

UV-BASED ADVANCED OXIDATION PROCESSES AND NANOSCALE  
ANTIMICROBIALS FOR ANTIBIOTIC RESISTANCE MITIGATION

by

Adeola Julian Sorinolu

A dissertation submitted to the faculty of  
The University of North Carolina at Charlotte  
in partial fulfillment of the requirements  
for the degree of Doctor of Philosophy in  
Civil Engineering

Charlotte

2022

Approved by:

---

Dr. Mariya Munir

---

Dr. Olya Keen

---

Dr. Juan L. Vivero-Escoto

---

Dr. Eric P. Vejerano

---

Dr. Cynthia Gibas

©2022  
Adeola Julian Sorinolu  
ALL RIGHTS RESERVED

## ABSTRACT

ADEOLA JULIAN SORINOLU. UV-Based Advanced Oxidation Processes and Nanoscale Antimicrobials for Antibiotic Resistance Mitigation. (Under the direction of DR. MARIYA MUNIR)

Antibiotic resistance (AR) is an ongoing pandemic that is unnoticed by many. AR is a global public health issue that challenges therapeutic potential against pathogens of humans and animals. Predictably, the environment has been implicated in the widespread AR in clinical settings. Wastewater treatment plants (WWTPs) are considered major sources for the release of antibiotic resistant bacteria (ARB) and antibiotic resistance genes (ARGs) into the environment. In this regard, effective wastewater treatment can serve as a barrier to the release of AR determinants to the environment. Also, addressing AR threats involves eliminating the development of new resistant traits by developing alternative antimicrobials with novel non-specific low-mutation bacterial targets.

This study presented advanced oxidation processes (AOPs) that utilize the strong oxidizing power of hydroxyl radical ( $HO\cdot$ ) and sulphate radical ( $SO_4\cdot^-$ ) as promising technologies for ARGs degradation. Also, we evaluated antimicrobial nanoparticles (NPs) that inactivate microorganisms via non-specific actions as alternatives to conventional antibiotics against pathogens of clinical concerns.

The reaction kinetics study, in Chapter 2, investigated the degradation of intracellular (i-) and extracellular (e-) plasmid-encoded *tetA*, *amp<sup>R</sup>* and *sull* ARGs using  $UV_{254}$ ,  $HO\cdot$  and  $SO_4\cdot^-$  UV-based AOP ( $UV_{254}/H_2O_2$  and  $UV_{254}/S_2O_8^{2-}$ , respectively). The degradation of *tetA*, *amp<sup>R</sup>* and *sull* was quantified using quantitative polymerase chain reaction (qPCR). Damages to each ARG were observed using two qPCR amplicons ranging

between 162-1054 bp. Culture-based horizontal gene transformation experiments were used to estimate the deactivation kinetics of pCR™2.1-TOPO AR plasmid. The results from this study provide data useful for setting operating conditions in WWTPs, drinking water treatments, and reactor designs for effective ARGs removal.

In Chapter 3, we investigated the antibacterial synergy of photosensitizer (PS) - AgNP conjugates using protoporphyrin IX (PpIX) as PS. The study examined the oxidation of AgNPs for an accelerated release of Ag<sup>+</sup> and the influence of positive surface coating of polyethyleneimine (PEI) in promoting NPs-bacterial interactions. The antimicrobial activities of three NPs: AgNPs and cysPpIX-AgNPs, PEI-cysPpIX-AgNPs against a methicillin-resistant *Staphylococcus aureus* (MRSA) strain and a wild-type multidrug-resistant (MDR) *E. coli* were reported. This study outlined the crucial role of optimized Ag<sup>+</sup> release for enhanced performance of AgNP-based antimicrobials.

Furthermore, Chapter 4 evaluated the use of nanoscale monocaprin as the first line of defense agent against the entrance of intracellular pathogens like *E. coli* and SARS-CoV-2. The sonochemistry technique was applied for the synthesis of nano-monocaprin to improve the solubility and antimicrobial activity of monocaprin. The study compared the inactivation of phi6 and *E. coli* using nano-monocaprin and bulk-monocaprin by plaque assay and drop plate colony count method, respectively. This study showed that nano-monocaprin formulations have improved antimicrobial properties relative to monocaprin at the molecular scale.

**Key Words:** Antibiotic resistance; Horizontal gene transfer; Advanced oxidation processes; Nanoscale antimicrobial; Photodynamic inactivation.

## DEDICATION

This dissertation is dedicated to my parents. Thank you for all you do.

## ACKNOWLEDGEMENTS

I sincerely thank my advisor, Dr Mariya Munir, for her constant support and guidance during this PhD program. Completing a PhD is demanding, but your confidence in me helped me scale through every challenge.

My thesis committee members, Dr. Olya Keen, Dr. Juan Vivero-Escoto, Dr. Eric Vejerano and Dr. Cynthia Gibas were more than just that. Thank you for your mentorship and insightful recommendations. I appreciate your effort and time.

I extend my appreciation to the North Carolina Water Resources Research Institute (NC WRRI) for the Student Fellowship Award to support my research work.

Munir Lab group is a friendly group, and I am glad to be a part of the team. Thank you to Dr Sol Park, Ariful Juel, Mohammad Khalid and Nita Khanal for creating a relaxed and friendly work environment. This thesis would not have been possible without Varsha Godakhindi, Mustafa Mamun, and Ted Brown who helped with the fabrication of nanoparticles and the UV apparatus used in this work. Kelsey Sikon, I appreciate your thoughtful updates and effort on the UV dose spreadsheet. I appreciate Dr Xiuli Lin, Dr Amir Alansari, Dr Amirhossein Adaryani and Dr Rui He for their training and help with lab equipment. I thank Dr Hemapriyadarshini Vadarevu and Dr Kevin Lambirth for their help with the cell culture work and microorganism sequence data analysis, respectively.

Life in Charlotte would have been lonesome without Shirley Geraldine and Binesh Kumar. Thank you both for being a family to me here. I am ever grateful for the blessing of a family in your family. I especially thank Tumininu Mbanisi and Chiamaka Fatoki for providing a rich growth experience for me during my PhD program. I thank Dr Alice Olorede, Mavis Mensah, Aanuoluwapo and Michael Uduebor, Suresh and Esther William,

Jeff and Debbie Washburn for providing amazing support communities during this PhD program.

My family: mum, dad, Adebunmi, Omolola, and Abiodun, thank you for your love and faith in me. Everything I have accomplished is because of your support. Mum and dad, this achievement is for you.

## TABLE OF CONTENTS

LIST OF FIGURES	XIII
LIST OF TABLES	XVIII
LIST OF ABBREVIATIONS	XVIII
LIST OF SYMBOLS	XXI
CHAPTER 1. INTRODUCTION	1
1.1. Antibiotic Resistance: A Silent Pandemic	1
1.2. Development and Spread of Antibiotic Resistance	2
1.3. Tackling Antibiotic Resistance in the Environment	5
1.3.1. Conventional Disinfection in Antibiotic Resistance Mitigation	6
1.3.2. Advanced Oxidation Processes (AOPs) – Promising Technologies for ARGs Degradation	9
1.4. Tackling Antibiotic Resistance in Clinical Settings: Nano-antimicrobials	11
1.4.1. Nanoparticles in Photodynamic Therapy	13
1.4.2. Nanoscale Antimicrobial Lipids Formulations	13
1.5. Study Objectives	14
1.6. Significance of the Study	14
1.7. Dissertation Overview	15
CHAPTER 2. DEGRADATION OF ANTIBIOTIC RESISTANCE GENES USING HYDROXYL RADICAL AND SULPHATE RADICAL (FUNDED BY: NC WRII)	17
2.1. Literature Review	17

2.2.	Hypothesis and Objectives of this Chapter	18
2.3.	Study Overview	19
2.4.	Materials and Method	20
2.4.1.	Chemical and Biological Reagents	20
2.4.2.	ARB Origin and Plasmids Identification	21
2.4.3.	Extracellular and Intracellular Plasmid Extraction	22
2.4.4.	Extracellular and Intracellular ARG Degradation Experiment	24
2.4.5.	qPCR Standard Preparation and Limit of Detection	26
2.4.6.	qPCR Quantification	28
2.4.7.	Radical Probe Quantification	30
2.4.8.	Preparation of Chemically Competent TOP10 <i>E. coli</i> Cells	30
2.4.9.	Bacterial Transformation Assay	31
2.4.10.	Gel Electrophoresis Analysis	32
2.4.11.	Data and Statistical Analysis	33
2.5.	Results and Discussion	33
2.5.1.	Extracellular ARG Degradation during UV <sub>254</sub> , UV <sub>254</sub> /H <sub>2</sub> O <sub>2</sub> and UV <sub>254</sub> /S <sub>2</sub> O <sub>8</sub> <sup>2-</sup>	34
2.5.2.	The Roles of HO· and SO <sub>4</sub> · <sup>-</sup> in ARGs Degradation during UV <sub>254</sub> /H <sub>2</sub> O <sub>2</sub> and UV <sub>254</sub> /S <sub>2</sub> O <sub>8</sub> <sup>2-</sup>	38

2.5.3.	Analysis of Amplicon Length and Nucleotide Contents on ARG	
	Degradation Rate	40
2.5.4.	Intracellular ARG Degradation during UV <sub>254</sub> , UV <sub>254</sub> /H <sub>2</sub> O <sub>2</sub> and UV <sub>254</sub> /S <sub>2</sub> O <sub>8</sub> <sup>2-</sup>	
	44	
2.5.5.	Impact of Initial Oxidant Concentration and pH	47
2.5.6.	Structural Changes and Loss of Transforming Activity	52
2.6.	Summary	56
CHAPTER 3. INACTIVATION OF ANTIBIOTIC RESISTANCE BACTERIA		
USING PHOTO-ACTIVATED SILVER NANOPARTICLES (FUNDED BY: FRG) 59		
3.1.	Literature Review	59
3.2.	Hypothesis and Objectives of this Chapter	63
3.3.	Study Overview	63
3.4.	Materials and Method	64
3.4.1.	Test Organisms	64
3.4.2.	MDR <i>E. coli</i> Library Preparation and Sequencing	65
3.4.3.	Nanoparticles Synthesis and Characterization	66
3.4.4.	Bacterial Inactivation Experiment	67
3.4.5.	ARG Degradation Experiment	68
3.4.6.	qPCR Quantification of ARG Degradation	68
3.5.	Results and Discussion	69
3.5.1.	MDR <i>E. coli</i> Sequence Data Analysis, Classification and Identification	69

3.5.2.	Bacterial Inactivation Experiment	70
3.5.3.	Roles of ROS in ARB Inactivation using Porphyrin-AgNP Conjugates	77
3.5.4.	ARG Degradation using Porphyrin-AgNPs	80
3.6.	Summary	83
CHAPTER 4. ANTIBACTERIAL AND ANTIVIRAL ACTIVITY OF MONOGLYCERIDE NANO-EMULSIONS		84
4.1.	Literature Review	84
4.2.	Objectives of the Chapter	87
4.3.	Study Overview	87
4.4.	Materials and Method	88
4.4.1.	Biological and Chemical Reagent	88
4.4.2.	Preparation of Bulk- and Nano-monocaprin	88
4.4.3.	Preparation of Bacteriophage Stock Suspension	89
4.4.4.	Bacteriophage Inactivation using Nano- and Bulk-monocaprin	89
4.4.5.	<i>E. coli</i> Inactivation using Nano-monocaprin	90
4.4.6.	Cytotoxicity of Nano-monocaprin	91
4.5.	Results and Discussion	92
4.5.1.	Characterization of Nano-monocaprin	92
4.5.2.	Antimicrobial Effect of Nano-monocaprin and Bulk-monocaprin	93
4.5.3.	Cytotoxicity of nano-monocaprin	99

4.6. Summary	99
CHAPTER 5. CONCLUSIONS AND RECOMMENDATIONS	101
5.1. Conclusions	101
5.2. Novel Contributions	102
5.3. Recommendations	103
LIST OF PUBLICATIONS	105
REFERENCES	106
APPENDIX A: QPCR AMPLICON SEQUENCE	120
APPENDIX B: REACTION EQUATIONS IN $UV_{254}$ , $UV_{254}/H_2O_2$ AND $UV_{254}/S_2O_8^{2-}$ SYSTEMS	122
APPENDIX C: LINEAR REGRESSION OF FIRST ORDER DEGRADATION RATE CONSTANT, $K$ ( $CM^2/MJ$ ) VERSUS SPECIFIC NUCLEOTIDE CONTENTS OF QPCR AMPLICON	128
APPENDIX D: UV FLUENCE CALCULATION EQUATIONS	129

## LIST OF FIGURES

FIGURE 1. 1 Pathway for the dissemination of antibiotic resistance.	4
FIGURE 1. 2 Stages involved in conventional wastewater treatment processes. The treatment stages are shown in the top flowchart and the functions of each of the treatment stages are briefly described in the bottom flowchart.	8
FIGURE 2. 1 Schematics of the ARG degradation experiments	20
FIGURE 2. 2 a) QIAGEN-extracted plasmids and linearized plasmids i. linearized MDR <i>E. coli</i> plasmid by restriction enzyme EcoRV-HF <sup>®</sup> ii. Extracted MDR <i>E. coli</i> plasmid iii. Linearized pCR <sup>™</sup> 2.1-TOPO by restriction enzyme EcoR1-HF <sup>®</sup> iv. Extracted pCR <sup>™</sup> 2.1-TOPO plasmid b) qPCR amplicons of <i>sulI</i> , <i>tetA</i> and <i>amp<sup>R</sup></i> .	22
FIGURE 2. 3 Standard curves for ARG amplicons. (A) <i>sulI</i> (162 bp), (B) <i>sulI</i> (841 bp), (C) <i>tetA</i> (210 bp), (D) <i>tetA</i> (1054 bp), (E) <i>amp<sup>R</sup></i> (192 bp), and (F) <i>amp<sup>R</sup></i> (851 bp). Standard curves were prepared by 10-fold serial dilutions of concentrated extracellular plasmids (for <i>amp<sup>R</sup></i> ) or PCR amplicons (for <i>sulI</i> and <i>tetA</i> ) (~ 108 copies/ $\mu$ L).	29
FIGURE 2. 4 Degradation of e-ARGs in PBS (pH 7, 10 mM) during UV <sub>254</sub> , UV <sub>254</sub> /H <sub>2</sub> O <sub>2</sub> and UV <sub>254</sub> /S <sub>2</sub> O <sub>8</sub> <sup>2-</sup> . The concentrations of H <sub>2</sub> O <sub>2</sub> and S <sub>2</sub> O <sub>8</sub> <sup>2-</sup> were 0.2 mM for UV <sub>254</sub> /H <sub>2</sub> O <sub>2</sub> and UV <sub>254</sub> /S <sub>2</sub> O <sub>8</sub> <sup>2-</sup> . Concentration of plasmids is ~2ng/ $\mu$ L. The error bars are the standard error of mean (SEM) of independent triplicate experiments. The LOD is 3 copies/reaction.	36
FIGURE 2. 5 Degradation of extracellular AR <i>E. coli</i> plasmids by 0.2mM H <sub>2</sub> O <sub>2</sub> and S <sub>2</sub> O <sub>8</sub> <sup>2-</sup> oxidants.	38
FIGURE 2. 6 Degradation of pCBA during the treatment of extracellular AR plasmids with UV <sub>254</sub> , UV <sub>254</sub> /H <sub>2</sub> O <sub>2</sub> and UV <sub>254</sub> /S <sub>2</sub> O <sub>8</sub> <sup>2-</sup> .	41
FIGURE 2. 7 Degradation of extracellular <i>tetA</i> and <i>sulI</i> during UV <sub>254</sub> /S <sub>2</sub> O <sub>8</sub> <sup>2-</sup> with and without HO. scavenger (BtOH represents tert-Butanol) at pH 7.	42
FIGURE 2. 8 First order degradation constants of qPCR amplicons as a function of the number of nucleotide base pair contents per qPCR amplicon.	43
FIGURE 2. 9 First order degradation constants ( <i>k</i> ) of qPCR amplicons versus the total number of intrastrand 5'-bipyrimidine-3' in each amplicon. Bipyrimidine are TT, TC, CT and CC within a single DNA strand.	44

FIGURE 2. 10 Degradation of i-ARGs in PBS (pH 7, 10 mM) during UV<sub>254</sub>, UV<sub>254</sub>/H<sub>2</sub>O<sub>2</sub> and UV<sub>254</sub>/S<sub>2</sub>O<sub>8</sub><sup>2-</sup>. The concentrations of H<sub>2</sub>O<sub>2</sub> and S<sub>2</sub>O<sub>8</sub><sup>2-</sup> were 0.2 mM for UV<sub>254</sub>/H<sub>2</sub>O<sub>2</sub> and UV<sub>254</sub>/S<sub>2</sub>O<sub>8</sub><sup>2-</sup>. The concentration of *E. coli* cells is ~1.5 x 10<sup>8</sup>. The error bars are the SEM of independent triplicate experiments. 46

FIGURE 2. 11 Comparison of first-order rate constants of e-ARG and i-ARG for UV<sub>254</sub>, UV<sub>254</sub>/H<sub>2</sub>O<sub>2</sub> and UV<sub>254</sub>/S<sub>2</sub>O<sub>8</sub><sup>2-</sup>. The largest difference between  $k_{e-ARG}$  and  $k_{i-ARG}$  degradation rates were observed for *amp<sup>R</sup>* (851 bp). 49

FIGURE 2. 12: Effect of initial H<sub>2</sub>O<sub>2</sub> and S<sub>2</sub>O<sub>8</sub><sup>2-</sup> concentrations on the degradation of i-ARG and e-ARG during UV<sub>254</sub>/H<sub>2</sub>O<sub>2</sub> and UV<sub>254</sub>/S<sub>2</sub>O<sub>8</sub><sup>2-</sup> treatments. UV fluence in all cases was 500 mJ/cm<sup>2</sup>. Error bars are SEM of duplicate independent experiments. The symbol \*, \*\* and \*\*\* denote statistically significant differences with p < 0.05, p < 0.01 and p < 0.001, respectively using one-way ANOVA test with Bonferroni correction between the different test samples at a given initial oxidant concentration. 50

FIGURE 2. 13 Influence of pH on the degradation of extracellular MDR *E. coli* plasmid (~1 ng/μL) using 0.1 mM and 0.2 mM concentrations of H<sub>2</sub>O<sub>2</sub> and S<sub>2</sub>O<sub>8</sub><sup>2-</sup> during UV<sub>254</sub>/H<sub>2</sub>O<sub>2</sub> and UV<sub>254</sub>/S<sub>2</sub>O<sub>8</sub><sup>2-</sup> treatments. UV fluence was 500 mJ/cm<sup>2</sup>. Error bars are SEM of duplicate independent experiments. The symbol \*, \*\* and \*\*\* denote statistically significant differences with p < 0.05, p < 0.01 and p < 0.001, respectively using one-way ANOVA test with Bonferroni correction between the different test samples in each experimental pH group. 51

FIGURE 2. 14: Stability of qPCR amplicons of tetA and sulI genes in MDR *E. coli* plasmid in various pH solutions over the same time exposure as pH impact experiment for UV<sub>254</sub>/H<sub>2</sub>O<sub>2</sub> and UV<sub>254</sub>/S<sub>2</sub>O<sub>8</sub><sup>2-</sup>. 52

FIGURE 2. 15 Changes in structural conformation of extracellular pCR<sup>TM</sup>2.1-TOPO<sup>®</sup> (~3 ng/μL) shown on gel electrophoresis during treatment with a) UV<sub>254</sub>, b) UV<sub>254</sub>/H<sub>2</sub>O<sub>2</sub> and c) UV<sub>254</sub>/S<sub>2</sub>O<sub>8</sub><sup>2-</sup> (pH = 7, 0.2 mM H<sub>2</sub>O<sub>2</sub> and S<sub>2</sub>O<sub>8</sub><sup>2-</sup>). The numbers presented above each column represent the UV fluence applied during all treatments. The 'linear plasmid' column is linearized pCR<sup>TM</sup>2.1-TOPO<sup>®</sup> by restriction enzyme EcoR1-HF<sup>®</sup>. 53

FIGURE 2. 16 (a) Loss of amp<sup>R</sup> gene transformation activity in TOP10 *E. coli* competent cells after treatment of extracellular pCR<sup>TM</sup>2.1-TOPO<sup>®</sup> (~1 ng/μL) with UV<sub>254</sub>, UV<sub>254</sub>/H<sub>2</sub>O<sub>2</sub> and UV<sub>254</sub>/S<sub>2</sub>O<sub>8</sub><sup>2-</sup> (pH=7, 0.2 mM H<sub>2</sub>O<sub>2</sub> and S<sub>2</sub>O<sub>8</sub><sup>2-</sup>) (b) Comparison of the first-order degradation rate constants of qPCR amplicons with first-order deactivation rate constant from TOP10 *E. coli* transformation with treated extracellular pCR<sup>TM</sup>2.1-TOPO<sup>®</sup>. Error bars are SEM of triplicate independent experiments. 55

FIGURE 3. 1 Schematics of the ARB inactivation experiments using porphyrin-AgNP conjugates. **A)** Synthesis and Characterization of cysPpIX-AgNPs and PEI-cysPpIX-AgNPs. **B)** Ag<sup>+</sup> release profile obtained post light activation using ICP-OES. **C)**

Antimicrobial activity of the light irradiated nanoparticles assessed by drop plate colony count method.	64
FIGURE 3. 2 Evaluating the Bacterial inactivation of MRSA after 20 minutes irradiation.	72
FIGURE 3. 3 Bacterial inactivation between MRSA and MDR <i>E. coli</i> after 20 minutes irradiation (30 minutes dark incubation prior to irradiation).	73
FIGURE 3. 4 Changes in the bacteria cell count in PBS with time (microbe stability test).	73
FIGURE 3. 5 Inactivation of MRSA under light activated conditions. 0 h time point indicates the achieved inactivation after light irradiation for 20 minutes. 4 h and 24 h show the bactericidal effect post-irradiation. Error bar is the standard error of mean (SEM) of three independent replicate experiments.	74
FIGURE 3. 6 Inactivation of MDR <i>E. coli</i> under light activated conditions. 0 h time point indicates the achieved inactivation after light irradiation for 20 minutes. 4 h and 24 h show the bactericidal effect post-irradiation. Error bar is the standard error of mean (SEM) of three independent replicate experiments.	76
FIGURE 3. 7 Ag <sup>+</sup> release profile of AgNP, cysPpIX-AgNP and PEI-cysPpIX-AgNP under light condition. (Experiment by Varsha Godakhindi, 2022. Details in publication: <i>Enhancing the Inactivation of Antibiotic- Bacteria using Light-Activated Silver Nanoparticles: Influence of Silver Ion Release</i> . Article no 2 in List of Publications).	77
FIGURE 3. 8 Tolerance of MDR <i>E. coli</i> to PDI using cysPpIX (30 min dark incubation and 20 min irradiation time).	79
FIGURE 3. 9 Inactivation of bacteria using AgNO <sub>3</sub> . Concentration is expressed in µg/L AgNO <sub>3</sub> as Ag <sup>+</sup> .	80
FIGURE 3. 10 Standard curves for <i>sulI</i> and <i>tetA</i> ARG amplicons.	81
FIGURE 3. 11 Degradation of extracellular ARG encoded on MDR <i>E. coli</i> plasmid using AgNP, cysPpIX-AgNP and cysPpIX (1.5 µg/mL AgNP and 1 µM cysPpIX). Contact time was 24 hrs. Control refers to samples that were not treated with any of the NPs or PS.	81
FIGURE 3. 12 Degradation of intracellular ARG in MDR <i>E. coli</i> plasmid using AgNP and cysPpIX-AgNP (1.5 µg/mL AgNP and 1 µM cysPpIX). Control refers to samples that were not treated with any of the NPs or PS.	82
FIGURE 3. 13 Effect of Ag <sup>+</sup> on the degradation of <i>sulI</i> gene in MDR <i>E. coli</i> plasmid after 24 hrs exposure.	83

FIGURE 4. 1 Chemical structure of capric acid (Free fatty acid) and Monocaprin (Monoglyceride).	86
FIGURE 4. 2 The generation of organic nanoparticle due to acoustic cavitation phenomenon during sonochemistry. During sonication, bubbles are generated in the liquid and organic molecules form a shell around bubbles. Bubbles grow in volume as solvent or solute vapour diffuses into the bubbles. A stage is reached when bubbles become unstable resulting in implosion and the collapse of molecules shell into the center of the bubble. This process creates nanoparticles (NPs) shown in the magnified form at the end of the process. Adapted from Yariv et al. (2015).	86
FIGURE 4. 3 Schematics of the antiviral and antibacterial assays using nano-monocaprin.	92
FIGURE 4. 4 Physical appearance of nano-monocaprin and bulk-monocaprin at 4 mM concentration.	94
FIGURE 4. 5 Absorbance spectra of bulk-monocaprin and nano-monocaprin (20 min sonication, continuous) (4 mM, in nano-pure water).	94
FIGURE 4. 6 Optimization of nano-monocaprin preparation method (2 mM, pH 7). Error bars are the standard deviation of triplicate plaque counts for each experiment condition.	95
FIGURE 4. 7 Inactivation of phi6 using bulk- and nano-monocaprin solutions at pH 7 with exposure time of 5 min. (*) indicates the limit of quantification. Error bars are the standard deviation of triplicate plaque counts for each experiment condition.	96
FIGURE 4. 8 Effect of surfactant tween20 on the on phi6 inactivation using nano-monocaprin (2 mM, pH 7).	97
FIGURE 4. 9 Effect of nano-monocaprin solution pH on phi6 inactivation for 5 min exposure time. (*) indicates the limit of quantification. Error bars are the standard deviation of triplicate plaque counts for each experiment condition. Control experiment indicates that pH 4 buffer + nano pure water achieved 0.21 ( $\pm$ 0.02) log inactivation of phi6.	97
FIGURE 4. 10 Plaque assay results of the antiviral experiment of samples against MS2. A). MS2 + TSB (control); B) MS2 + 2.5 mM bulk-monocaprin; C) MS2 + 2.5 mM nano-monocaprin. Treatment conditions are 5 min contact time and pH 7. Images show comparable number of plaques at 10 <sup>-4</sup> dilution.	98
FIGURE 4. 11 Inactivation of <i>E. coli</i> using nano-monocaprin solution at pH 4 with exposure time of 5 min. No bacterial inactivation was observed when <i>E. coli</i> cells were exposed to pH 4 buffer solution alone in a control experiment. (*) indicates the limit of quantification.	98

FIGURE 4. 12 Cytotoxicity of nano-monocaprin on HeLa and HPDE cells.

100

## LIST OF TABLES

TABLE 2. 1 Specific nucleotide compositions of the qPCR amplicons.	25
TABLE 2. 2 List of primers and qPCR amplification conditions.	28
TABLE 2. 3 First order kinetic degradation rate constants during UV <sub>254</sub> , UV <sub>254</sub> /H <sub>2</sub> O <sub>2</sub> and UV <sub>254</sub> /S <sub>2</sub> O <sub>8</sub> <sup>2-</sup> treatment of extracellular plasmid-encoded ARGs.	34
TABLE 2. 4: Degradation kinetics of pCBA and steady-state concentrations of <i>HO</i> . and <i>SO4</i> . –.	39
TABLE 2. 5 Estimated first-order and second order degradation rate constants of ARGs due to only <i>HO</i> . and <i>SO4</i> . –.	42
TABLE 2. 6 First-order kinetic degradation rate constants during UV <sub>254</sub> , UV <sub>254</sub> /H <sub>2</sub> O <sub>2</sub> and UV <sub>254</sub> /S <sub>2</sub> O <sub>8</sub> <sup>2-</sup> treatments of intracellular plasmid-encoded ARGs ( $k = 2.303 \times \text{slope}$ ).	48
TABLE 2. 7 First-order rate constant for <i>amp</i> <sup>R</sup> , pCR <sup>TM</sup> 2.1 degradation and pCR <sup>TM</sup> 2.1 deactivation.	57
TABLE 3. 1 List of primers and qPCR amplification conditions.	69

## LIST OF ABBREVIATIONS

<i>amp<sup>R</sup></i>	Ampicillin Resistance Gene
<i>cys</i>	Cysteamine
pCBA	Parachlorobenzoic Acid
qPCR	Quantitative Polymerase Chain Reaction
<i>sulI</i>	Sulfonamide Resistance Gene
<i>tetA</i>	Tetracycline Resistance Gene Class A
AgNPs	Silver Nanoparticles
AMR	Antimicrobial Resistance
AOPs	Advanced Oxidation Processes
AR	Antibiotic Resistance
ARB	Antibiotic Resistant Bacteria
ARG	Antibiotic Resistance Gene
ATCC	American Type Culture Collection
CFU	Colony Forming Unit
DBPs	Disinfection Byproducts
DMEM	Dulbecco's modified Eagle's medium
DNA	Deoxyribonucleic Acid
DOMs	Dissolved Organic Matters
DPBS	Dulbecco's phosphate buffer saline
EPS	Extracellular Polymeric Substances
FBS	Fetal Bovine Serum
HGT	Horizontal Gene Transfer

HPDE Human Pancreatic Duct Epithelial Cell

LB Luria Bertani

LOD Limit of Detection

MDR Multidrug Resistant Bacteria

MGE Mobile Genetic Elements

MIC Minimum Inhibitory Concentration

MRSA Methicillin Resistant *Staphylococcus aureus*

NPs Nanoparticles

PBS Phosphate Buffered Saline Solution

PDI Photodynamic Inactivation

PEI Polyethyleneimine

PFU Plaque Forming Unit

PMS Peroxymonosulfate

PpIX Protoporphyrin IX

PS Photosensitizer

RNA Ribonucleic Acid

ROS Reactive Oxygen Species

RPMI Roswell Park Memorial Institute

TSA Tryptic Soy Agar

TSB Tryptic Soy Broth

TWW Treated Wastewater

VGT Vertical Gene Transfer

WWTPs Wastewater Treatment Plants

## LIST OF SYMBOLS

$HO\cdot$  Hydroxyl radical

$SO_4\cdot^-$  Sulphate radical

$k_i$  First-order degradation rate constant of ARG.  $i$  represents  $UV_{254}$ .

$k'_i$  pseudo First-order degradation rate constant of ARG  $i$  represents  $UV_{254}/H_2O_2$ ,  $UV_{254}/S_2O_8^{2-}$ ,  $HO\cdot$  or  $SO_4\cdot^-$ .

$k_{i,ARG}$  Second order degradation rate constant of ARG with respect to oxidant  $i$ .  $i$  represents  $HO\cdot$  or  $SO_4\cdot^-$ .

$k_{i,pCBA}$  Second order degradation rate constant of pCBA with respect to oxidant  $i$ .  $i$  represents  $HO\cdot$  or  $SO_4\cdot^-$ .

## CHAPTER 1. INTRODUCTION

### 1.1. Antibiotic Resistance: A Silent Pandemic

The introduction of penicillin in 1942 began the invaluable contribution of antibiotics to human health (Walsh and Wright, 2005). Since then, the widespread use of antibiotics for human and animal therapy has been followed by the rise of bacteria that are resistant to them. Antibiotic resistance (AR) is a phenomenon exhibited by a bacterium when it resists the bactericidal effect of an antibiotic after exposure to the antibiotic at a concentration equal to or above the minimum inhibitory concentration (MIC) (Michael-Kordatou et al., 2018). Nowadays, common and treatable illnesses (such as urinary tract infections and tuberculosis) are often fatal due to the dwindling effectiveness of current antimicrobial drugs against pathogenic organisms (WHO, 2014). In the United States, more than 2.8 million antibiotic-resistant infections occur annually resulting in more than 35,000 deaths (CDC, 2019).

According to Monnet and Harbarth (2020), AR is an ongoing pandemic that is unnoticed. Larry Kerr, the co-chair of the Transatlantic Task Force on Antimicrobial Resistance, likened antimicrobial resistance to “a multitude of small fires that are less visible than the single massive firestorm of the pronounced COVID-19 pandemic” (Monnet and Harbarth, 2020). AR is a global public health issue because it challenges therapeutic potential against pathogens of human and animals. Arguably there a minimum of one mechanism of bacterial resistance to all the classes of antibiotics available today (Levy and Marshall, 2004). The report on the Global Antimicrobial Resistance Surveillance by the World Health Organization (WHO) emphasised that the inability to mitigate the spread of

antibacterial resistance (AR) and develop new antibiotics will subject the 21<sup>st</sup> century to a post-antibiotic era (WHO, 2014). Antibiotic resistance affects humans, animals and the environment across the world (CDC, 2019). This implies that AR can be spread through these routes, and everyone is at the risk of contracting an antibiotic resistant infection.

## 1.2. Development and Spread of Antibiotic Resistance

Naturally, AR in some microorganisms is an evolutionary process that increases their chances of survival against other microbes (Calero-Cáceres and Muniesa, 2016). The acquisition of antibiotic resistance genes (ARGs) by an organism is either by vertical gene transfer (VGT), or horizontal gene transfer (HGT). VGT refers to the transfer of genetic information from parent cells to offspring which is rapidly driven by the selective pressure of antibiotics used in therapeutic settings (Michael-Kordatou et al., 2018). In HGT, a bacterium without resistance acquires the resistance genes from mobile genetic elements (MGEs) such as plasmids, integrons, and transposons. HGT mediated processes include conjugation, transduction and natural transformation. Conjugation is a process in which DNA is passed from a cell (the donor) to another cell (the acceptor) through direct cell to cell contact; transduction is the introduction of ARGs into microbial cells by bacteriophages; and natural transformation refers to the process in which competent microbes take up free (extracellular) DNA from their surroundings (Keen and Montforts, 2012).

Despite the diverse natural background of antibiotic resistant bacteria (ARB) and ARGs, the prevalence of ARB and ARGs has been linked to the indiscriminate use of antibiotics for human and animal treatment (Figure 1.1). This is because antibiotics select

for resistant bacteria in a bacterial population by killing susceptible bacteria while resistant bacteria proliferate (WHO, 2014, Berendonk et al., 2015). Sir Alexander Fleming – the Scottish Bacteriologist who discovered penicillin, in his Nobel Prize lecture in 1945 warned of the tendency of bacteria to develop resistance to antibiotics (WHO, 2014). In Sir Alexander Fleming’s words, “It is not difficult to make microbes resistant to penicillin in the laboratory by exposing them to concentrations not sufficient to kill them, and the same thing has occasionally happened in the body.”(Fleming, 1945).

AR in the clinical setting is previously known. However, the spread of AR in the environment is an emerging issue. Nowadays, there are frequent reports of the occurrence of ARB and ARGs in rivers, soils, treated drinking water, sewage, and air (Xi et al., 2009, Yuan et al., 2015, Czekalski et al., 2016, Ma et al., 2017, Yu et al., 2017, He et al., 2019). The dissemination of antibiotics in the environment could be by the direct disposal of excess antibiotics or the presence of antibiotics and their metabolites in faeces and urine. According to Kümmerer (2009) and Tran et al. (2016), about 50 to 90% of antibiotics taken by humans or animals are passed out in excrement and urine in their original forms and (or) their metabolites. Also, the widespread use of antibiotics in agriculture and aquaculture contributes immensely to the prevalence of antibiotics and AR in the environment. In most developed countries, livestock production (cattle, chickens, and pigs) accounts for 50 to 80% of the total antibiotic usage (Cully, 2014). These antibiotics, ARB and ARGs end up the aquatic environment and soil (Figure 1.1).

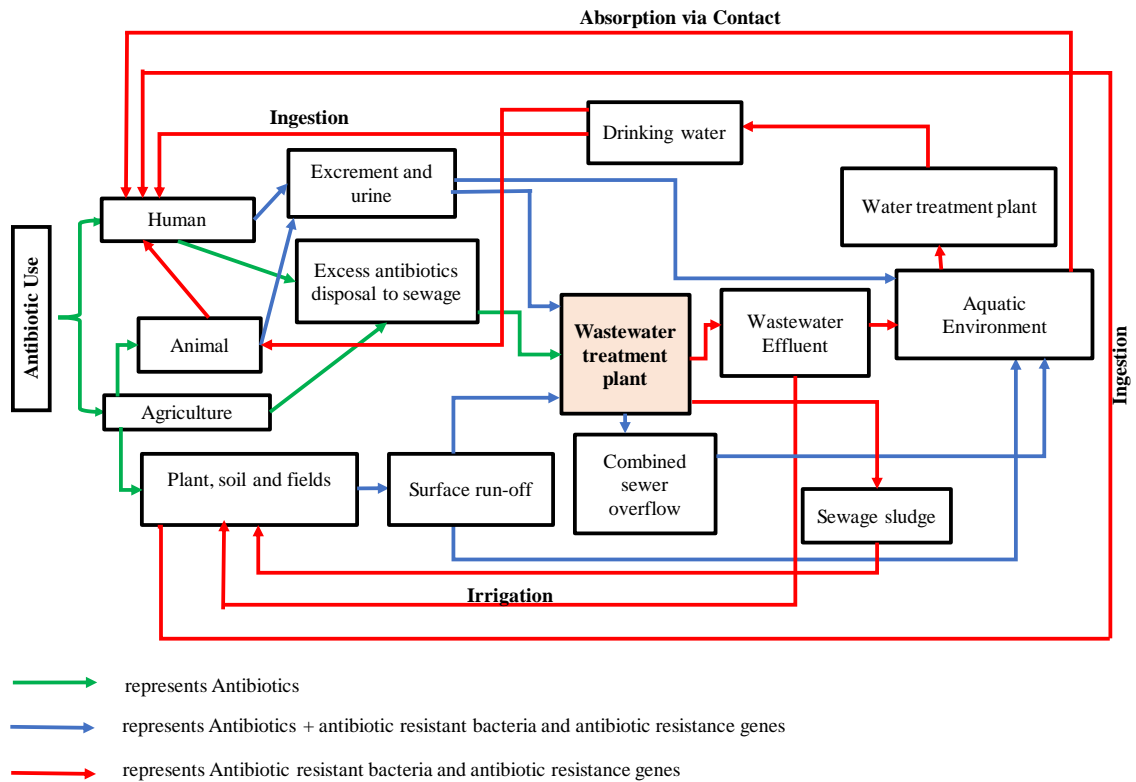


FIGURE 1. 1 Pathway for the dissemination of antibiotic resistance.

Wastewater treatment plants (WWTPs) are one of the main sources of ARB and ARGs release into the environment (Rizzo et al., 2013) (Figure 1.1). Wastewater is considered favorable for the development of new resistance traits via HGT because human-commensal, pathogenic and environmental bacteria are in close contact, nutrients are abundant and antimicrobial agents are present (Lindberg et al., 2004, Michael-Kordatou et al., 2018, Sorinolu et al., 2021). Furthermore, wastewater carries different forms of ARGs; including DNA within bacteria and viruses, and extracellular DNA (Colomer-Lluch et al., 2011, Sorinolu et al., 2021). Also, there are reports that metals, biocides and quaternary ammonium compounds which are commonly present in wastewater have greater potential to select for ARGs (Pal et al., 2015).

The reuse of wastewater (an effort to address the scarce water resources) and sewage sludge for agricultural purposes potentially compounds this problem (Michael-Kordatou et al., 2018, Sorinolu et al., 2021). The use of treated wastewater (TWW) and biosolids in agriculture results in the introduction of subtherapeutic amounts of antibiotics in the environment. Subtherapeutic antibiotic concentrations are known to promote the development of AR in microorganisms (Chang et al., 2015, Sorinolu et al., 2021). Usually, the concentration of antibiotics in the environment is below therapeutically used lethal concentrations. Nevertheless, these sublethal antibiotic concentrations are well known to favor the development of AR in microbial communities (Jørgensen and Halling-Sørensen, 2000, Rizzo et al., 2013). ARB and ARGs are microbiological hazards related to AR human health risks assessment during TWW irrigation and biosolids amendment. The routes of exposure to these hazards during wastewater reuse include (i) inhalation of ARB/ARGs/antibiotics in aerosols produced during irrigation and soil amendment, (ii) absorption through the skin following contact with TWW, biosolids or contaminated crop and (iii) ingestion (mostly via consumption of contaminated crops) (Figure 1.1) (Manaiia, 2017, Ben et al., 2019, Amarasiri et al., 2020, Sorinolu et al., 2021).

### 1.3. Tackling Antibiotic Resistance in the Environment

Tackling AR threat involves slowing and stopping the development of resistance through better antibiotic use (CDC, 2019). Conventional wastewater treatment processes (such as activated sludge process, oxidation ditch etc.) involve a combination of physical, chemical and biological processes to treat wastewater (Figure 1.2) (Moura et al., 2012). These processes cannot efficiently remove ARB and ARGs from wastewater because they

are primarily designed for the removal of solids, organic pollutants and (sometimes) nutrients (Zhang and Li, 2011, Lamba and Ahammad, 2017). Unlike most environmental contaminants that can be attenuated by natural processes, AR tends to persist in the environment since it is associated with biological organisms that actively reproduce and multiply. The ability of many antibiotic-susceptible bacteria to incorporate ARGs into their cells via HGT makes ARGs persistent in the environment (Matyar, 2012, Yu et al., 2018). Consequently, for WWTPs to serve as a barrier against AR spread, effluent discharge with no detectable ARB/ARG is desirable.

It is common knowledge that ARB and ARGs are widespread in water environments (He et al., 2019, Sharma et al., 2019). ARB and ARGs have been observed in rivers, wastewater, effluent from wastewater treatment plants (WWTPs) and drinking water distribution systems (Xi et al., 2009, Yuan et al., 2015, Czekalski et al., 2016, Ma et al., 2017, Yu et al., 2017, He et al., 2019). In this regard, effective wastewater treatment can serve as a barrier against the release of ARB and ARGs into the environment. Disinfection process, as an integral part of the wastewater treatment process, is vital in controlling the spread of ARB and ARGs in the environment (Figure 1.2).

### 1.3.1. Conventional Disinfection in Antibiotic Resistance Mitigation

Conventional disinfection processes, such as chlorination and ultraviolet (UV) irradiation, have been widely adopted for wastewater effluent disinfection; particularly when it discharges into sensitive rivers and drinking water sources (Jacangelo and Trussell, 2002). The main advantages associated with chlorination are its high efficacy, low operating cost and ease of application (Huang et al., 2011). However, the formation of

disinfection by-products (DBPs) due to the reaction of chlorine with dissolved organic matters (DOM) in effluents is a disadvantage of this disinfection process. Furthermore, the tendency for the formation of DBPs during chlorination may limit the application concentration because toxicity increases with increasing chlorine concentration and contact time. UV irradiation does not form DBPs and usually requires a shorter contact time than chlorination. One disadvantage associated with UV irradiation is the ability of organisms to repair UV damage through photoreactivation or dark repair (Solomon et al., 1998, Cutler and Zimmerman, 2011). Thus, to reduce AR dissemination using UV irradiation, it is important to establish operating conditions that will not result in bacterial regrowth.

Studies have shown that chlorination and ultraviolet irradiation considerably inactivate ARB; however, ARGs are not effectively removed at doses typically used in WWTPs (Yu et al., 2017, Yu et al., 2018, Sharma et al., 2019, Zhang et al., 2019). For instance, in a UV irradiation experiment conducted by Zhang et al. (2015b), the maximum log reduction of *tet(X)* achieved was only 0.58 at a UV fluence of 249.5 mJ/cm<sup>2</sup>; whereas the conventional UV fluence for wastewater treatment is between 20 mJ/cm<sup>2</sup> to 100 mJ/cm<sup>2</sup> (Templeton et al., 2009, Michael-Kordatou et al., 2018). Also, a study by Furukawa et al. (2017) on the removal of *vanA* using chlorination revealed that at a chlorine dose of 3 mg/L with contact time of 3 min, vancomycin-resistant enterococci were below detection limit (> 7 log reduction) but *vanA* genes were still present at the same chlorine dose. Furthermore, at a higher chlorine dose of 160 mg/L with a contact time of 120 min, the maximum log reductions of ARGs in a chlorination experiment was just 3.24 log (Zhuang et al., 2015). Meanwhile, the chlorine concentration examined in this study was higher than the conventional chlorine dose (5 to 20 mg/L) used in wastewater treatment (US EPA,

1999). The results of these studies buttress that stronger oxidants or disinfection techniques are needed to degrade ARGs. Moreover, issues regarding the potential for HGT promotion during these treatment process have been raised. Some studies have shown that subinhibitory chlorination conditions increase the frequency of HGT between microbes (Guo et al., 2015, Zhang et al., 2017, Sanganyado and Gwenzi, 2019). This is particularly of concern in chlorine contact tanks with dead corners. Consequently, there exist questions regarding the efficiencies of these disinfection processes in reducing AR in the environment (Huang et al., 2011, Czekalski et al., 2016).

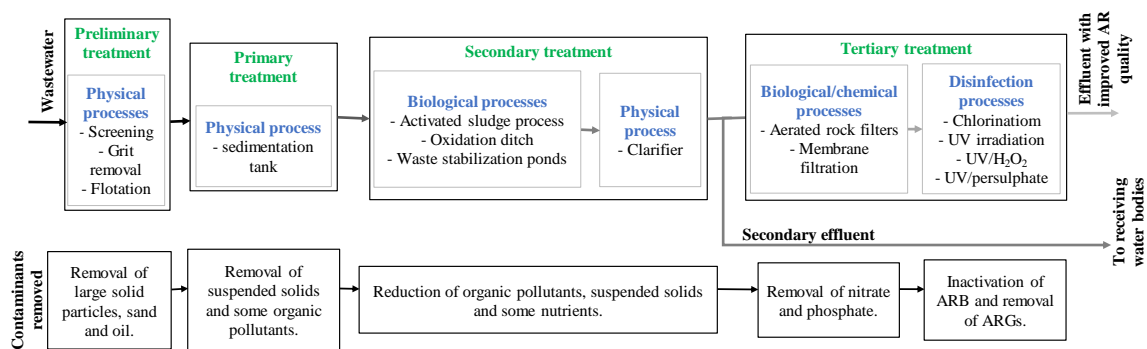


FIGURE 1. 2 Stages involved in conventional wastewater treatment processes. The treatment stages are shown in the top flowchart and the functions of each of the treatment stages are briefly described in the bottom flowchart.

In the quest for mitigating AR proliferation, complete inactivation of ARB without degradation of the resistance determinants (such as plasmids, integrons, gene cassettes, or transposons) in wastewater is not ‘enough’. Intact resistance determinants within the cell debris in the environment can confer resistance to bacterial populations downstream via HGT. Thus, HGT is by far the most important route by which ARG is transferred from

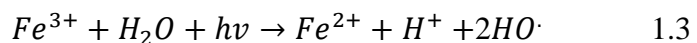
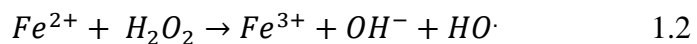
environmental and(or) commensal ARB to antibiotic-susceptible human pathogens (Chang et al., 2015). Also, it has been reported that this mechanism of ARG transfer is accelerated by environmental stressors such as biocides, toxic metals, and nanomaterials (Qiu et al., 2012, Soumet et al., 2012). Furthermore, wastewater is considered favorable for the development of new resistant traits via horizontal transfer of resistance gene since human-commensal, pathogenic and environmental bacteria are in close contact, nutrients are abundant and antimicrobial agents are present (Lindberg et al., 2004, Michael-Kordatou et al., 2018). Hence, disinfection processes must be designed for ARG degradation while eliminating HGT propagation which could occur due to insufficient disinfectant dose and residual disinfectant discharge into the environment.

### 1.3.2. Advanced Oxidation Processes (AOPs) – Promising Technologies for ARGs Degradation

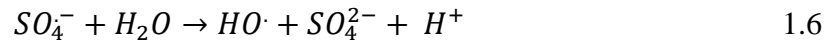
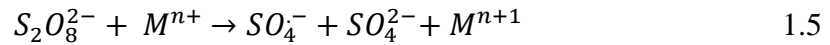
AOPs such as ozonation, UV/H<sub>2</sub>O<sub>2</sub>, peroxymonosulfate (PMS) and other homogeneous and heterogeneous photocatalysis; have received a growing interest in the inactivation of ARB and reduction of ARGs (Michael-Kordatou et al., 2018). The relatively high oxidative potentials of these oxidizing agents make AOPs attractive for the removal of recalcitrant organic matter and trace inorganic contaminants in water. In some countries (e.g., Switzerland), AOPs have been successfully used to eliminate different micropollutants e.g., hormones and personal care products (Eggen et al., 2014). According to Czekalski et al. (2016), the abatement of ARB and intracellular ARG can be achieved under conditions optimized for micropollutant removal. UV-based AOPs are oxidative disinfection processes that utilize strong oxidizing power of hydroxyl radical ( $HO\cdot$ ) and sulphate radical ( $SO_4^{\cdot-}$ ) (Deng and Zhao, 2015). AOPs inactivate bacteria by causing

oxidative stress via the reactions of cell lipids, proteins and DNA with reactive oxygen species (ROS) (Deng and Zhao, 2015, Michael-Kordatou et al., 2018). This reaction leads to the loss of protein activity, DNA damage and cell death.

$HO\cdot$  has an oxidizing potential between 2.8 V (pH 0) and 1.95 V (pH 14). It is the strongest oxidizing agent in water treatment (Deng and Zhao, 2015). The high reactivity of  $HO\cdot$  is attributed to its nonselective reactivity with numerous species.  $HO\cdot$  is produced by the dissociation of  $H_2O_2$  by UV light, the reaction of  $H_2O_2$  and  $O_3$ , and the reaction  $H_2O_2$  and  $Fe^{2+}$  (called Fenton process) (Deng and Zhao, 2015).  $HO\cdot$  inactivate bacteria by inducing oxidative stress to cellular component leading to cell death. Also, due to the high permeability of  $H_2O_2$ , it readily penetrates the cell membrane and reacts with non-protein bound ferrous iron ( $Fe^{2+}$ ) in the bacterial cell. This results in Fenton oxidation and the production of additional  $HO\cdot$  (Michael-Kordatou et al., 2018) (Equations 1.1 to 1.3). The chain reactions involved in the AOP processes make it an area of interest for the mitigation of ARB and ARGs propagation. However, it has been documented that bacterium can use active catalases and peroxidases ( $HO\cdot$  scavenging enzymes) to degrade  $H_2O_2$  and keep it below harmful concentration (Michael-Kordatou et al., 2018). Therefore, the use of appropriate  $H_2O_2$  concentration is vital to the successful control of ARB and ARGs using  $HO\cdot$  disinfection. Another concern with  $HO\cdot$  disinfection is that  $HO\cdot$  is short-lived ( $10^{-10}$  s) (Phaniendra et al., 2015) and may require longer detention time for bacterial inactivation if produced in small concentrations (Tchobanoglous et al., 1991, Deng and Zhao, 2015).



Sulphate radical is generated when peroxymonosulfate or persulfate ( $S_2O_8^{2-}$ ) is activated by heat, ultraviolet light, high pH and transition metals (Equations 1.4 to 1.5) (Zhang et al., 2015a).  $SO_4^{\cdot-}$  has an oxidation potential of 2.6 V and it is very reactive (Kolthoff and Miller, 1951, House, 1962). Also,  $SO_4^{\cdot-}$  are known to generate hydroxyl radical (Deng and Zhao, 2015) (Equations 1.6 to 1.7). Thus, the optimization of these oxidation technologies in terms of operating parameters will play a key role in coping with the spread of ARB and ARGs in the environment. However, there are limited studies regarding factors (such as exposure time, water pH, water temperature, nitrite concentration and the presence of other reducing agents) that may influence the inactivation of ARB and the removal of ARGs during the application of these processes.



#### 1.4.Tackling Antibiotic Resistance in Clinical Settings: Nano-antimicrobials

Most antibiotics kill or inhibit microorganisms by interfering with specific cellular function or metabolic pathway in microbes resulting in cell death (Aruguete et al., 2013, Jackman et al., 2016). Bacteria develop resistance to antibiotics by modifying the target site for antibiotic activity, modifying the pathway of the target synthesis, reducing the antibiotic concentration in the cell or destroying the antibiotics. Poor intracellular bioavailability of antibiotics at target sites also exacerbate the problem of antibiotic

resistance (Abed et al., 2015). Addressing antimicrobial resistance calls for the development of alternative antimicrobial agents that inhibit microorganisms via multiple mechanisms (Aruguete et al., 2013, Singh et al., 2014, Jackman et al., 2016). There is a need for antibacterial agents whose bactericidal actions do not involve specific biochemical pathway. Also, there is a great demand for broad-spectrum antibacterial agents with novel bacterial targets for which microorganisms cannot develop resistance via genetic evolution or mutation (Jackman et al., 2016).

Nanotechnology exploits the high chemical reactivity and large surface area to volume ratio of materials with sizes between 1 to 100 nm known as nanoparticles (NPs) (Mamun et al., 2021). The physico-chemical properties of the NPs such as the surface area, size, surface charge, aggregation state, hydrophobicity and chemical composition of the NP are determined by the method of synthesis and the surface coating mediums (Xu et al., 2012, Zhang et al., 2012, Yu et al., 2017, Yu et al., 2018, Anjum et al., 2019). It is reported that the size of NPs influences the surface area to volume ratio which affects the reactivity of NPs (Pareek et al., 2018, Anjum et al., 2019). The smaller the size of NPs, the greater the reactivity and adsorption capacity of NPs (Aruguete et al., 2013, Pareek et al., 2018). NPs usually exhibit unique properties that are not present in their corresponding bulk materials since matter is easily manipulated on the atomic scale (Tiwari et al., 2008, Xu et al., 2012, Singh et al., 2014). For instance, ferric oxide ( $\text{Fe}_2\text{O}_3$ ) NPs display antibacterial property which is not present in its bulk form (Singh et al., 2014). Consequently, several studies have explored the use of NPs with antimicrobial activity as alternative defense against multidrug resistant organisms (Taylor et al., 2012, Zhang et al., 2012, Aruguete et al., 2013, Singh et al., 2014, Ma et al., 2015, Sengupta et al., 2019).

#### 1.4.1. Nanoparticles in Photodynamic Therapy

Nanomaterials possess antibacterial properties that inactivate microorganisms via non-specific actions. The bactericidal activity of NPs usually involves a combination of cell membrane lysis, generation of ROS for degrading a wide range of organic compounds including DNA, RNA, and proteins (Aruguete et al., 2013). Moreover, the use of nanoscale antimicrobials allows for increased bioavailability promoting transport through the cell membrane to the target site (Gao et al., 2014, Abed et al., 2015). Thus, NPs have gained attention as alternative defense against multidrug resistance organisms.

#### 1.4.2. Nanoscale Antimicrobial Lipids Formulations

Monoglycerides and free fatty acids are antimicrobial lipids whose antimicrobial properties have been long known for several decades (Kabara et al., 1972, Kabara et al., 1977, Jackman et al., 2016). Monoglycerides and free fatty acids formulations are membrane-active antimicrobial agents that are effective against including algae, bacteria, fungi, protozoa and viruses (Kabara et al., 1972, Kabara et al., 1977, Jackman et al., 2016). The rise in AR has fostered renewed attention on antimicrobial lipids as alternative bactericidal agents to conventional antibiotics. Antimicrobial Lipids have become attractive because they are broad-spectrum antimicrobial agents with unique mechanism of action (Jackman et al., 2016). These molecules are cheap, biocompatible and have a low frequency of bacterial resistance development (Kabara, 1978, Jackman et al., 2016). Moreover, lipids contribute to the innate immune system in humans (Thorgeirsdottir et al., 2003).

## 1.5. Study Objectives

The objectives of this research work were defined broadly as follows:

- i. Assess the degradation of antibiotic resistance genes using  $HO\cdot$  and  $SO_4^-$  advanced oxidation process.
- ii. Evaluate the inactivation of antibiotic resistance bacteria using photo-activated nanoparticles.
- iii. Examine the antimicrobial and antiviral activity of monoglyceride nano-emulsions.

## 1.6. Significance of the Study

The increase in AR amongst pathogens of human and animal is a major global public health issue. Moreover, AR infections complicate treatment and recovery from other illnesses of public health concerns such as the severe acute respiratory syndrome coronavirus 2 (SARS-CoV-2) (CDC, 2019). Although the economic implications of AR cannot be accurately measured, the CDC estimated an increase in medical cost by \$4.8 billion for a subset of AR infections in 2017 (CDC, 2019). Taylor et al. (2014) estimated that, by 2050, failure to curb the AR threat will reduce the world population by 11 million (provided AR rate is kept relatively low) and 444 million (for a scenario in which no antimicrobial drug is effective). Depending on the gravity of the situation, Taylor et al. (2014) expounded that the impact of this estimated reduction on the world population will result in a decrease in the world economy by between 0.06% and 3.10%. These estimates buttress the need to combat the continued spread of AR. The onus is on all sectors linked

to this global threat to understand the development of AR in clinically relevant bacteria and mitigate the spread.

Addressing AR threats involves developing efficient methods to eliminate ARB and ARGs from the environment and reducing the development of new resistant traits by developing alternative antimicrobials with novel non-specific low-mutation bacterial target sites. The reaction kinetics study in this work provides quantitative information for deciding treatment processes for effective ARGs degradation. This study promotes an understanding of factors that influence ARGs degradation using  $HO\cdot$  and  $SO_4^{\cdot-}$  AOPs. The results from the study provide data useful for setting operating conditions in WWTPs, drinking water treatments, and reactor designs for effective ARGs removal. Furthermore, this work evaluated the potential of nanoscale antimicrobials as alternative antibacterial agents against pathogens of clinical concerns. The novelty of the photoactivated silver-NPs study is based on the combination of PS with NPs to improve the performance of PDI for clinical AR control. Also, the study explored the use of nanoscale monoglycerides as a first line of defense antimicrobials against the entrance of intracellular pathogens due to their biocompatibility and broad-spectrum antimicrobial activity.

### 1.7. Dissertation Overview

The overall goal of this study was to evaluate the role of UV-based AOPs and nanoscale antimicrobials for the mitigation of AR in environmental and clinical settings. This dissertation is presented in five chapters. Chapter 1 details the introduction to the work and research objectives. In Chapter 2, the results of the degradation of ARGs using hydroxyl radical and sulphate radical AOPs are discussed. Details of the inactivation of

antibiotic resistance bacteria using photo-activated nanoparticles can be found in Chapter 3. Chapter 4 describes the antimicrobial and antiviral activity of monoglyceride nano-emulsions. Lastly, conclusions, the summary of contributions, and recommendations for future work are included in Chapter 5. The peer-reviewed articles on the studies presented in this dissertation document is found in the List of Publications given after Chapter 5.

## CHAPTER 2. DEGRADATION OF ANTIBIOTIC RESISTANCE GENES USING HYDROXYL RADICAL AND SULPHATE RADICAL (FUNDED BY: NC WRRI)

### 2.1. Literature Review

Recent studies have focused on the use of AOPs that use strong oxidizing abilities of  $SO_4^{\cdot-}$  and  $HO^{\cdot}$  for ARB inactivation and ARG degradation (Yoon et al., 2017, Yoon et al., 2018b, Hu et al., 2019, Rodríguez-Chueca et al., 2019a, Rodríguez-Chueca et al., 2019b, Nihemaiti et al., 2020, Xiao et al., 2020, Zhou et al., 2020, Choi et al., 2021, Yoon et al., 2021, Yao et al., 2022). Relatively fewer studies have evaluated and compared the fundamental kinetic parameters of extracellular and intracellular plasmid-encoded ARGs degradation using UV-based  $SO_4^{\cdot-}$  and  $HO^{\cdot}$  AOPs (Yoon et al., 2017, Yoon et al., 2018b, Nihemaiti et al., 2020, Yoon et al., 2021). These studies reported that the reduction in the observed absolute concentration of ARGs is influenced by the length of target qPCR amplicons (Chang et al., 2017, He et al., 2019, Zhang et al., 2019, Nihemaiti et al., 2020, Choi et al., 2021, Yoon et al., 2021), amplicon nucleotide base pair (bp) composition (Zhang et al., 2015b, Yoon et al., 2017, Yoon et al., 2018b), chemical structure and morphological conformation (plasmid-borne or chromosomal ARG) (Yoon et al., 2017, Yoon et al., 2018b, He et al., 2019, Zhang et al., 2019), oxidative damage mechanism, the operating parameters (e.g. oxidant dose, contact time, water composition) (Chen and Zhang, 2013, Pak et al., 2016, Michael-Kordatou et al., 2018). However, some of these studies were carried out using complex wastewater matrices making the comparison and generalization of treatment performance for other ARGs impracticable. Fundamental reaction rate constants will help determine whether the results of different studies can be generalized for various ARGs or not. It will provide generally applicable rate constants for

predicting the fate of ARG with similar conformation, length and nucleotide composition. Also, many of the studies focused on UV/H<sub>2</sub>O<sub>2</sub> (Yoon et al., 2017, Yoon et al., 2018b, He et al., 2019). The studies did not examine the influence of pH on the optimization of these AOPs for ARGs degradation.

Very few studies have investigated the biological activities of the ARG downstream of the disinfection process (He et al., 2019, Nihemaiti et al., 2020, Choi et al., 2021, Yoon et al., 2021). Studies on the role of  $HO\cdot$  and  $SO_4^{\cdot-}$  in the propagation or mitigation of AR via HGT are scarce (Nihemaiti et al., 2020). It is noted that ARGs encoded on plasmids are principal ways for the spread of resistance genes since plasmids reproduce independently (Walsh, 2000). This study addressed the following research questions:

1. Does  $SO_4^{\cdot-}$  readily degrade ARGs than  $HO\cdot$  under typical environmental conditions?
2. What operating conditions promote HGT when using  $HO\cdot$  and  $SO_4^{\cdot-}$  AOPs?
3. Is DNA degradation (qPCR assay) a good measure of the loss of biological activities of the ARGs (transformation assay)?

## 2.2. Hypothesis and Objectives of this Chapter

It was hypothesized that  $SO_4^{\cdot-}$  AOP will outperform  $HO\cdot$  AOP as the former selectively react with contaminants in water while  $HO\cdot$  is a non-selective oxidant. This is because  $SO_4^{\cdot-}$  has a relatively higher redox potential than  $HO\cdot$  at near neutral pH - the typical pH of wastewater and drinking water from which the ARGs are to be removed. Furthermore, the redox potential of  $HO\cdot$  decreases from 2.7 V under acidic condition to 1.8 V under alkaline condition; whereas the redox potential of  $SO_4^{\cdot-}$  is between 2.5 and 3.1 V

in acidic or neutral pH (Zhang et al., 2015a). The following objectives were designed to answer the above questions:

- i. Determination of the rate of extracellular and intracellular ARGs degradation using  $HO\cdot$  and  $SO_4\cdot^-$ .
- ii. Assessment of the kinetics of extracellular ARGs degradation under typical effluent pH and various oxidant concentrations.
- iii. Identification of the operating conditions that could promote HGT during  $HO\cdot$  and  $SO_4\cdot^-$  AOPs.

### 2.3. Study Overview

This bench-scale study investigated and compared the degradation kinetics of intracellular and extracellular plasmid-encoded sulphonamide resistance gene (*sulI*), tetracycline resistance gene (*tetA*) and ampicillin resistance gene (*amp<sup>R</sup>*) hosted in *Escherichia coli* using  $UV_{254}$ ,  $UV_{254}/H_2O_2$  and  $UV_{254}/S_2O_8^{2-}$ . The experiment was carried out in phosphate-buffered solution (pH 7,  $25 \pm 2$  °C) to provide fundamental and more generally applicable kinetic parameters. The impacts of ARG nucleotide composition, nucleotide arrangements and length on the observed degradation kinetics were investigated by monitoring the degradation of two qPCR target amplicons for each ARG. Kinetic parameters were derived for the degradation of *sulI* (162 bp), *sulI* (841 bp), *tetA* (210 bp), *tetA* (1054 bp), *amp<sup>R</sup>* (192 bp), and *amp<sup>R</sup>* (851 bp). The contributions of  $HO\cdot$  and  $SO_4\cdot^-$  to the measured ARG degradation during  $UV_{254}/H_2O_2$  and  $UV_{254}/S_2O_8^{2-}$  were evaluated. Other analyses examined the effects of initial oxidant concentration and reaction pH on ARG degradation during  $UV_{254}/H_2O_2$  and  $UV_{254}/S_2O_8^{2-}$ . ARG degradation measured by

qPCR was compared with the loss of transforming activity of treated plasmids (deactivation) by culture techniques in HGT transformation experiments using chemically competent TOP10 *E. coli*. The overall schematic of the experimental setup is presented in Figure 2.1.

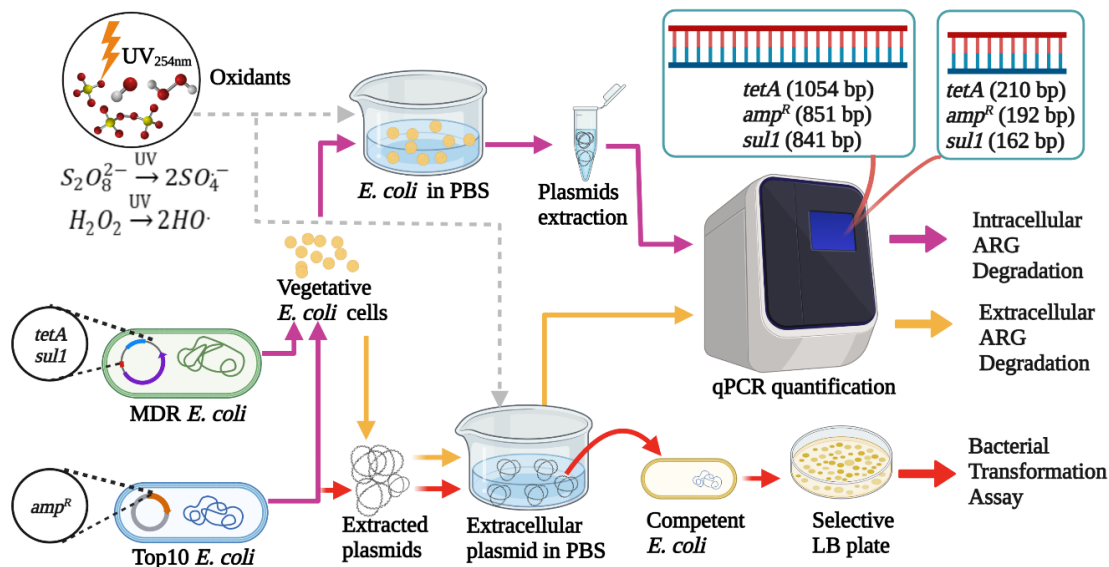


FIGURE 2. 1 Schematics of the ARG degradation experiments

## 2.4. Materials and Method

### 2.4.1. Chemical and Biological Reagents

All chemicals and biological media were of reagent grade purity and certified nuclease-free and were used without further purification. Ampicillin sodium salt, para-chlorobenzoic acid (pCBA, 99%), acetonitrile (>99.9%), hydrogen peroxide (30% w/w, H<sub>2</sub>O<sub>2</sub>), tert-Butanol (99.7%), phosphate-buffered saline solution (PBS) (10 mM) and sodium persulphate (Na<sub>2</sub>S<sub>2</sub>O<sub>8</sub>, 98%) were purchased from Sigma-Aldrich. Luria Bertani (LB) broth, LB agar (VWR Life Science), SsoAdvanced Universal SYBR Green (Biorad),

primers (IDT), SOC medium (Corning), hydrogen peroxide test kit (K-5510) and persulphate test kit (K-7870) (CHEMetrics), formic acid (>99.0%, Fisher Chemical™). Calcium chloride dihydrate (CaCl<sub>2</sub>·2H<sub>2</sub>O), glycerol, magnesium chloride hexahydrate (MgCl<sub>2</sub>·6H<sub>2</sub>O), manganese (II) chloride tetrahydrate (MnCl<sub>2</sub>·4H<sub>2</sub>O), potassium acetate (KOAc), hydrochloric acid (HCl).

#### 2.4.2. ARB Origin and Plasmids Identification

Plasmids were extracted from two *E. coli* bacteria cells: multidrug resistant (MDR) *E. coli* and TOP10 *E. coli* (Figure 2.1). The MDR *E. coli* is a wild-type *E. coli* K-12 isolated from Class B biosolids amended soil hosting a plasmid that contained *tetA* and *sulI* genes and confers resistance to tetracycline, gentamicin, ampicillin, sulfamethoxazole-trimethoprim and ciprofloxacin using the CLSI M100 Performance Standards (Mays et al., 2021). Details of the MDR *E. coli* sequence (accession number PRJNA806466) and characterization are provided in the Section 3.5.1 (Chapter 3). Gel electrophoresis of PCR amplification products using published primers for *tetA* and *sulI* conserved regions suggested the presence of these ARGs and their presence was confirmed by sequencing. The size of the plasmid was ~ 7000 bp by restriction enzyme analysis using EcoRV-HF® (NEB) (Figure 2.2).

Plasmid pCR™2.1-TOPO® (3931 bp), extracted from TOP10 *E. coli*, is a commercially available plasmid that contains *amp<sup>R</sup>*. These two plasmids were used to observe the degradation of GC-rich (*tetA* and *sulI*) and AT-rich (*amp<sup>R</sup>*) ARGs (Table 2.1).

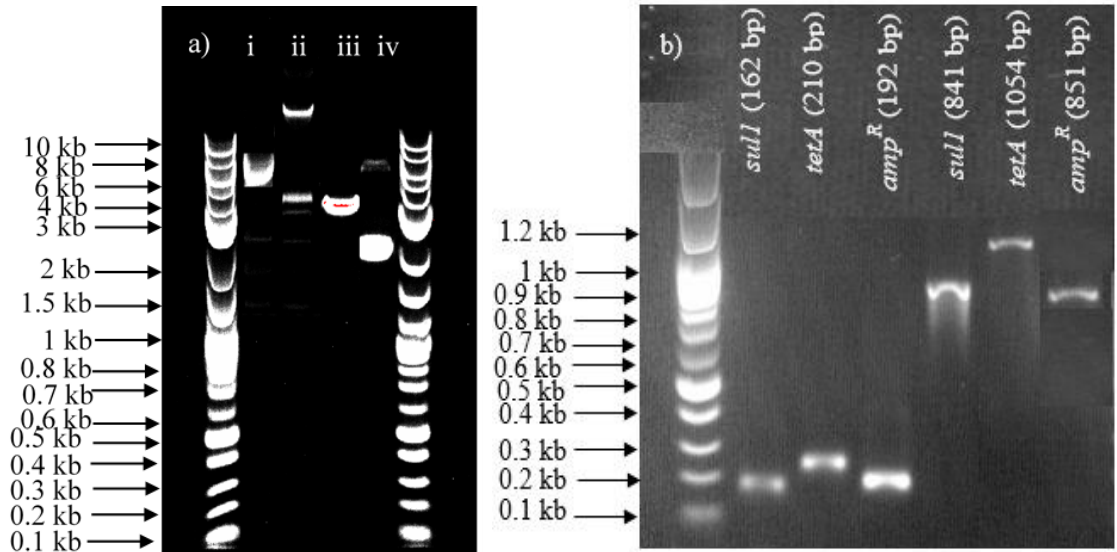


FIGURE 2. 2 a) QIAGEN-extracted plasmids and linearized plasmids i. linearized MDR *E. coli* plasmid by restriction enzyme EcoRV-HF<sup>®</sup> ii. Extracted MDR *E. coli* plasmid iii. Linearized pCR<sup>™</sup>2.1-TOPO by restriction enzyme EcoR1-HF<sup>®</sup> iv. Extracted pCR<sup>™</sup>2.1-TOPO plasmid b) qPCR amplicons of *sulI*, *tetA* and *amp<sup>R</sup>*.

#### 2.4.3. Extracellular and Intracellular Plasmid Extraction

Plasmids were extracted from two *E. coli* bacteria cells: TOP10 *E. coli* and MDR *E. coli* using QIAGEN Plasmids Maxi kit for extracellular ARGs (e-ARGs) degradation experiment and QIAprep spin miniprep kit for intracellular ARGs (i-ARGs) degradation experiment. For e-ARGs, 500 mL of TOP10 and MDR *E. coli* were cultured separately under gentle mixing at 200 rpm and 35°C for ~ 18 h in LB broth with 100 µg/mL of ampicillin (plus 50 µg/mL tetracycline 200 µg/mL sulfamethoxazole-trimethoprim for MDR *E. coli*). Cells were pelleted by centrifugation at 6000 g for 15 min at 4°C and resuspended in 10 mL Buffer P1 (containing 100 µg/mL RNase and LyseBlue reagent added at a ratio of 1 to 1000). 10 mL Buffer P2 was added to the suspension and thoroughly

mixed by inversion until homogeneous. The mixture was left at room temperature to allow cell lysis for about 5 min. Thereafter, 10 mL ice-cold Buffer P3 was added to neutralize the cell lysis step and the suspension was incubated on ice for 20 min. The suspension was centrifuged at  $> 20,000$  g for 30 min at  $4^{\circ}\text{C}$  to obtain clear lysate. The clear lysate was transferred into an equilibrated QIAGEN-tip column and allowed to drain out of the column by gravity. Flowthrough was discarded and the column was washed twice using 30 mL Buffer QC. DNA was eluted using 15 mL of pre-warmed ( $\sim 45^{\circ}\text{C}$ ) Buffer QF. Thereafter, eluted DNA was precipitated with 10.5 mL room temperature isopropanol and centrifuged at  $15,000$  g for 30 min at  $4^{\circ}\text{C}$ . The supernatant was gently decanted and precipitated DNA was washed with 5 mL of 70% ethanol. The solution was mixed and then centrifuged at  $15,000$  g for 10 min at  $4^{\circ}\text{C}$  to precipitate the plasmids. Plasmids were allowed to air-dry in a biosafety cabinet and dry DNA pellets were redissolved in 1 mL of TE buffer. The concentration of eluted plasmids ranged between 70 to  $120$  ng/ $\mu\text{L}$  measured by Qubit<sup>®</sup> 3.0 fluorometer using dsDNA HS Assay (Thermo Scientific<sup>™</sup>). The structural conformation of the extracted plasmids was mostly supercoiled as seen on gel electrophoresis (Figure 2.2a).

For i-ARGs, plasmids were extracted from 1 mL TOP10 *E. coli* or MDR *E. coli* bacterial suspension ( $\sim 1.5 \times 10^8$  CFU/mL) withdrawn at specific time intervals during  $\text{UV}_{254}$ ,  $\text{UV}_{254}/\text{H}_2\text{O}_2$  and  $\text{UV}_{254}/\text{S}_2\text{O}_8^{2-}$  treatments. Cells were pelleted by centrifugation at 7000 rpm for 5 min at  $4^{\circ}\text{C}$ . Pelleted cells were resuspended in 250  $\mu\text{L}$  of Buffer P1 (with LyseBlue reagent added at ratio of 1 to 1000) by gentle vortexing. Thereafter, 250  $\mu\text{L}$  of Buffer P2 was added and mixing was done by inversion 6 to 8 times. Cell lysis was allowed to occur by incubating the mixture for at most 5 minutes. Cell lysis was stopped by adding

350  $\mu\text{L}$  of buffer N3 followed by precipitation of cell components at 13000 rpm for 10 min. The supernatant was transferred into the QIAprep spin column and centrifuged at 13000 rpm for 1 min. Flow-through was discarded and DNA was washed using 500  $\mu\text{L}$  of Buffer PB followed by 750  $\mu\text{L}$  of Buffer PE (supplemented with ethanol). Catch-tubes were changed for every wash step to avoid carryover of wash solution or contamination. A final centrifugation step at 13000 rpm for 1 min was taken to remove residual wash solutions. Plasmid DNA was eluted using 40  $\mu\text{L}$  of Buffer EB and was stored at  $-20\text{ }^{\circ}\text{C}$  for qPCR analysis. The concentration of eluted plasmids ranged between 0.8-1 ng/  $\mu\text{L}$  using Qubit<sup>®</sup> 3.0 fluorometer. The purity of the extracted plasmids was assessed by Nanodrop<sup>™</sup> UV-Vis spectrophotometer at 260 nm.

#### 2.4.4. Extracellular and Intracellular ARG Degradation Experiment

The photochemical experiments were carried out in a collimated UV beam apparatus equipped with four low-pressure germicidal lamps (13 watt each) emitting light at 254 nm. The batch reactor was a 50 mL (40 mm  $\times$  30 mm) crystallization dish mounted on a stir plate for gentle continuous stirring by a magnetic bar while avoiding a vortex. Lamps were warmed up at least 30 min before the experiments to ensure a stable energy output. The average UV fluence was estimated using standard protocols (Bolton and Linden, 2003) (Appendix D). The average irradiance at the centre of the dish was  $\sim 1.35 \pm 0.04\text{ mW/cm}^2$  measured using a calibrated radiometer (Model ILT1400A, SEL 240/W). Extracellular plasmid-encoded ARGs (e-ARGs) and intracellular plasmid-encoded ARGs (i-ARGs) degradation experiments were carried out using 20 mL of  $\sim 2\text{ }\mu\text{g/ul}$  of plasmid

and *E. coli* cells at  $\sim 1.5 \times 10^8$  (0.5 McFarland turbidity standard), respectively, suspended in autoclaved PBS (10 mM) at pH 7.

TABLE 2. 1 Specific nucleotide compositions of the qPCR amplicons

qPCR Amplicons	Specific Nucleotide Count <sup>a</sup>					
	AT bp/amplicon	GC bp /amplicon	5'-TT- 3'/amplicon	5'-TC- 3'/amplicon	5'-CT- 3'/amplicon	5'-CC- 3'/amplicon
<i>tetA</i> (210 bp)	79 (37.6%)	131 (62.4%)	12 (5.7%)	30 (14.3%)	26 (12.4%)	37 (17.6%)
<i>tetA</i> (1054 bp)	383 (36.3%)	671 (63.7%)	81 (7.7%)	135 (12.8%)	104 (9.9%)	185 (17.6%)
<i>amp<sup>R</sup></i> (192 bp)	103 (53.6%)	89 (46.4%)	42 (21.9%)	26 (13.5%)	21 (10.9%)	22 (11.5%)
<i>amp<sup>R</sup></i> (851 bp)	431 (50.6%)	420 (49.4%)	118 (13.9%)	105 (12.3%)	104 (12.2%)	87 (10.2%)
<i>sulI</i> (162 bp)	66 (40.7%)	96 (59.3%)	22 (13.6%)	21 (13.0%)	19 (11.7%)	26 (16.0%)
<i>sulI</i> (841 bp)	323 (38.4%)	518 (61.6%)	67 (8.0%)	134 (15.9%)	94 (11.2%)	133 (15.8%)

<sup>a</sup> The values given for 5'-TT-3', 5'-TC-3', 5'-CT-3' and 5'-CC-3' represent the total bipyrimidine contents of both complementary DNA strands in a given amplicon. For instance, 5'-TT-3' is the sum of the number of 5'-TT-3' and 5'- AA-3' in one DNA strand for an amplicon region. The latter (5'- AA-3') accounts for 5'-TT-3' the second DNA strand. 5'- TT-3' and 5'-CC-3' contents in contiguous sequences such as 5'-TTT-3' or 5'-CCC-3' and 5'-TTTT-3' or 5'-CCCC-3' were counted as 2 and 3 for 5'- TT-3' or 5'-CC-3' respectively. The numbers in brackets are the relative AT bp, GC bp, 5'-GG-3', 5'-TT-3', 5'-TC-3', 5'-CT-3', and 5'-CC-3' in % of total amplicon length.

The examined UV fluences ranged from 0 to 1000 mJ/cm<sup>2</sup>. For UV<sub>254</sub>/H<sub>2</sub>O<sub>2</sub> and UV<sub>254</sub>/S<sub>2</sub>O<sub>8</sub><sup>2-</sup> systems, stock solutions of H<sub>2</sub>O<sub>2</sub> and Na<sub>2</sub>S<sub>2</sub>O<sub>8</sub> were prepared in nuclease-free Milli-Q water (18 MΩ.cm, Millipore) and used at a working concentration of 0.2 mM, confirmed by Ferric Thiocyanate method (CHEMetrics kits). The steady-state concentrations of HO· and SO<sub>4</sub><sup>·-</sup> ([HO·]<sub>ss</sub> and [SO<sub>4</sub><sup>·-</sup>]<sub>ss</sub>) were determined by dosing

samples in  $UV_{254}/H_2O_2$  and  $UV_{254}/S_2O_8^{2-}$  systems with pCBA probe to a final concentration of 10  $\mu M$ . At predefined time (corresponding to UV fluence), for e-ARGs, 500  $\mu L$  of samples were withdrawn at specific time points, and residual oxidant was quenched with excess sodium thiosulphate for DNA and probe analyses. For i-ARGs, 1 mL samples were withdrawn, residual oxidants were quenched with excess sodium thiosulphate, and plasmids were extracted using QIAprep spin miniprep kit and DNA degradation was quantified using qPCR. The contributions of  $HO\cdot$  to ARG degradation in  $UV_{254}/S_2O_8^{2-}$  system was analyzed by irradiating samples in the presence of 0.2 mM  $Na_2S_2O_8$  and 50 mM tert-Butanol (t-BuOH) at pH 7. The impact of the starting oxidants concentrations and pH on ARG degradation kinetics was investigated by varying  $H_2O_2$  and  $Na_2S_2O_8$  concentrations (0.5 – 1mM) and PBS pH (5-9) using the same plasmids and bacteria concentrations at 500  $mJ/cm^2$  as above. Control experiments using  $H_2O_2$  and  $Na_2S_2O_8$  alone were carried out to account for possible direct chemical degradation ARGs. All experiments were performed in triplicate at room temperature ( $25\pm 2^\circ C$ ).

#### 2.4.5. qPCR Standard Preparation and Limit of Detection

ARG standards used for quantification of *tetA*, *amp<sup>R</sup>* and *sull* in plasmids were prepared using PCR products following recommended procedures (Dhanasekaran et al., 2010). PCR products were obtained by amplifying DNA segments of *sull* (162 bp), *sull* (841 bp), *tetA* (210 bp), *tetA* (1054 bp), *amp<sup>R</sup>* (192 bp), and *amp<sup>R</sup>* (851 bp) using primers described in Table 2.2. The total volume of the qPCR reaction mixture was 25  $\mu L$  consisting of 0.5  $\mu L$  of each primer, 2  $\mu L$  of DNA sample, 12.5  $\mu L$  of *Taq* 2X Master Mix (NEBioLabs), and 9.5  $\mu L$  of sterile nuclease-free water. The PCR reaction cycle included

one cycle at 95 °C for 10 min, 30 cycles at 95 °C for 1 min, an annealing step at  $T_A$  (Table 2.2) for 60 s, an elongation at 72°C for 1 min and a final elongation cycle at 72°C for 10 min. The PCR products were confirmed for the presence of target amplicons by viewing on 2% agarose gel using gel electrophoresis (Figure 2.2b). PCR products were cleaned up to remove unreacted nucleotides and enzymes using the QIAquick PCR Purification kit (QIAGEN) according to the manufacturer's instructions. The resulting PCR products were quantified using Qubit<sup>®</sup> 3.0 fluorometer (3.0) based on the Qubit dsDNA HS Assay (Thermo Scientific<sup>™</sup>). qPCR standards were prepared using purified PCR products in 10-fold serial dilutions to cover a concentration range of  $10^8$  to  $10^1$  for stock standards (i.e.  $10^7$  to 1 in qPCR reaction). Standards were aliquoted in single-use volumes (5 $\mu$ L) and stored at -20 °C. Freezing and thawing of standards were avoided in all cases. Each of these standard samples was analyzed in 6 replicates. Standard curves generated for the six qPCR amplicons are given in Figure 2.3 showing the R-squared value and amplification efficiency (E).

The limit of detection (LOD) for each amplicon was determined by measuring the concentration of two-fold serially diluted samples in the lower concentration range between 1 to 32 DNA copies/reaction (He et al., 2019) in 12 replicates. The LOD is defined as the lowest ARG concentration at which 95% of the positive samples are detected (He et al., 2019). The experimental LODs for all amplicons were less than 3 copies per reaction. Hence, this study used the theoretical LOD of 3 copies per reaction for all amplicons.

TABLE 2. 2 List of primers and qPCR amplification conditions

qPCR Amplicons	Forward primer (5' – 3')	Reverse primer (5' – 3')	T <sub>A</sub> * (°C)	Reference
<i>tetA</i> (210 bp)	GCTACATCCTGCTTGCCTTC	CATAGATCGCCGTGAAG AGG	55	(Zhang et al., 2019)
<i>tetA</i> (1054 bp)	GTAATTCTGAGCACTGTCGC	CATAGATCGCCGTGAAG AGG	55	
<i>amp<sup>R</sup></i> (192 bp)	GTATTCAACATTTCCGTGTC GC	TTGGAAAACGTTCTTCGG GG	55	(Yoon et al., 2021)
<i>amp<sup>R</sup></i> (851 bp)	GTATTCAACATTTCCGTGTC GC	ATGCTTAATCAGTGAGGC ACC	55	
<i>sulI</i> (162 bp)	CGCACCGGAAACATCGCTG CAC	TGAAGTTCCGCCGCAAGG CTCG	55.9	(Pei et al., 2006)
<i>sulI</i> (841 bp)	ATGGTGACGGTGTTCCGGCAT TCTG	GCTAGGCATGATCTAACC CTCGG	60	(Briggs and Fratamico, 1999)

\* Annealing temperature

#### 2.4.6. qPCR Quantification

UV or AOP treated and untreated plasmids were examined for the concentrations of *tetA*, *amp<sup>R</sup>* and *sulI* by qPCR. Primers were designed to target long and short amplicons of each ARG to produce a total of six qPCR amplicons (Appendix A). The total volume of the qPCR reaction mixture was 20 µL consisting of 0.5 µL of each primer, 2 µL of DNA sample, 10 µL of SYBR green, and 7 µL of sterile nuclease-free water. The qPCR reaction cycle included one cycle at 95 °C for 2 min, 30 cycles at 95 °C for 5 s, an annealing step at T<sub>A</sub> (Table 2.2) for 1 min, and an elongation at 72 °C for 30 s, followed by a melt curve analysis from 65 °C to 95 °C. Each sample was analyzed in triplicate independent experiments.

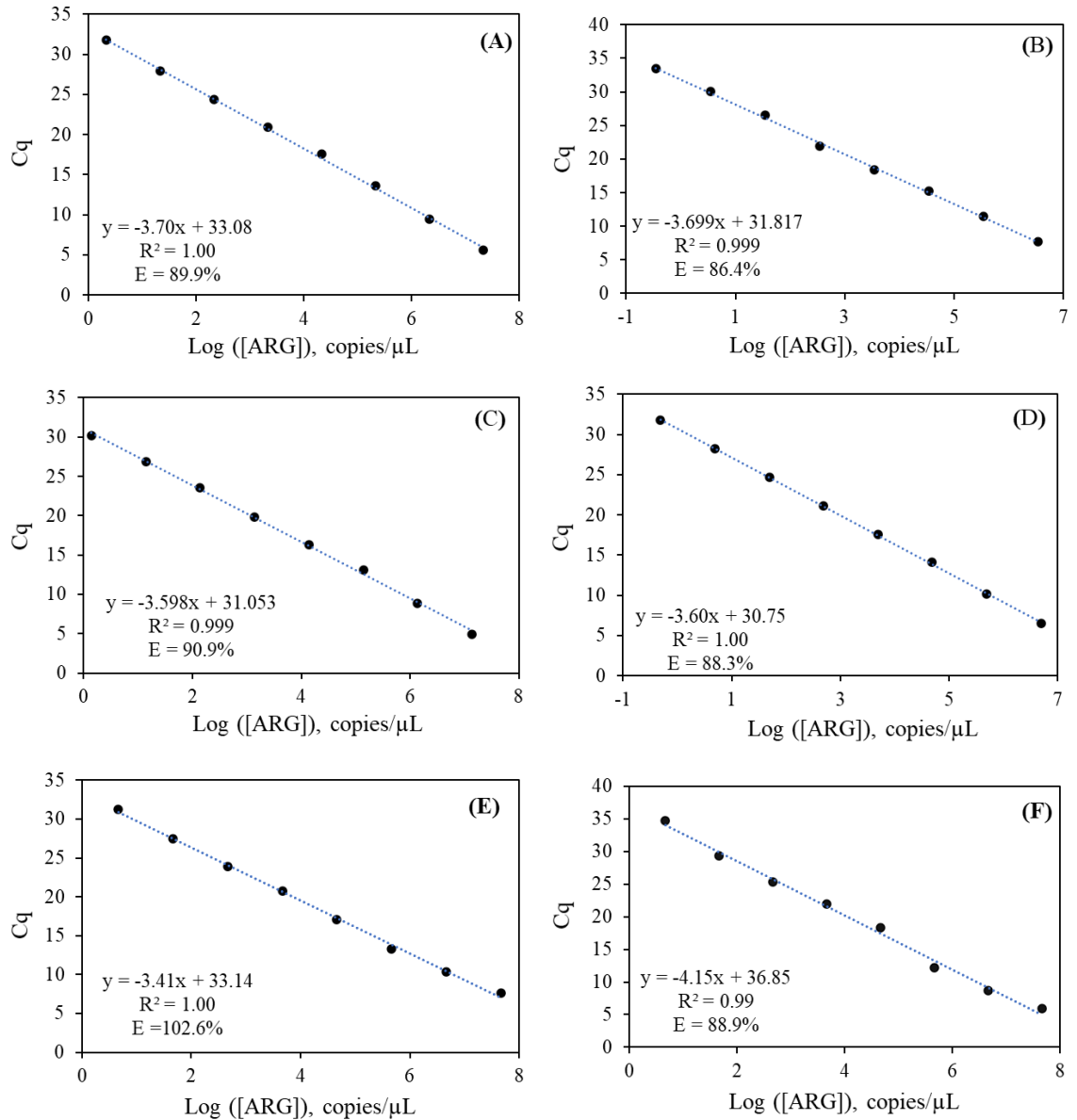


FIGURE 2. 3 Standard curves for ARG amplicons. (A) *sulI* (162 bp), (B) *sulI* (841 bp), (C) *tetA* (210 bp), (D) *tetA* (1054 bp), (E) *amp<sup>R</sup>* (192 bp), and (F) *amp<sup>R</sup>* (851 bp). Standard curves were prepared by 10-fold serial dilutions of concentrated extracellular plasmids (for *amp<sup>R</sup>*) or PCR amplicons (for *sulI* and *tetA*) ( $\sim 10^8$  copies/μL).

#### 2.4.7. Radical Probe Quantification

pCBA was used as  $HO\cdot$  and  $SO_4\cdot^-$  probe to quantify the steady-state concentrations of radicals. The second-order rate constants of  $HO\cdot$  and  $SO_4\cdot^-$  with pCBA are  $k_{HO\cdot,pCBA} = 5.0 \times 10^9 M^{-1}s^{-1}$  and  $k_{SO_4\cdot^-,pCBA} = 3.6 \times 10^8 M^{-1}s^{-1}$  respectively (Ahn et al., 2017). Here, 200 mL of the sample withdrawn at predefined time intervals (corresponding to specific UV fluences) were quenched immediately with sodium thiosulphate and used to quantify pCBA degradation using HPLC (Agilent 1100 Series - UV–diode array detector). The HPLC was fitted with a ZORBAX Eclipse Plus C8 column (4.6 x 50 mm, 5.0  $\mu$ m, Agilent). The column temperature was maintained at 30°C. The mobile phase consisted of 65:35% v/v of 0.1% formic:acetonitrile at a flow rate of 1 mL/min and an injection volume was 40  $\mu$ L. The retention time was 2.1 min based on the absorption at 234 nm.

#### 2.4.8. Preparation of Chemically Competent TOP10 *E. coli* Cells

Competent cells were prepared using detergent-free sterile glassware in a biosafety cabinet using CCMB80 buffer. CCMB80 buffer was prepared by combining 10 mM KOAc (pH 7.0), 80 mM  $CaCl_2 \cdot 2H_2O$ , 20 mM  $MnCl_2 \cdot 4H_2O$ , 10 mM  $MgCl_2 \cdot 6H_2O$  and 10% glycerol (Hanahan et al., 1991). The pH of the solution was adjusted to 6.4 using HCl. The solution was sterile filtered and stored at 4°C. Sterile LB broth (250 ml) was inoculated with 1 mL overnight TOP10 *E. coli* cell culture and grown at  $20 \pm 3$  °C to an optical density (OD 600nm) of 0.3. The cells were harvested by centrifugation at 3000g and 4°C for 10 minutes in 50 mL centrifuge tubes. The supernatant was discarded, pelleted cells were resuspended in 80 mL ice-cold CCMB80 buffer and incubated on ice for 20 minutes. Thereafter, the cells were pelleted by centrifugation at 3000g and 4°C, the supernatant was

decanted, and cells were resuspended in 10 ml of ice-cold CCMB80 buffer. The OD of the cell suspension was measured and adjusted to yield a final OD of 1.0 using chilled CCMB80. The suspension was incubated on ice for 20 min to obtain the chemically competent TOP10 *E. coli* cells used for the bacterial transformation experiment. Subsequently, 50  $\mu\text{L}$  of chemically competent cells were aliquoted into 2 mL cryogenic tubes and stored at  $-80^{\circ}\text{C}$  for later use. The concentration of recipient cells was  $\sim 1 \times 10^8$  CFU/mL as measured by culturing on nonselective agar plates (without ampicillin). The transformation efficiency of the competent cells was determined using pUC19. Competent cells were incubated with 1  $\mu\text{L}$  of 10  $\text{pg}/\mu\text{L}$  for 30 minutes, subjected to heat shock at  $42^{\circ}\text{C}$  for 30 s and incubated with 200  $\mu\text{L}$  of SOC medium at  $37^{\circ}\text{C}$  for 1 hr under continuous gentle mixing at 200 rpm. Thereafter, cells were serially diluted with PBS and grown on ampicillin supplemented LB agar plates (100  $\mu\text{g}/\text{mL}$ ) overnight. The transforming efficiency of the competent cells using pUC19 was obtained as  $\sim 1 \times 10^9$  CFU/ $\mu\text{g}$  based on Equation 2.1. This value is in agreement with the transforming efficiency of the commercially available chemically competent One Shot<sup>®</sup> competent cell (Invitrogen) using pUC19. The transforming efficiency TOP10 *E. coli* using 20  $\mu\text{L}$  of  $\sim 2$   $\text{ng}/\mu\text{L}$  pCR<sup>™</sup>2.1-TOPO was between  $10^7$  - $10^8$ .

$$\text{transforming efficiency} = \frac{\text{number of colonies on selective plate (CFU)}}{\text{Volume plated } (\mu\text{L}) \times \text{dilution factor} \times \text{plasmid concentration (ng}/\mu\text{L})} \quad (2.1)$$

#### 2.4.9. Bacterial Transformation Assay

The biological activity of the treated plasmids (pCR<sup>™</sup>2.1-TOPO) was examined by checking their transforming activity using chemically competent TOP10 *E. coli* cells. Chemically competent TOP10 *E. coli* cells, prepared using CCMB80 buffer (Hanahan et

al., 1991), were used as the recipient cells. The concentration of recipient cells was  $\sim 1 \times 10^8$  CFU/mL as measured by culturing on nonselective agar plates (without ampicillin). The bacterial transformation assay was carried out by mixing 20  $\mu$ L of treated DNA samples (1 ng/ $\mu$ L) with 50  $\mu$ L of competent TOP10 *E. coli* cells. The mixed samples were incubated on ice for 30 minutes and subjected to heat shock at 42°C for 30 s. Thereafter, 900  $\mu$ L of SOC medium was added to each sample and incubated horizontally at 35 °C for 1 hr. Subsequently, 100  $\mu$ L was serially diluted and grown on ampicillin supplemented LB agar plates (100  $\mu$ g/mL) to determine the transforming activity of the treated AR plasmids. Transforming activity was determined by comparing the number of transformants of treated plasmids to untreated plasmids (Equation 2.2). Control experiments were conducted by directly plating the recipient cells without heat shock on non-selective agar plates.

$$\text{Loss of transforming activity} = \log \frac{C_o}{C_t} \quad (2.2)$$

where  $C_o$  is the concentration (CFU/mL) of competent TOP10 cell on selective LB agar plate with untreated pCR™2.1-TOPO plasmid and  $C_t$  is the bacterial concentration on selective LB agar plate with UV<sub>254</sub>, UV<sub>254</sub>/H<sub>2</sub>O<sub>2</sub> and UV<sub>254</sub>/S<sub>2</sub>O<sub>8</sub><sup>2-</sup>-treated pCR™2.1-TOPO plasmids at time  $t$ .

#### 2.4.10. Gel Electrophoresis Analysis

Gel electrophoresis was used to examine conformational changes in plasmids (pCR™2.1-TOPO as a model plasmid) after treatment with UV<sub>254</sub>, UV<sub>254</sub>/H<sub>2</sub>O<sub>2</sub> and UV<sub>254</sub>/S<sub>2</sub>O<sub>8</sub><sup>2-</sup> at different UV fluence and 0.2 mM oxidants concentration. pCR™2.1-TOPO ( $\sim 3$  ng/ $\mu$ L) was linearized using the restriction enzyme EcoR1-HF® (NEB) following the manufacturer's instruction. Plasmids were incubated at 37°C with enzymes

for 15 min and enzymes were inactivated at 65°C for 20 min. The linear plasmid was used as a reference for comparison with treated and untreated supercoiled pCR™2.1-TOPO. Treated plasmids, untreated plasmids, linearized plasmids and 1 kb Plus DNA molecular ladder (NEB) were loaded onto 1% (in 1X TAE) agarose gel stained with GelRed (Biotium). DNA was separated in a mini sub-cell at 60 V for 1 hr (BIO-RAD). DNA bands were viewed under UV Transilluminator (Gel Doc EZ, BIO-RAD).

#### 2.4.11. Data and Statistical Analysis

Microsoft Excel was used to generate graphs, perform linear regressions, and statistical significance by one-way analysis of variance (ANOVA) between treatment trials (except otherwise mentioned). Data from independent replicate experiments were pooled to perform linear regression to obtain the (pseudo)first-order kinetic parameters. The null hypothesis that ARG degradation/deactivation was not different between different treatments was rejected at  $P < 0.05$  (95% confidence level).

## 2.5. Results and Discussion

In the environment, ARGs are present in free form (e-ARG) or enclosed within dead bacteria cells (i-ARG). The degradation of e-ARG and i-ARG namely *sulI*, *tetA* and *amp<sup>R</sup>* were examined in this study. *sulI* and *tetA* are ARGs encoded on a plasmid hosted by a MDR *E. coli* while *amp<sup>R</sup>* gene is carried on plasmid pCR™2.1-TOPO® hosted by a TOP10 *E. coli*. ARG degradation kinetics were obtained by measuring the decrease in the concentrations of 6 qPCR target amplicons: *sulI* (162 bp), *sulI* (841 bp), *tetA* (210 bp), *tetA* (1054 bp), *amp<sup>R</sup>* (192 bp), and *amp<sup>R</sup>* (851 bp) after the exposure of plasmids (e-ARG)

and plasmids carrying *E. coli* cells (i-ARG) in PBS (10 mM, pH 7) to UV<sub>254</sub> only, a combination of UV<sub>254</sub> with 0.2 mM H<sub>2</sub>O<sub>2</sub>, and a combination UV<sub>254</sub> with 0.2 mM S<sub>2</sub>O<sub>8</sub><sup>2-</sup> at different fluence.

TABLE 2. 3 First order kinetic degradation rate constants during UV<sub>254</sub>, UV<sub>254</sub>/H<sub>2</sub>O<sub>2</sub> and UV<sub>254</sub>/S<sub>2</sub>O<sub>8</sub><sup>2-</sup> treatment of extracellular plasmid-encoded ARGs

<i>ARG</i>	Amplicon length	$k_{UV_{254}}$ (cm <sup>2</sup> /mJ)	$k'_{UV_{254}/H_2O_2}$ (cm <sup>2</sup> /mJ)	$k'_{UV_{254}/S_2O_8^{2-}}$ (cm <sup>2</sup> /mJ)
<i>tetA</i>	210 bp	4.65(±0.16) x10 <sup>-3</sup> (r <sup>2</sup> =0.99)	4.88(±0.12) x10 <sup>-3</sup> (r <sup>2</sup> =1.00)	4.54(±0.62) x10 <sup>-3</sup> (r <sup>2</sup> =0.90)
	1054 bp	2.65(±0.23) x10 <sup>-2</sup> (r <sup>2</sup> =0.97)	2.67(±0.21) x10 <sup>-2</sup> (r <sup>2</sup> =0.98)	2.65(±0.44) x10 <sup>-2</sup> (r <sup>2</sup> =0.95)
<i>sull</i>	162 bp	5.41(±0.41) x10 <sup>-3</sup> (r <sup>2</sup> =0.97)	5.57(±0.99) x10 <sup>-3</sup> (r <sup>2</sup> =0.97)	5.62(±0.16) x10 <sup>-3</sup> (r <sup>2</sup> =0.84)
	841 bp	4.08(±0.58) x10 <sup>-2</sup> (r <sup>2</sup> =0.94)	3.92(±0.53) x10 <sup>-2</sup> (r <sup>2</sup> =0.95)	3.71(±0.62) x10 <sup>-2</sup> (r <sup>2</sup> =0.95)
<i>amp<sup>R</sup></i>	192 bp	9.14(±0.53) x10 <sup>-3</sup> (r <sup>2</sup> =0.98)	1.47(±0.07) x10 <sup>-2</sup> (r <sup>2</sup> =0.99)	2.35(±0.32) x10 <sup>-2</sup> (r <sup>2</sup> =0.93)
	851 bp	5.73(±0.64) x10 <sup>-2</sup> (r <sup>2</sup> =0.96)	7.16(±0.67) x10 <sup>-2</sup> (r <sup>2</sup> =0.97)	9.95(±0.21) x10 <sup>-2</sup> (r <sup>2</sup> =1.00)

### 2.5.1. Extracellular ARG Degradation during UV<sub>254</sub>, UV<sub>254</sub>/H<sub>2</sub>O<sub>2</sub> and UV<sub>254</sub>/S<sub>2</sub>O<sub>8</sub><sup>2-</sup>

The degradation of extracellular *tetA*, *amp<sup>R</sup>* and *sull* by UV<sub>254</sub>, UV<sub>254</sub>/H<sub>2</sub>O<sub>2</sub> and UV<sub>254</sub>/S<sub>2</sub>O<sub>8</sub><sup>2-</sup> is presented in Figure 2.4. Figure 2.4a gives the log reduction in ARG amplicons upon exposure to UV<sub>254</sub>. The logarithmic concentration of ARGs decreased as UV fluence increased from 0 to 1000 mJ/cm<sup>2</sup>. The observed damage to DNA was slower for short qPCR amplicons i.e., *tetA* (210 bp), *amp<sup>R</sup>* (192 bp) and *sull* (162 bp) than for long qPCR amplicons i.e., *tetA* (1054 bp), *amp<sup>R</sup>* (851 bp) and *sull* (841 bp) under the same treatment conditions. For the long qPCR amplicons, significant DNA damage (~4 logs) was recorded between 200 – 400 mJ/cm<sup>2</sup>. However, only *amp<sup>R</sup>* (192 bp) achieved 4 logs

degradation at ~1000 mJ/cm<sup>2</sup> UV fluence while lower DNA damages (~2.1 and 2.5 logs) were obtained for *tetA* (210 bp) and *sull* (162 bp). The pattern of slower/lower ARG degradation using short qPCR amplicon is consistent with reports in literature (He et al., 2019, Zhang et al., 2019, Nihemaiti et al., 2020, Choi et al., 2021, Yoon et al., 2021). One explanation for this observation is that an increase in the number of nucleotide bp per amplicon means a proportional increase in potential reaction sites (Nihemaiti et al., 2020). Thus, an increase in the probability of damaged nucleotide sites that prevents qPCR amplification process (He et al., 2019). Regardless of the qPCR amplicon in this study, the maximum ARG reduction was only 2.1 log at typical UV fluence (between 40 – 100 mJ/cm<sup>2</sup>) for water disinfection (Yoon et al., 2017, Michael-Kordatou et al., 2018). The first-order rate constant for ARGs degradation by UV ( $k_{UV_{254}}$ ) is presented in Table 2.3.  $k_{uv}$  for all amplicons were obtained as the slope of the plot following linear regression ( $k_{UV_{254}} = 2.303 \times \text{slope}$ ) (Appendix B).  $k_{UV_{254}}$  was in the range of  $4.65 \times 10^{-3} - 5.73 \times 10^{-2} \text{ cm}^2/\text{mJ}$  with the highest value for *amp<sup>R</sup>* (851 bp) and lowest value for *tetA* (210 bp).  $k_{UV_{254}}$  are comparable with previous studies, however, values were slightly higher than recorded here for *amp<sup>R</sup>* ( $2.4 \times 10^{-2} - 8.2 \times 10^{-2} \text{ cm}^2/\text{mJ}$ ) and *tetA* ( $4.0 \times 10^{-3} - 5.8 \times 10^{-2} \text{ cm}^2/\text{mJ}$ ) (Chang et al., 2017, Yoon et al., 2018b, Nihemaiti et al., 2020). Sources of variations could be differences in experimental conditions such as initial plasmid concentration (0.3 vs 1 ng/μL) and PBS concentration (2 mM vs 10 mM).

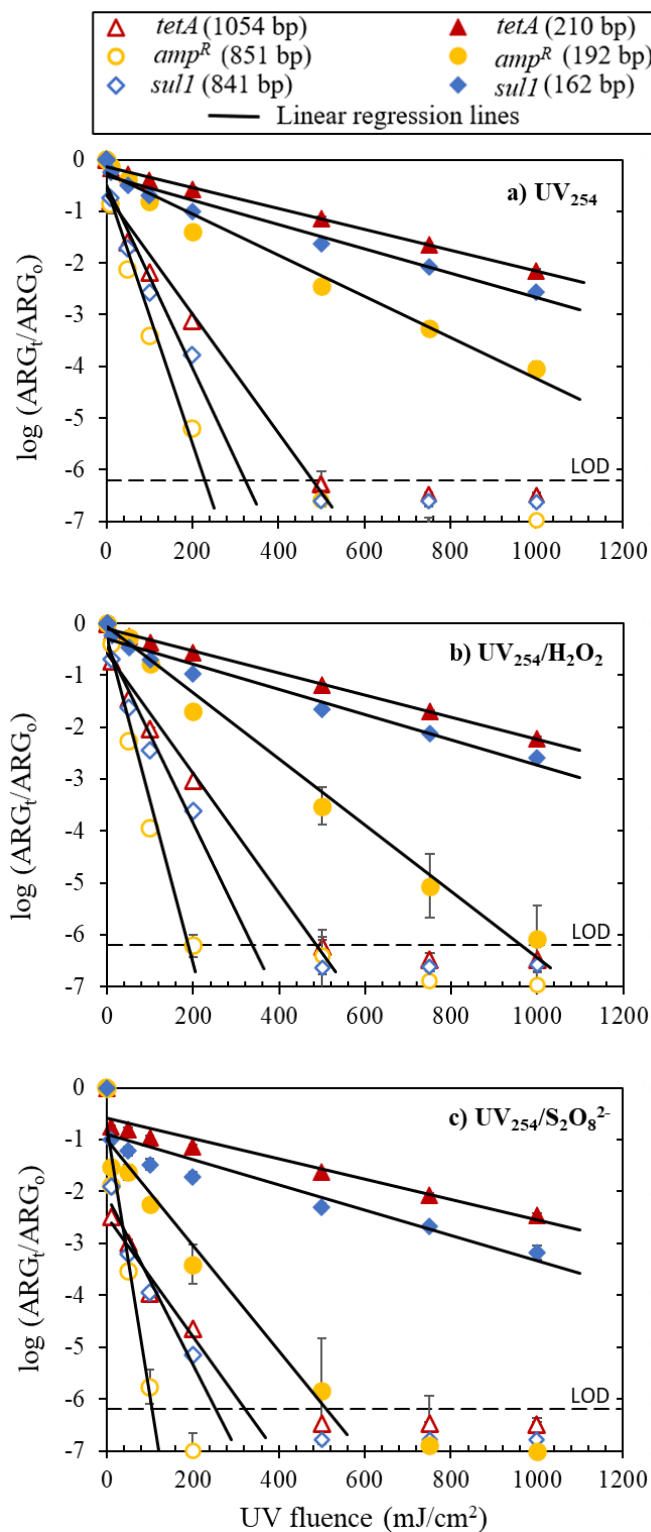


FIGURE 2. 4 Degradation of e-ARGs in PBS (pH 7, 10 mM) during  $\text{UV}_{254}$ ,  $\text{UV}_{254}/\text{H}_2\text{O}_2$  and  $\text{UV}_{254}/\text{S}_2\text{O}_8^{2-}$ . The concentrations of  $\text{H}_2\text{O}_2$  and  $\text{S}_2\text{O}_8^{2-}$  were 0.2 mM for  $\text{UV}_{254}/\text{H}_2\text{O}_2$

and  $UV_{254}/S_2O_8^{2-}$ . Concentration of plasmids is  $\sim 2\text{ng}/\mu\text{L}$ . The error bars are the standard error of mean (SEM) of independent triplicate experiments. The LOD is 3 copies/reaction.

The log reduction of *tetA*, *amp<sup>R</sup>* and *sulI* amplicons by  $UV_{254}/H_2O_2$  also followed the first-order kinetics with respect to UV fluence ( $r^2 \geq 0.95$ ) (Figure 2.4b). As observed with  $UV_{254}$ , higher ARG degradation were recorded for long qPCR amplicons (i.e., *tetA* (210 bp), *amp<sup>R</sup>* (192 bp), *sulI* (162 bp)) than for short qPCR amplicons (i.e., *tetA* (210 bp), *amp<sup>R</sup>* (192 bp), *sulI* (162 bp)). Again, *amp<sup>R</sup>* was the most susceptible to degradation and *tetA* had the lowest degradation for both the short and long amplicon. The pseudo first-order kinetic constants ( $k'_{UV_{254}/H_2O_2} = 2.303 \times \text{slope}$ ) of the amplicons were in the range of  $4.88 \times 10^{-3} - 7.16 \times 10^{-2} \text{ cm}^2/\text{mJ}$  (Table 2.3) which are larger than  $k_{UV_{254}}$  by only a factor of  $\sim 1.2$  (i.e.  $k'_{UV_{254}/H_2O_2}/k_{UV_{254}}$ ). This suggests that  $HO\cdot$  did not contribute significantly to the overall ARG degradation during  $UV_{254}/H_2O_2$  treatment in this study. It is necessary to mention that a relatively low concentration of  $H_2O_2$  (0.2 mM) was used here. A minimum of 10 mg/L (0.3 mM)  $H_2O_2$  is typical for a noticeable yield of  $HO\cdot$  due to the low molar extinction coefficient of  $H_2O_2$  during  $UV_{254}/H_2O_2$  (Liu et al., 2015, Lee et al., 2016, Yoon et al., 2017). Studies that used higher concentration of  $H_2O_2$  ( $\geq 0.3$  mM) have reported greater role of  $HO\cdot$  (about 75%) to DNA degradation during  $UV_{254}/H_2O_2$  (Yoon et al., 2017, He et al., 2019, Nihemaiti et al., 2020).

Figure 2.4c shows the decrease in the logarithmic concentration of *tetA*, *amp<sup>R</sup>* and *sulI* amplicons with increasing UV fluence during  $UV_{254}/S_2O_8^{2-}$  exposure. *amp<sup>R</sup>* amplicons degradation was faster than other ARGs with *amp<sup>R</sup>* (192 bp) attaining  $\sim 6$  log reduction at  $500 \text{ mJ}/\text{cm}^2$ . All qPCR amplicons achieved up to 4 log reductions at  $1000 \text{ mJ}/\text{cm}^2$ . Between 1-2 logs reduction in qPCR amplicon was observed from exposure of plasmids to 0.2 mM

$S_2O_8^{2-}$  only for exposure durations that corresponded to UV fluence used in the study (Figure 2.5). However, no DNA damage was recorded after exposure of plasmids to 0.2 mM  $H_2O_2$  for the same contact time. This is consistent with the higher oxidation potential of  $S_2O_8^{2-}$  than  $H_2O_2$  (2v vs 1.77v) (Memming, 1969). The degradation rate constants of the qPCR amplicons ( $k'_{UV_{254}/S_2O_8^{2-}} = 2.303 \times \text{slope}$ ) were in the range of  $4.54 \times 10^{-3} - 9.95 \times 10^{-2} \text{ cm}^2/\text{mJ}$  (Table 1).  $k'_{UV_{254}/S_2O_8^{2-}}$  was 1.4 times larger than  $k_{UV_{254}}$  ( $k_{UV_{254}}/k'_{UV_{254}/S_2O_8^{2-}}$ ). Under the same conditions evaluated here,  $UV_{254}/S_2O_8^{2-}$  resulted in higher overall ARG degradation than  $UV_{254}/H_2O_2$ .

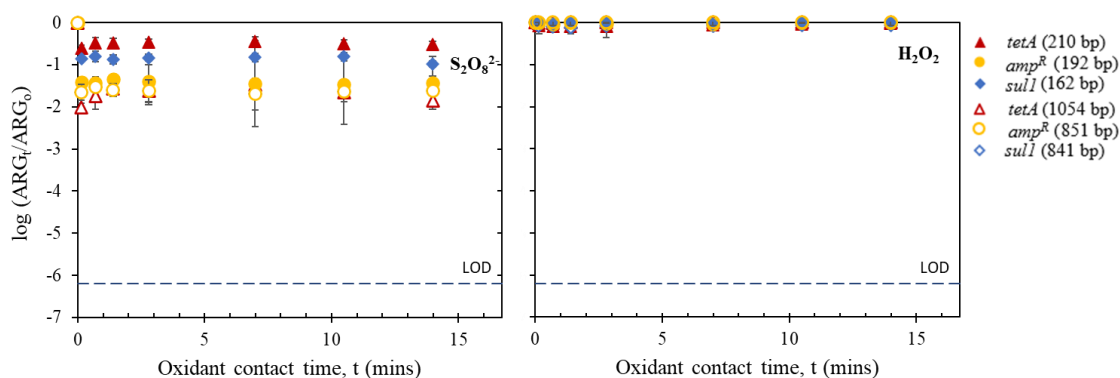


FIGURE 2. 5 Degradation of extracellular ARG *E. coli* plasmids by 0.2mM  $H_2O_2$  and  $S_2O_8^{2-}$  oxidants.

### 2.5.2. The Roles of $HO\cdot$ and $SO_4^{\cdot-}$ in ARGs Degradation during $UV_{254}/H_2O_2$ and $UV_{254}/S_2O_8^{2-}$

To understand the relative reactivities of the qPCR amplicons with  $HO\cdot$  and  $SO_4^{\cdot-}$ , the second order degradation rate constants for *tetA*, *amp<sup>R</sup>* and *sulI* were obtained in a competitive kinetic study using pCBA as radical probe compound (Table 2.5). pCBA was resistant to direct degradation by  $S_2O_8^{2-}$  and  $H_2O_2$  alone at 0.2mM but susceptible to

degradation by  $UV_{254}$ ,  $UV_{254}/H_2O_2$  and  $UV_{254}/S_2O_8^{2-}$  (Figure 2.6).  $HO\cdot$  is the only radical generated in  $UV_{254}/H_2O_2$  system. Control experiment showed that no direct chemical degradation of ARG occurred at 0.2 mM  $H_2O_2$  (Figure 2.5). Therefore, ARG damage in the  $UV_{254}/H_2O_2$  system resulted from direct  $UV_{254}$  photolysis and free  $HO\cdot$  attack. The  $[HO\cdot]_{ss}$  was estimated as  $1.06 \times 10^{-13}M$  (Table 2.4). In the  $UV_{254}/S_2O_8^{2-}$  system,  $SO_4\cdot^-$  is the primary radical generated from the direct photolysis of  $S_2O_8^{2-}$ . Additionally,  $SO_4\cdot^-$  can react with  $H_2O$  and  $OH^-$  to produce  $HO\cdot$  (Equations B21 and B22 in Appendix B).

TABLE 2. 4: Degradation kinetics of pCBA and steady-state concentrations of  $HO\cdot$  and  $SO_4\cdot^-$

Kinetic parameters	From linear regression		
	$(s^{-1})$	$cm^2/mJ$	$r^2$
$k_{pCBA UV}$	$3.23(\pm 0.04) \times 10^{-4}$	$2.75(\pm 0.03) \times 10^{-4}$	1
$k'_{pCBA UV/H_2O_2}$	$8.52(\pm 0.06) \times 10^{-4}$	$7.08(\pm 0.05) \times 10^{-4}$	1
$k'_{pCBA UV/S_2O_8^{2-}}$	$3.54(\pm 0.02) \times 10^{-4}$	$3.01(\pm 0.02) \times 10^{-4}$	1
$k'_{pCBA H_2O_2}$	0	0	-
$k'_{pCBA S_2O_8^{2-}}$	0	0	-
Calculated			
	$(s^{-1})$	$cm^2/mJ$	Eq. no
$k'_{pCBA HO\cdot}$	$5.29(\pm 0.02) \times 10^{-4}$	$4.33(\pm 0.02) \times 10^{-4}$	B14
$k'_{pCBA SO_4\cdot^-}$	$3.11(\pm 0.20) \times 10^{-5}$	$2.60(\pm 0.10) \times 10^{-5}$	B34
$[HO\cdot]_{ss}$ (M)	$1.06(\pm 0.00) \times 10^{-13}$		B17
$[SO_4\cdot^-]_{ss}$ (M)	$8.64(\pm 0.56) \times 10^{-14}$		B38

The contributions of  $HO\cdot$  to ARG degradation in the  $UV_{254}/S_2O_8^{2-}$  system at pH 7 was examined in a radical scavenging experiment using t-BuOH (Figure 2.7). Figure 2.7 shows that the contributions of  $HO\cdot$  to the degradation of ARG was insignificant in the

UV<sub>254</sub>/S<sub>2</sub>O<sub>8</sub><sup>2-</sup> system. Thus, the degradation of ARG observed in the UV<sub>254</sub>/S<sub>2</sub>O<sub>8</sub><sup>2-</sup> system was a result of direct photolysis, direct chemical oxidation by S<sub>2</sub>O<sub>8</sub><sup>2-</sup> and oxidation by free SO<sub>4</sub><sup>·-</sup>. The higher ARG degradation observed in the UV/S<sub>2</sub>O<sub>8</sub><sup>2-</sup> system did not necessarily mean a larger amount of SO<sub>4</sub><sup>·-</sup> was generated in the system ([SO<sub>4</sub><sup>·-</sup>]<sub>SS</sub> = 8.64 × 10<sup>-14</sup>M). The base pair specific kinetic constants with respect to HO<sup>·</sup> and SO<sub>4</sub><sup>·-</sup> were between 1.86×10<sup>9</sup>-1.65×10<sup>11</sup> M<sup>-1</sup>s<sup>-1</sup> and 2.87×10<sup>9</sup>-5.84×10<sup>11</sup> M<sup>-1</sup>s<sup>-1</sup> respectively (Table 2.5). SO<sub>4</sub><sup>·-</sup> is a known selective oxidant that is highly reactive towards conjugated electron-rich sites of nucleotides. HO<sup>·</sup> is also a highly non-selective radical that causes oxidation via addition of hydroxyl group or hydrogen abstraction. As expected, the reactivity of HO<sup>·</sup> and SO<sub>4</sub><sup>·-</sup> towards each amplicon occurred at a diffusion-controlled rate (von Sonntag, 2006, Nihemaiti et al., 2020).

### 2.5.3. Analysis of Amplicon Length and Nucleotide Contents on ARG Degradation Rate

The rate constants of the six qPCR amplicons were compared to the nucleotide contents of each amplicon to examine whether the dependences of first-order rate constants (*k*) on the amplicon lengths and nucleotide contents have a consistent predictable pattern (Figures 2.8 and 2.9). This was done using a single-variable regression analysis between *k* values and DNA sequence elements (Appendix C) (He et al., 2019). Specific nucleotide contents in terms of AT and GC composition for *tetA*, *sull* and *amp<sup>R</sup>* amplicons are given in Table 2.1. Generally, longer amplicons resulted in larger *k* (Table 2.3). However, *k* (cm<sup>2</sup>/mJ) for all treatments showed weak relationships with amplicon length (i.e., AT+GC bps) 0.34 ≤ *r*<sup>2</sup> ≤ 0.67 (Figure 2.8). Whereas *k*<sub>UV<sub>254</sub></sub> values had a stronger correlation with the number of interstrand AT bps *r*<sup>2</sup>= 0.85 than *k*'<sub>UV<sub>254</sub>/H<sub>2</sub>O<sub>2</sub></sub> and *k*'<sub>UV<sub>254</sub>/S<sub>2</sub>O<sub>8</sub><sup>2-</sup></sub>. This

suggests that other specific nucleotide element such as isolated singlets (A, T, G, C), doublets (AA, TT, CC, GG), triplets (AAA, TTT, CCC, GGG) etc. or a combination of these, influenced the relative reactivities of the qPCR amplicon to the treatments and not simply the numbers of ATs and GCs (Fukuzumi et al., 2005, He et al., 2019). Also, the role of the number of intrastrand bipyrimidine (TT, TC, CT and CC) sites within each qPCR amplicon on the observed degradation kinetics ( $k$ ) was examined.

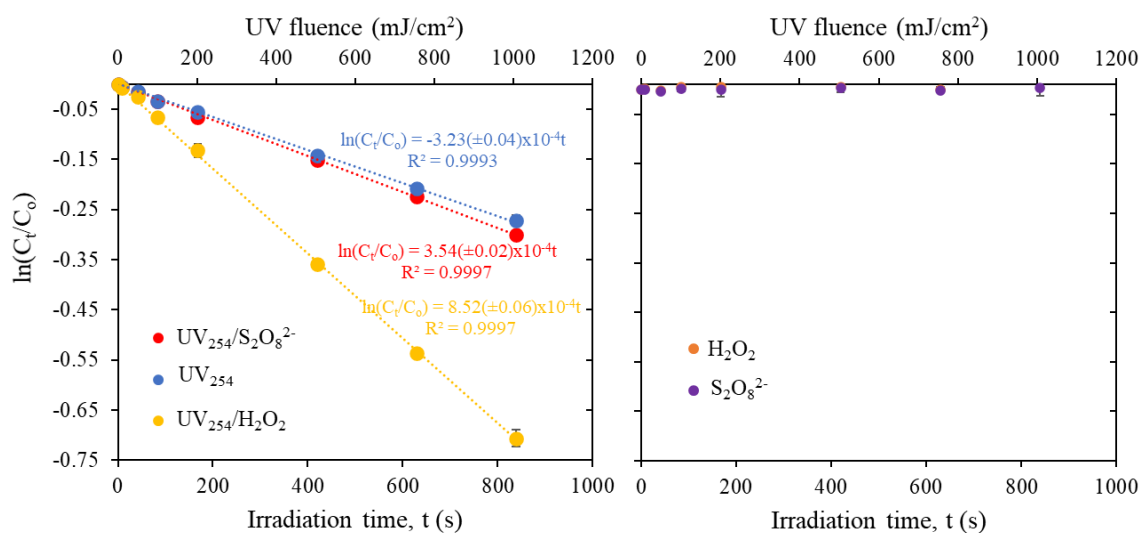


FIGURE 2. 6 Degradation of pCBA during the treatment of extracellular AR plasmids with  $\text{UV}_{254}$ ,  $\text{UV}_{254}/\text{H}_2\text{O}_2$  and  $\text{UV}_{254}/\text{S}_2\text{O}_8^{2-}$ .

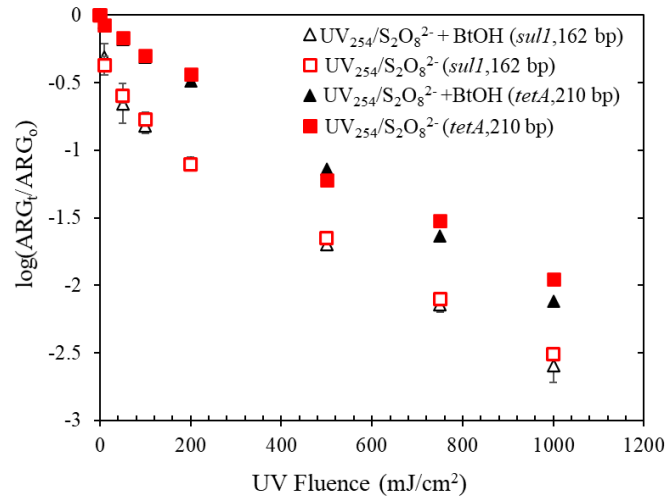


FIGURE 2. 7 Degradation of extracellular *tetA* and *sull* during  $UV_{254}/S_2O_4^{2-}$  with and without  $HO\cdot$  scavenger (BtOH represents tert-Butanol) at pH 7.

TABLE 2. 5 Estimated first-order and second order degradation rate constants of ARGs due to only  $HO\cdot$  and  $SO_4^{\cdot-}$

ARG	Amplicon length	$(cm^2/mJ)$		$(M^{-1}s^{-1})$	
		$k'_{HO\cdot}$ <sup>a</sup>	$k'_{SO_4^{\cdot-}}$ <sup>b</sup>	$k_{HO\cdot}$ <sup>c</sup>	$k_{SO_4^{\cdot-}}$ <sup>d</sup>
<i>amp<sup>R</sup></i>	192 bp	$1.07(\pm 0.01) \times 10^{-2}$	$1.95 (\pm 0.27) \times 10^{-2}$	$1.24(\pm 0.02) \times 10^{11}$	$2.70(\pm 0.37) \times 10^{11}$
	851 bp	$1.43(\pm 0.02) \times 10^{-2}$	$4.21(\pm 0.44) \times 10^{-2}$	$1.65(\pm 0.03) \times 10^{11}$	$5.84(\pm 0.61) \times 10^{11}$
<i>sull</i>	162 bp	$1.61(\pm 0.44) \times 10^{-4}$	$2.07(\pm 0.60) \times 10^{-4}$	$1.86(\pm 0.69) \times 10^9$	$2.87(\pm 0.69) \times 10^9$
	841 bp	-	-	-	-
<i>tetA</i>	210 bp	$2.30 (\pm 0.46) \times 10^{-4}$	-	$2.66(\pm 0.53) \times 10^9$	-
	1054 bp	$2.30(\pm 0.23) \times 10^{-4}$	-	$2.66(\pm 0.27) \times 10^9$	-

<sup>a</sup> pseudo first-order rate constant of hydroxyl radical obtained from Eq B15.

<sup>b</sup> pseudo first-order rate constant of  $SO_4^{\cdot-}$  calculated from Eq B36.

<sup>c</sup> second-order rate constant of  $HO\cdot$  obtained from Eq B19.

<sup>d</sup> second-order rate constant of  $SO_4^{\cdot-}$  obtained from Eq B40.

- Estimate is not presented due to potential experimental artifacts in regression analysis data.

Adjacent pyrimidine sites are potential sites for  $UV_{254}$  to generate cyclobutane pyrimidine dimers, the major UV-induced DNA lesions (Görner and Biology, 1994, Sinha

et al., 2002). The strength of correlation of  $k$  for all treatments was in the order 5'-TT-3' > 5'-CT-3' > 5'-TC-3' > 5'-CC-3' (Figure 2.9). This result is consistent with other reports in literature for UV-based treatments of ARGs (He et al., 2019, Yao et al., 2022). This observation provides an explanation for the faster degradation rate observed for  $amp^R$  qPCR amplicons than  $tetA$  despite the longer AT+GC bps of  $tetA$  amplicons (Figure 2.4).  $amp^R$  (192 bp and 851 bp) are more enriched in AT which make them contain more 5'-TT-3' than  $tetA$  and  $sull$  (Table 2.1). The relatively lower regression values ( $0.8 \leq r^2 < 0.99$ ) here suggest that other 'secondary' targets sites influenced DNA reactivities to  $UV_{254}$ ,  $HO^\cdot$  and  $SO_4^{\cdot-}$ . For instance, very strong linear relationships were observed between target site 5'-TA-3' and  $k'_{UV_{254}/H_2O_2}$  as well as for  $k'_{UV_{254}/S_2O_8^{2-}}$  ( $r^2 > 0.95$ ) (Appendix C). This means that a single variable regression analysis may not fully account for the dependences of  $k$  on DNA sequence elements. Nevertheless, results herein provide insights for predicting the degradation efficiencies for other ARGs of known sequences.

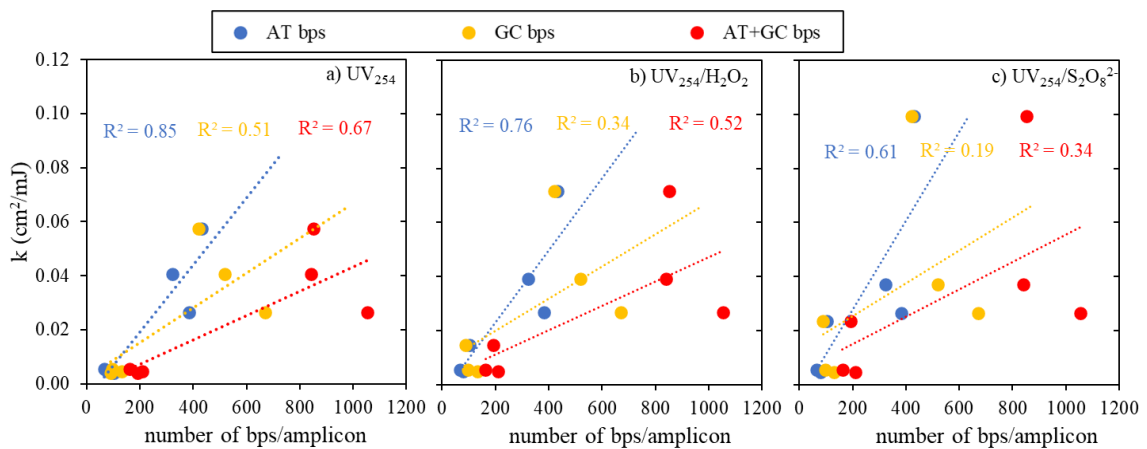


FIGURE 2. 8 First order degradation constants of qPCR amplicons as a function of the number of nucleotide base pair contents per qPCR amplicon.

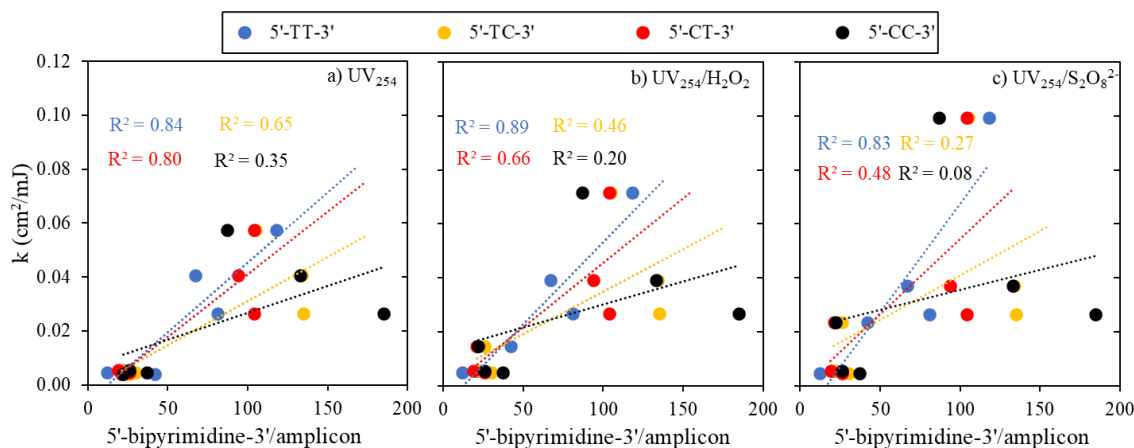


FIGURE 2. 9 First order degradation constants ( $k$ ) of qPCR amplicons versus the total number of intrastrand 5'-bipyrimidine-3' in each amplicon. Bipyrimidine are TT, TC, CT and CC within a single DNA strand.

#### 2.5.4. Intracellular ARG Degradation during $UV_{254}$ , $UV_{254}/H_2O_2$ and $UV_{254}/S_2O_8^{2-}$

The degradation kinetics of i-ARG by  $UV_{254}/H_2O_2$  and  $UV_{254}/S_2O_8^{2-}$  were not significantly higher than those of  $UV_{254}$  only (Figure 2.10). The first-order degradation rate constants for the qPCR amplicons indicate that degradation was mainly from direct  $UV_{254}$  photolysis (Table 2.6). This suggests that  $HO\cdot$  and  $SO_4^{\cdot-}$  had negligible contributions to i-ARG degradation. Cytoplasmic organic matters released into solution, following cell membrane rupture by radical attacks, scavenge radicals before they can interact with DNA (Huang et al., 2017, Yoon et al., 2017). The rate of i-ARG damage was slower than the damage to the corresponding e-ARG ( $k_{e-ARG}/k_{i-ARG} \sim 1.3$  to 3). The largest difference between  $k_{e-ARG}$  and  $k_{i-ARG}$  degradation rates were observed for  $amp^R$  (851 bp) in  $UV_{254}/S_2O_8^{2-}$  because of the significant contribution of  $SO_4^{\cdot-}$  to e- $amp^R$  degradation and its relatively high AT content (Figure 2.11). This shows that cellular components screen DNA and act as a protective layer against damage. Yoon et al. (2017) and Yoon et al. (2018b)

also reported that the rate of degradation of intracellular *kan<sup>R</sup>* and *amp<sup>R</sup>* were at least 1.5 fold lower than e-ARGs. Conversely, some studies have reported increased degradation rates of i-ARGs in *Pseudomonas sp* during UV<sub>254</sub>/H<sub>2</sub>O<sub>2</sub>, UV<sub>254</sub>/S<sub>2</sub>O<sub>8</sub><sup>2-</sup> and UV<sub>254</sub>/PMS systems relative to UV<sub>254</sub> irradiation only (Hu et al., 2019, Meng et al., 2022). The mechanistic study by Meng et al. (2022) on the role of radicals in i-ARG degradation showed that the degradation rates of plasmid-encoded i-ARGs and chromosomal i-ARGs of *Pseudomonas putida* increased by 71%-136% during UV<sub>254</sub>/H<sub>2</sub>O<sub>2</sub> and UV<sub>254</sub>/S<sub>2</sub>O<sub>8</sub><sup>2-</sup> compared to UV<sub>254</sub>. The study demonstrated that the increased i-ARG degradation did not result from direct interactions of HO· and SO<sub>4</sub><sup>-</sup> with i-ARG but was the aftermath of the degradation of extracellular polymeric substances (EPS) by these radicals. That is, EPS degradation resulted in higher cellular UV transmittance leading to increased i-ARG degradation. It is noteworthy that the compositions of polysaccharides, humic substances, lipids and protein in EPS of *Pseudomonas sp.* and *E. coli* strains are different. This difference in EPS compositions potentially affects the reactivities of radicals with EPS of these different organisms (Long et al., 2009, Tong et al., 2010, Di Martino, 2018). Besides, a study by Long et al. (2009) on the influence of EPS on bacteria deposition kinetics reported higher humic acids (a major UV absorbing component) in the EPS of *E. coli* BL21 (18.6±1.3 mg/g) than in *Pseudomonas sp.* QG6 (2.8±1.3 mg/g). This may explain the insignificant contributions of radicals to the i-ARG degradation reported by Yoon et al. (2017), Yoon et al. (2018b) and this study in which i-ARG of *E. coli* strains were studied. Nevertheless, i-ARG degradation kinetics increased with % AT nucleotide per amplicon and amplicon length as described in Section 2.5.3 above.

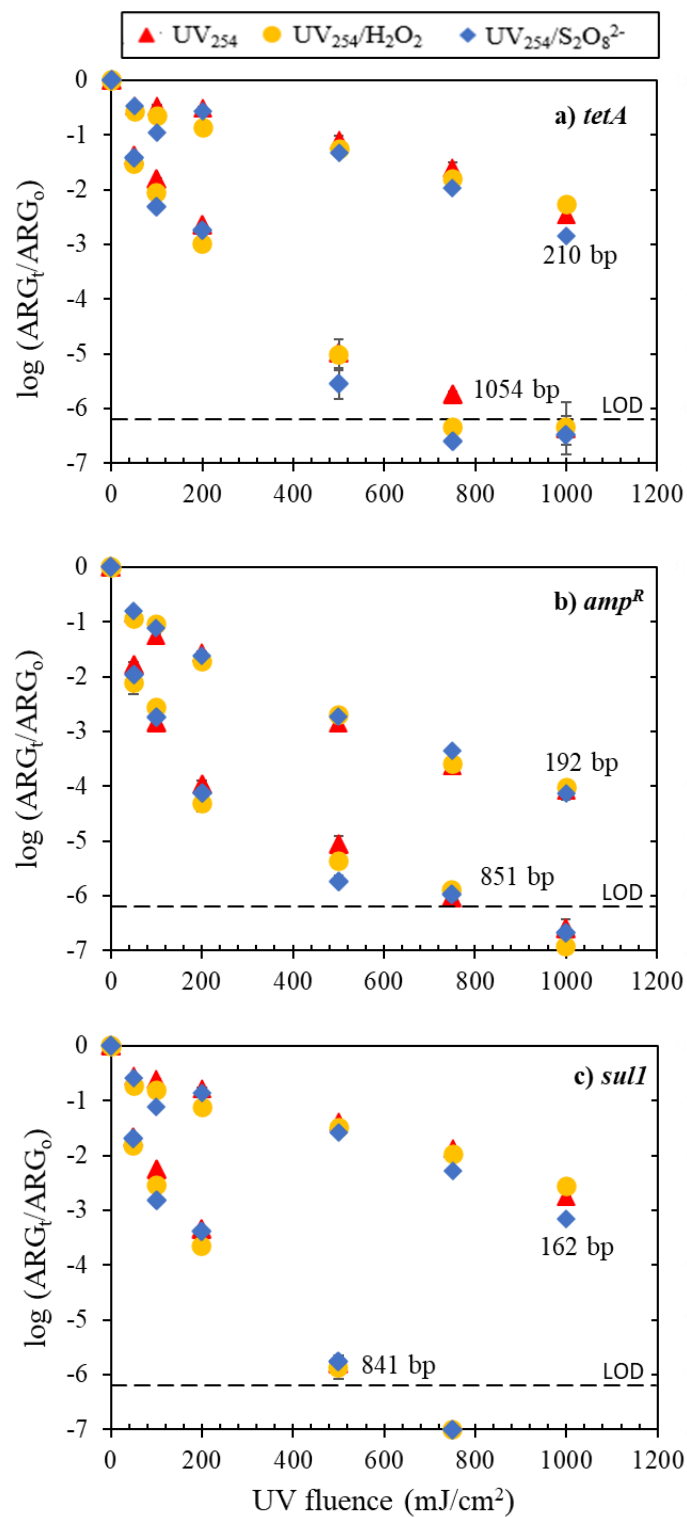


FIGURE 2. 10 Degradation of i-ARGs in PBS (pH 7, 10 mM) during UV<sub>254</sub>, UV<sub>254</sub>/H<sub>2</sub>O<sub>2</sub> and UV<sub>254</sub>/S<sub>2</sub>O<sub>8</sub><sup>2-</sup>. The concentrations of H<sub>2</sub>O<sub>2</sub> and S<sub>2</sub>O<sub>8</sub><sup>2-</sup> were 0.2 mM for UV<sub>254</sub>/H<sub>2</sub>O<sub>2</sub>

and UV<sub>254</sub>/S<sub>2</sub>O<sub>8</sub><sup>2-</sup>. The concentration of *E. coli* cells is  $\sim 1.5 \times 10^8$ . The error bars are the SEM of independent triplicate experiments.

#### 2.5.5. Impact of Initial Oxidant Concentration and pH

The efficiencies of UV<sub>254</sub>/H<sub>2</sub>O<sub>2</sub> and UV<sub>254</sub>/S<sub>2</sub>O<sub>8</sub><sup>2-</sup> for contaminants degradation are impacted by the starting oxidant concentration and reaction pH (Zhang et al., 2016, Li et al., 2018, Hu et al., 2019, Yao et al., 2022). The roles of initial H<sub>2</sub>O<sub>2</sub> and S<sub>2</sub>O<sub>8</sub><sup>2-</sup> (0.05 mM to 1 mM) on the degradation of e-ARG and i-ARG were examined at 500 mJ/cm<sup>2</sup> using *tetA* (210bp) and *sull* (162bp) amplicons as model ARGs (Figure 2.12). As H<sub>2</sub>O<sub>2</sub> and S<sub>2</sub>O<sub>8</sub><sup>2-</sup> concentrations increased, the log degradation of e-ARG increased with a higher increase for UV<sub>254</sub>/S<sub>2</sub>O<sub>8</sub><sup>2-</sup> than UV<sub>254</sub>/H<sub>2</sub>O<sub>2</sub> at 0.2, 0.3 and 0.5 mM ( $p < 0.05$ ) (Figures 2.12a and 2.12b). At 1 mM oxidant concentration, similar e-ARG log degradation ( $> 5$  logs) was observed for UV<sub>254</sub>/H<sub>2</sub>O<sub>2</sub> and UV<sub>254</sub>/S<sub>2</sub>O<sub>8</sub><sup>2-</sup> at 500 mJ/cm<sup>2</sup> UV fluence for *sull* (162bp) (T-test,  $P = 0.59$ ) (Figure 2.12b). These results agree with findings that oxidant doses are rate-limiting factors in UV-AOPs (Liu et al., 2015, Zhang et al., 2016, Hu et al., 2019). However, studies have shown that increasing the initial amount of H<sub>2</sub>O<sub>2</sub> and S<sub>2</sub>O<sub>8</sub><sup>2-</sup> beyond a certain concentration (called optimum concentration) can be unproductive due to radicals quenching by excess oxidants (Liu et al., 2015, Zhang et al., 2016). This phenomenon was not observed in the concentration range examined in this study. Therefore, 0.5 -1 mM oxidant concentrations are acceptable for optimum performance of UV<sub>254</sub>/H<sub>2</sub>O<sub>2</sub> and UV<sub>254</sub>/S<sub>2</sub>O<sub>8</sub><sup>2-</sup> for ARG degradation.

TABLE 2. 6 First-order kinetic degradation rate constants during UV<sub>254</sub>, UV<sub>254</sub>/H<sub>2</sub>O<sub>2</sub> and UV<sub>254</sub>/S<sub>2</sub>O<sub>8</sub><sup>2-</sup> treatments of intracellular plasmid-encoded ARGs ( $k = 2.303 \times \text{slope}$ )

ARG	Amplicon length	$k_{UV_{254}}$	$k'_{UV_{254}/H_2O_2}$	$k'_{UV_{254}/S_2O_8^{2-}}$
		(cm <sup>2</sup> /mJ)	(cm <sup>2</sup> /mJ)	(cm <sup>2</sup> /mJ)
<i>tetA</i>	210 bp	4.65 (±0.44) × 10 <sup>-3</sup> (r <sup>2</sup> =0.96)	4.61 (±0.12) × 10 <sup>-3</sup> (r <sup>2</sup> =0.95)	5.41 (±0.62) × 10 <sup>-3</sup> (r <sup>2</sup> =0.97)
	1054 bp	1.66 (±0.21) × 10 <sup>-2</sup> (r <sup>2</sup> =0.94)	1.77 (±0.21) × 10 <sup>-2</sup> (r <sup>2</sup> =0.95)	1.90 (±0.23) × 10 <sup>-2</sup> (r <sup>2</sup> =0.95)
<i>sulI</i>	162 bp	5.48 (±0.44) × 10 <sup>-3</sup> (r <sup>2</sup> =0.95)	4.88 (±0.60) × 10 <sup>-3</sup> (r <sup>2</sup> =0.93)	6.17 (±0.69) × 10 <sup>-3</sup> (r <sup>2</sup> =0.93)
	841 bp	2.06 (±0.02) × 10 <sup>-2</sup> (r <sup>2</sup> =0.95)	1.94 (±0.29) × 10 <sup>-2</sup> (r <sup>2</sup> =0.93)	1.93 (±0.29) × 10 <sup>-2</sup> (r <sup>2</sup> =0.92)
<i>amp<sup>R</sup></i>	192 bp	8.77 (±0.92) × 10 <sup>-3</sup> (r <sup>2</sup> =0.97)	8.59 (±0.90) × 10 <sup>-3</sup> (r <sup>2</sup> =0.95)	8.66 (±0.83) × 10 <sup>-3</sup> (r <sup>2</sup> =0.96)
	851 bp	4.38 (±0.90) × 10 <sup>-2</sup> (r <sup>2</sup> =0.78)	4.61 (±0.90) × 10 <sup>-2</sup> (r <sup>2</sup> =0.79)	4.47 (±0.90) × 10 <sup>-2</sup> (r <sup>2</sup> =0.85)

There was no significant increase in the log reduction of i-ARG with increasing H<sub>2</sub>O<sub>2</sub> and S<sub>2</sub>O<sub>8</sub><sup>2-</sup> concentrations (0.73 ≤ P ≤ 0.97). That is, the average log inactivation obtained with UV<sub>254</sub>/H<sub>2</sub>O<sub>2</sub> and UV<sub>254</sub>/S<sub>2</sub>O<sub>8</sub><sup>2-</sup> was similar to that obtained at 500 mJ/cm<sup>2</sup> UV<sub>254</sub> only (0.55 ± 0.08 vs 0.49 ± 0.02 vs 0.46 ± 0.05). This suggests that extracellularly produced HO· and SO<sub>4</sub>·<sup>-</sup> had negligible contributions to the degradation of i-ARG regardless of the reactivity of these radicals with DNA under the examined conditions. Similar results have been reported for i-ARGs degradation in *E. coli* cells using HO· and SO<sub>4</sub>·<sup>-</sup> (Ferro et al., 2017, Yoon et al., 2017, Yoon et al., 2018b, Yoon et al., 2021). This result may be due to radical scavenging by cell membrane and intracellular organic matters (Huang et al., 2017, Yoon et al., 2017). Besides, radicals are short-lived and may not

adequately diffuse through cell membranes and cytoplasm to effect i-ARG degradation (Michael-Kordatou et al., 2018). In contrast, Hu et al. (2019) observed a proportional increase in the degradation of intracellular chromosomal *sulI* and *intI1* in *pseudomonas* sp. with PMS concentration (5 to 30 mg/L) in UV<sub>254</sub>/PMS system. This difference could be due to conformational differences in plasmid and chromosomal DNA, UV fluence applied, the difference in bacterial species/concentration or an interplay between radicals in UV<sub>254</sub>/PMS distinct from UV<sub>254</sub>/S<sub>2</sub>O<sub>8</sub><sup>2-</sup>.

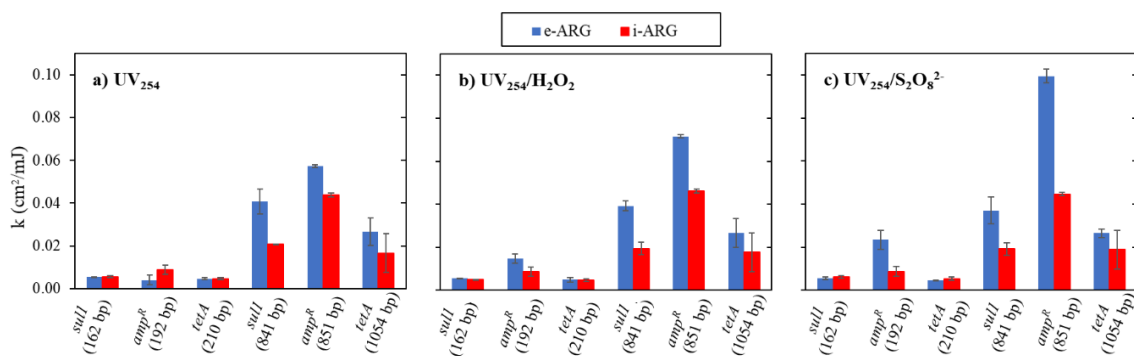


FIGURE 2. 11 Comparison of first-order rate constants of e-ARG and i-ARG for UV<sub>254</sub>, UV<sub>254</sub>/H<sub>2</sub>O<sub>2</sub> and UV<sub>254</sub>/S<sub>2</sub>O<sub>8</sub><sup>2-</sup>. The largest difference between  $k_{e-ARG}$  and  $k_{i-ARG}$  degradation rates were observed for *amp<sup>R</sup>* (851 bp).

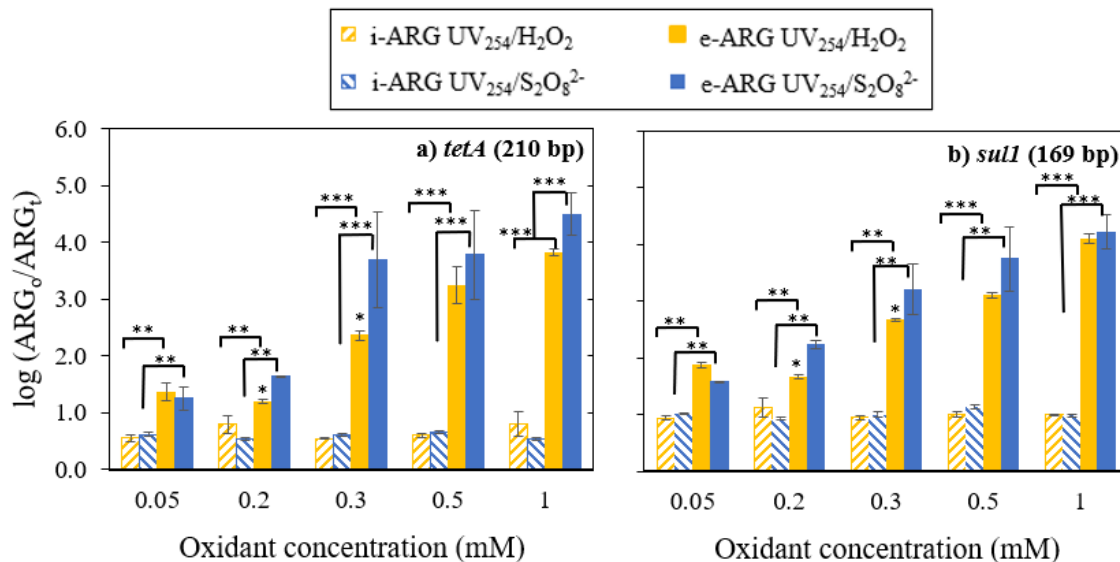


FIGURE 2. 12: Effect of initial H<sub>2</sub>O<sub>2</sub> and S<sub>2</sub>O<sub>4</sub><sup>2-</sup> concentrations on the degradation of i-ARG and e-ARG during UV<sub>254</sub>/H<sub>2</sub>O<sub>2</sub> and UV<sub>254</sub>/S<sub>2</sub>O<sub>8</sub><sup>2-</sup> treatments. UV fluence in all cases was 500 mJ/cm<sup>2</sup>. Error bars are SEM of duplicate independent experiments. The symbol \*, \*\* and \*\*\* denote statistically significant differences with p < 0.05, p < 0.01 and p < 0.001, respectively using one-way ANOVA test with Bonferroni correction between the different test samples at a given initial oxidant concentration.

pH is a factor that affects the oxidation potential of oxidants and radical generation reactions in UV<sub>254</sub>/H<sub>2</sub>O<sub>2</sub> and UV<sub>254</sub>/S<sub>2</sub>O<sub>8</sub><sup>2-</sup> systems (Zhang et al., 2016, Yao et al., 2022). The logarithmic degradation of extracellular *tetA* (210 bp) and *sull* (162 bp) were examined under pH 5-9 at 500 mJ/cm<sup>2</sup> using 0.1- and 0.2-mM oxidant concentrations (Figure 2.13). Control experiments showed that qPCR amplicons of *tet* (210 bp) and *sull* (162 bp) were stable under the range of pH examined. Thus, ARG degradation was not due to hydrolysis at relatively high or low pH (Figure 2.14). For UV<sub>254</sub>/H<sub>2</sub>O<sub>2</sub>, *tetA* (210 bp) and *sull* (162 bp) degradations decreased as pH increased past pH 8 or as pH decreased past pH 7 (P<0.01) for both 0.1 and 0.2 mM H<sub>2</sub>O<sub>2</sub> concentrations (Figure 2.13). This indicates

that UV<sub>254</sub>/H<sub>2</sub>O<sub>2</sub> has optimum performance for ARG degradation at near-neutral pH. A reason for this could be the reduction in the oxidation potential of HO· and hydrolysis of H<sub>2</sub>O<sub>2</sub> as pH increases (Zhang et al., 2016, Kilic et al., 2019).

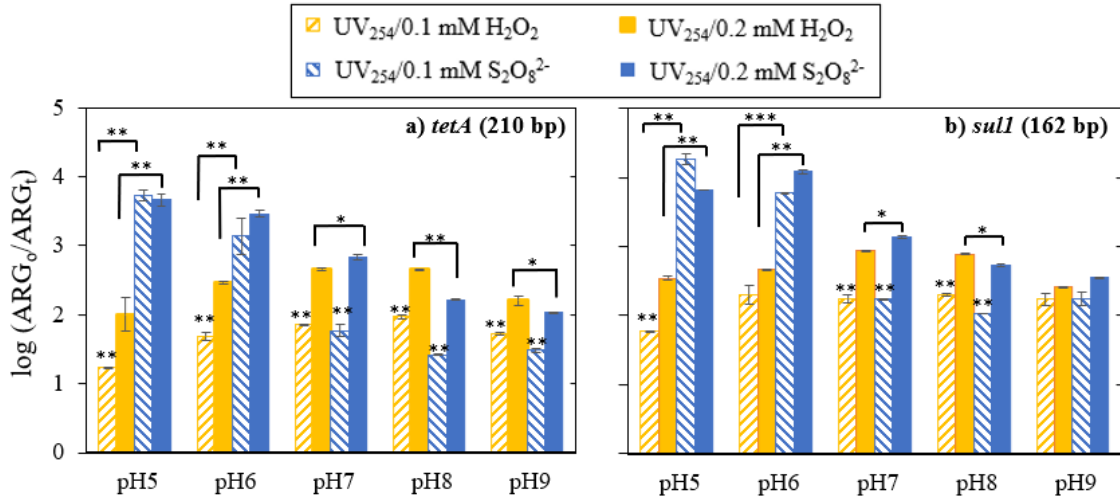


FIGURE 2. 13 Influence of pH on the degradation of extracellular MDR *E. coli* plasmid (~1 ng/μL) using 0.1 mM and 0.2 mM concentrations of H<sub>2</sub>O<sub>2</sub> and S<sub>2</sub>O<sub>4</sub><sup>2-</sup> during UV<sub>254</sub>/H<sub>2</sub>O<sub>2</sub> and UV<sub>254</sub>/S<sub>2</sub>O<sub>8</sub><sup>2-</sup> treatments. UV fluence was 500 mJ/cm<sup>2</sup>. Error bars are SEM of duplicate independent experiments. The symbol \*, \*\* and \*\*\* denote statistically significant differences with p < 0.05, p < 0.01 and p < 0.001, respectively using one-way ANOVA test with Bonferroni correction between the different test samples in each experimental pH group.

The degradation of *tetA* (210 bp) and *sulI* (162 bp) increased (~2 logs to ~4 logs) with decreasing pH (from 9 to 5) in the UV<sub>254</sub>/S<sub>2</sub>O<sub>8</sub><sup>2-</sup> system (Figure 2.13). The difference between log ARG damage using 0.1 mM and 0.2 mM initial S<sub>2</sub>O<sub>8</sub><sup>2-</sup> decreased as pH decreased in UV<sub>254</sub>/S<sub>2</sub>O<sub>8</sub><sup>2-</sup> systems. That is, comparable ARG degradations resulted from 0.1 mM and 0.2 mM initial S<sub>2</sub>O<sub>8</sub><sup>2-</sup> concentration at pH 5 and 6 (0.67 < P < 1). Yao et al.

(2022) and Hu et al. (2019) recorded the same trend for chromosomal ARG degradation in UV<sub>254</sub>/PMS system. This could be because the production of  $SO_4^{\cdot-}$  is enhanced under low pH by acid catalysis (Kilic et al., 2019). Besides, at high pH,  $SO_4^{\cdot-}$  reacts with  $OH^-$  forming  $HO\cdot$  of lower redox potential (Equation B22 in Appendix B). The pattern of ARG degradation using UV<sub>254</sub>/H<sub>2</sub>O<sub>2</sub> and UV<sub>254</sub>/S<sub>2</sub>O<sub>8</sub><sup>2-</sup> systems under different pH is consistent with that described by Zhang et al. (2016) and Kilic et al. (2019) in the degradation of other organic contaminants. Overall, UV<sub>254</sub>/S<sub>2</sub>O<sub>8</sub><sup>2-</sup> showed a relatively higher (~11%) ARG log reduction than UV<sub>254</sub>/H<sub>2</sub>O<sub>2</sub> at pH 7 and 0.2 mM oxidants concentration.

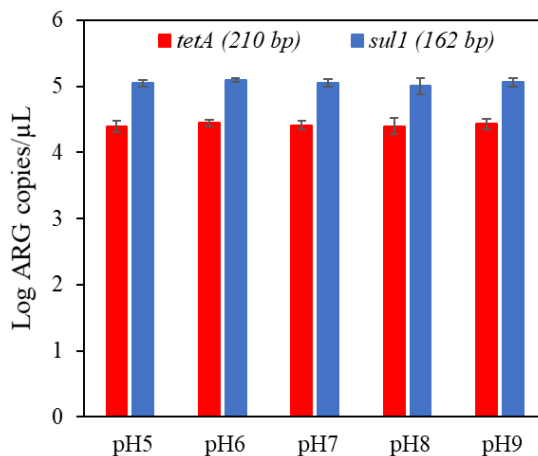


FIGURE 2. 14: Stability of qPCR amplicons of *tetA* and *sulI* genes in MDR *E. coli* plasmid in various pH solutions over the same time exposure as pH impact experiment for UV<sub>254</sub>/H<sub>2</sub>O<sub>2</sub> and UV<sub>254</sub>/S<sub>2</sub>O<sub>8</sub><sup>2-</sup>.

#### 2.5.6. Structural Changes and Loss of Transforming Activity

The mode of pCR<sup>TM</sup>2.1-TOPO degradation in UV<sub>254</sub>, UV<sub>254</sub>/H<sub>2</sub>O<sub>2</sub> and UV<sub>254</sub>/S<sub>2</sub>O<sub>8</sub><sup>2-</sup>-treated extracellular plasmids (e-plasmid) was viewed on gel electrophoresis. No change to the structural conformation of supercoiled pCR<sup>TM</sup>2.1-TOPO was observed by UV<sub>254</sub> at

UV fluences  $< 500 \text{ mJ/cm}^2$  (Figure 2.15a). During  $\text{UV}_{254}/\text{H}_2\text{O}_2$  and  $\text{UV}_{254}/\text{S}_2\text{O}_8^{2-}$  treatments, pCR<sup>TM</sup>2.1-TOPO gradually moved from the supercoiled band to the nicked band and finally to the linear band as treatment progressed (Figures 2.15b and 2.15c). This observation is consistent with the well-established DNA damage mechanisms of  $\text{UV}_{254}$  and radicals (i.e.,  $\text{HO}\cdot$  and  $\text{SO}_4\cdot^-$ ). UV damages DNA mainly via oxidation of nucleobase such as pyrimidine dimer formation (Görner and Biology, 1994, Sinha et al., 2002). Nucleobase dimerization does not change the structural conformation of DNA nor its size. Thus, they are not detectable by gel-electrophoresis. On the other hand,  $\text{HO}\cdot$  and  $\text{SO}_4\cdot^-$  react with phosphate backbone of DNA causing single-strand (ss) or double-strand (ds) breakage (Balasubramanian et al., 1998, von Sonntag, 2006). This explains the movement in the DNA band from supercoiled to linear band.

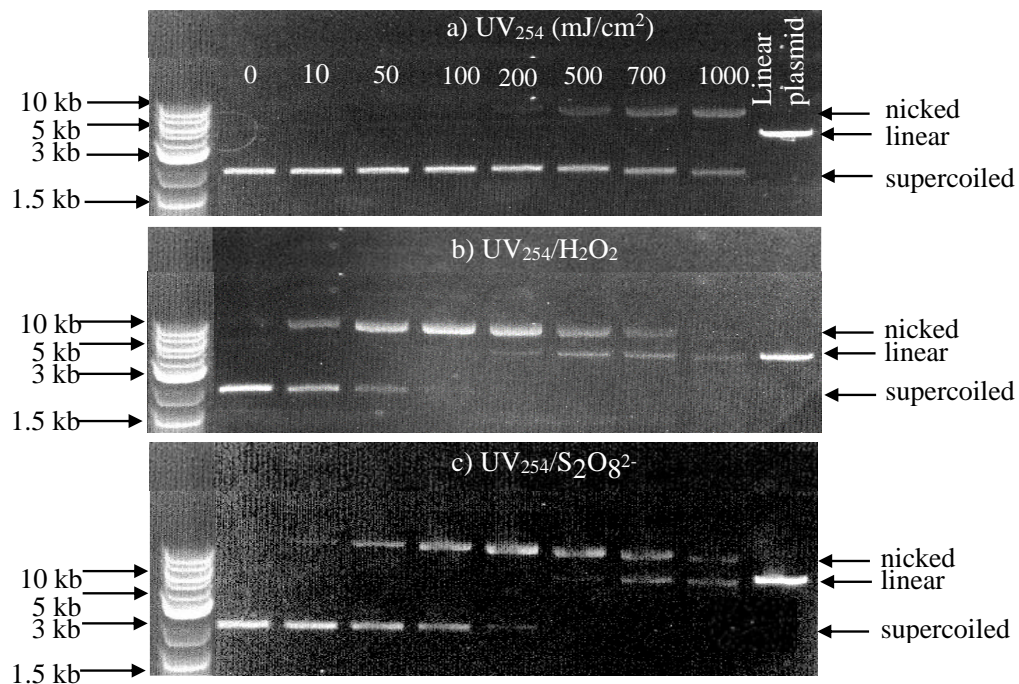


FIGURE 2. 15 Changes in structural conformation of extracellular pCR<sup>TM</sup>2.1-TOPO<sup>®</sup> (~3 ng/ $\mu\text{L}$ ) shown on gel electrophoresis during treatment with a)  $\text{UV}_{254}$ , b)  $\text{UV}_{254}/\text{H}_2\text{O}_2$  and

c)  $UV_{254}/S_2O_8^{2-}$  (pH = 7, 0.2 mM  $H_2O_2$  and  $S_2O_8^{2-}$ ). The numbers presented above each column represent the UV fluence applied during all treatments. The ‘linear plasmid’ column is linearized pCR™2.1-TOPO® by restriction enzyme EcoR1-HF®.

Although qPCR is a rapid analytical tool that captures DNA damages better than gel electrophoresis, culture-based transformation assays provide a more accurate evaluation of treatment impacts on AR dissemination risks (Chang et al., 2017, Vikesland et al., 2017). The replication efficiencies of damaged ARGs measured by qPCR are sometimes different from that observed when a bacterial cell is transformed by the same DNA (Chang et al., 2017, He et al., 2019, Nihemaiti et al., 2020, Yoon et al., 2021). The transformation activity of treated e-pCR™2.1-TOPO using  $UV_{254}$ ,  $UV_{254}/H_2O_2$  and  $UV_{254}/S_2O_8^{2-}$  was examined to correlate its biological deactivation to degradation measured by qPCR amplicons (Figure 2.16). The transformation efficiency of TOP10 *E. coli* using pCR™2.1-TOPO was in the range of  $10^7$  -  $10^8$ . This value was comparable with previous studies (Hanahan et al., 1991, Yoon et al., 2018b). The loss of transformation activity of pCR™2.1-TOPO (i.e., deactivation) followed first-order kinetics with respect to UV fluence ( $r^2 \geq 0.94$ ) (Figure 2.16a and Table 2.7). At least 3 logs deactivation of pCR™2.1-TOPO was obtained at  $100 \text{ mJ/cm}^2$  for all treatments (typical UV fluence for water disinfection is between  $40 - 100 \text{ mJ/cm}^2$ ). At UV fluence  $> 200 \text{ mJ/cm}^2$ , pCR™2.1-TOPO was completely deactivated for all treatments.

The rates of elimination of transforming activity by  $UV_{254}/H_2O_2$  and  $UV_{254}/S_2O_8^{2-}$  were 2.6-times higher than that of  $UV_{254}$  only (Figure 2.16b). This value is higher ~ 2 times higher than the relative rate of transforming activity loss (i.e.  $UV_{254}$  vs  $UV_{254}/H_2O_2$ ) reported by Nihemaiti et al. (2020) and (Yoon et al., 2018b) for *amp<sup>R</sup>* in pUC19. This

difference could be because of the lack of *recA* protein in the DH5 $\alpha$  strain used in these studies. *recA* protein is responsible for DNA repair via homologous recombination (Smith and Wang, 1989, Shinohara and Ogawa, 1995). Interestingly, the degradation rates  $k'_{UV_{254}/S_2O_8^{2-}}$  and  $k'_{UV_{254}/H_2O_2}$  monitored by qPCR were only greater 1.2 and 1.1 times greater than  $k_{UV_{254}}$  (compared to 2.6-times for deactivation rate) (Table 2.3 vs Figure 2.16b). One reason for this is that radical-induced damages (such as ss- or ds-DNA breaks) can occur in DNA regions outside qPCR monitored amplicons (He et al., 2019). qPCR only measures the degradation of a small fragment of DNA which may not give an accurate representation of the biological activity of the entire DNA.

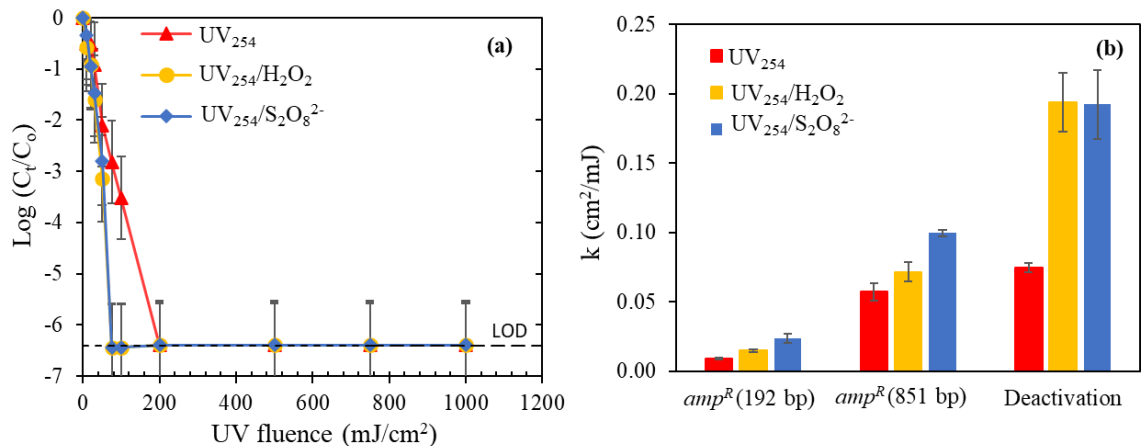


FIGURE 2. 16 (a) Loss of  $amp^R$  gene transformation activity in TOP10 *E. coli* competent cells after treatment of extracellular pCR™2.1-TOPO® (~1 ng/μL) with UV<sub>254</sub>, UV<sub>254</sub>/H<sub>2</sub>O<sub>2</sub> and UV<sub>254</sub>/S<sub>2</sub>O<sub>8</sub><sup>2-</sup> (pH=7, 0.2 mM H<sub>2</sub>O<sub>2</sub> and S<sub>2</sub>O<sub>8</sub><sup>2-</sup>) (b) Comparison of the first-order degradation rate constants of qPCR amplicons with first-order deactivation rate

constant from TOP10 *E. coli* transformation with treated extracellular pCR<sup>TM</sup>2.1-TOPO<sup>®</sup>. Error bars are SEM of triplicate independent experiments.

The higher rate of *amp<sup>R</sup>* degradation by UV<sub>254</sub>/S<sub>2</sub>O<sub>8</sub><sup>2-</sup> than UV<sub>254</sub>/H<sub>2</sub>O<sub>2</sub> did not result in a higher loss of transformation activity (T-test, P=0.98) (Figure 2.16b). *amp<sup>R</sup>* (192 bp) qPCR amplicon underestimated (~90%) the rate of deactivation of pCR<sup>TM</sup>2.1-TOPO for the three treatments while *amp<sup>R</sup>* (851 bp) gave a closer (~20%) estimate of the plasmid deactivation for UV<sub>254</sub> (Figure 2.16b). Nevertheless, *amp<sup>R</sup>* (851 bp) underestimated (~77%) pCR<sup>TM</sup>2.1-TOPO deactivation for UV<sub>254</sub>/H<sub>2</sub>O<sub>2</sub> and UV<sub>254</sub>/S<sub>2</sub>O<sub>8</sub><sup>2-</sup>. This could be due to the same reason for qPCR's inability to estimate DNA damages outside the amplification region. As reported herein, studies have shown that deactivation kinetics were faster than degradation kinetics when short (< 270 bp) qPCR amplicons were used (Chang et al., 2017, He et al., 2019, Nihemaiti et al., 2020, Yoon et al., 2021). The predicted degradation rate constants for the entire plasmid (i.e., k<sub>pCR<sup>TM</sup>2.1-TOPO</sub>) overestimated the deactivation of the plasmid for the three treatments (Table 2.7).

## 2.6. Summary

This study addresses the gap in knowledge of fundamental kinetic parameters for estimating and predicting ARGs degradation and deactivation during UV-based hydroxyl and sulphate radical AOPs. Herein, the impacts of the target qPCR amplicon length, nucleotide compositions, pH and initial oxidant concentrations on degradation kinetics of intracellular and extracellular plasmid-encoded *tetA*, *amp<sup>R</sup>* and *sulI* ARGs during UV<sub>254</sub>, UV<sub>254</sub>/H<sub>2</sub>O<sub>2</sub> and UV<sub>254</sub>/S<sub>2</sub>O<sub>8</sub><sup>2-</sup> treatments were assessed. The first-order degradation rate constants for UV<sub>254</sub>, UV<sub>254</sub>/H<sub>2</sub>O<sub>2</sub> and UV<sub>254</sub>/S<sub>2</sub>O<sub>8</sub><sup>2-</sup>; and second-order degradation kinetic

constants of ARGs with respect to  $HO\cdot$  and  $SO_4^{\cdot-}$  were determined. e-ARGs degradation efficiencies for the treatments followed the order  $UV_{254}/S_2O_8^{2-} > UV_{254}/H_2O_2 > UV_{254}$ . AT-rich  $amp^R$  amplicon degraded faster than GC-rich  $tetA$  and  $sulI$  for all treatments. The strength of correlation of first-order degradation rate constants with adjacent pyrimidine UV-active sites was in the order  $5'-TT-3' > 5'-CT-3' > 5'-TC-3' > 5'-CC-3'$ , for all treatments. Target amplicons reacted with  $HO\cdot$  and  $SO_4^{\cdot-}$  at diffusion-controlled rates ( $10^9$ - $10^{11} M^{-1}s^{-1}$ ), demonstrating that  $HO\cdot$  and  $SO_4^{\cdot-}$  AOPs are effective barriers for AR mitigation.

TABLE 2. 7 First-order rate constant for  $amp^R$ , pCR<sup>TM</sup>2.1 degradation and pCR<sup>TM</sup>2.1 deactivation

Amplicon length		$k_{UV_{254}}$	$k'_{UV_{254}/H_2O_2}$	$k'_{UV_{254}/S_2O_8^{2-}}$
		( $cm^2/mJ$ )	( $cm^2/mJ$ )	( $cm^2/mJ$ )
qPCR	192 bp	$9.14(\pm 0.53) \times 10^{-3}$ ( $r^2=0.98$ )	$1.47(\pm 0.07) \times 10^{-2}$ ( $r^2=0.99$ )	$2.35(\pm 0.32) \times 10^{-2}$ ( $r^2=0.93$ )
	851 bp	$5.73(\pm 0.64) \times 10^{-2}$ ( $r^2=0.96$ )	$7.16(\pm 0.67) \times 10^{-2}$ ( $r^2=0.97$ )	$9.95(\pm 0.21) \times 10^{-2}$ ( $r^2=1.00$ )
	$k_{pCR^{TM}2.1*}$			
	(192bp_etrp)	$1.87(\pm 0.11) \times 10^{-1}$	$3.01(\pm 0.14) \times 10^{-1}$	$4.81(\pm 0.66) \times 10^{-1}$
	$k_{pCR^{TM}2.1}$			
(851bp_etrp)	$2.64(\pm 0.29) \times 10^{-1}$	$3.31(\pm 0.31) \times 10^{-1}$	$4.60(\pm 0.01) \times 10^{-1}$	
Loss of transforming activity	$7.44(\pm 0.32) \times 10^{-2}$ ( $r^2=0.99$ )	$1.94(\pm 0.21) \times 10^{-1}$ ( $r^2=0.95$ )	$1.93(\pm 0.25) \times 10^{-1}$ ( $r^2=0.94$ )	

\*  $k_{pCR^{TM}2.1} = k_{qPCR \text{ amplicon}} \times \frac{\text{length of pCR}^{TM}2.1}{\text{length of qPCR amplicon}}$  assuming an equal sensitivity of DNA damage across the entire plasmid (Chang et al., 2017, Nihemaiti et al., 2020).

The effectiveness of UV<sub>254</sub>/S<sub>2</sub>O<sub>8</sub><sup>2-</sup> was highly pH-dependent compared to UV<sub>254</sub>/H<sub>2</sub>O<sub>2</sub>, with higher ARG degradation at pH 5 and 6. Nevertheless, a significant ARG degradation (e.g., 3 logs) was observed at near-neutral pH for 500 mJ/cm<sup>2</sup> UV fluence. Comparable log degradation of e-ARG resulted from 0.1 mM (3.2-3.8 logs) and 0.2 mM (3.8-4.1 logs) initial S<sub>2</sub>O<sub>8</sub><sup>2-</sup> concentration at pH 5 and 6. This observation has implications for chemical cost savings and reduced residual concentration in water during UV<sub>254</sub>/S<sub>2</sub>O<sub>8</sub><sup>2-</sup> treatment. H<sub>2</sub>O<sub>2</sub> and S<sub>2</sub>O<sub>8</sub><sup>2-</sup> at 0.2 mM (pH 7) did not significantly improve the degradation of i-ARG during UV<sub>254</sub>/H<sub>2</sub>O<sub>2</sub> and UV<sub>254</sub>/S<sub>2</sub>O<sub>8</sub><sup>2-</sup> treatments compared to UV<sub>254</sub> only.

The deactivation rates of plasmid pCR<sup>TM</sup>2.1-TOPO from HGT experiments were faster than the observed degradation rates of qPCR amplicons. About 3 logs deactivation of *amp*<sup>R</sup> in pCR<sup>TM</sup>2.1-TOPO was obtained at typical UV fluence (e.g, 100 mJ/ cm<sup>2</sup>) for water disinfection for UV<sub>254</sub>. Whereas, > 6 logs deactivation were recorded for UV<sub>254</sub>/H<sub>2</sub>O<sub>2</sub> and UV<sub>254</sub>/S<sub>2</sub>O<sub>8</sub><sup>2-</sup>. Short qPCR amplicons overestimated the potential risks of ARG presence as shown by the loss of transforming activity of plasmid encoding ARGs detected by short qPCR amplicon (i.e., *amp*<sup>R</sup>, 192 bp) in bacterial transformation experiments. This demonstrates that the effectiveness of treatment options against ARGs are best evaluated using longer qPCR amplicons that have better coverage of the resistance gene of interest. These findings herein present useful considerations for estimating the levels of ARGs, monitoring the AR status of environmental samples, assessing UV-based treatment strategies, and setting treatment operating conditions for effective ARGs degradation.

## CHAPTER 3. INACTIVATION OF ANTIBIOTIC RESISTANCE BACTERIA USING PHOTO-ACTIVATED SILVER NANOPARTICLES (FUNDED BY: FRG)

### 3.1. Literature Review

The emergence and spread of antibiotic resistance (AR) are one of the greatest global public health issues of the 21<sup>st</sup> century (WHO, 2014, WHO, 2017, CDC, 2019). The prevalence of AR is linked to the indiscriminate use of antibiotics for human and animal treatment because antibiotics impose selective pressure by killing susceptible bacteria while resistant bacteria proliferate (Berendonk et al., 2015). AR challenges therapeutic potential against pathogens of humans and animals resulting in overwhelming healthcare costs and deaths (Jackman et al., 2016, Mamun et al., 2021). Moreover, advancements in modern medicine become incapacitated with dwindling efficacy of antibacterial drugs (O'Connell et al., 2013). The AR problem is compounded by the fact that the evolution of antibiotic-resistant bacterial (ARB) strains has been faster than the development of new classes of antibiotics (O'Connell et al., 2013, Jackman et al., 2016, Richards et al., 2018).

Typically, conventional antibiotics kill or inhibit microorganisms by interfering with a specific cellular function or metabolic pathway resulting in their cell death (Aruguete et al., 2013, Jackman et al., 2016). Common antibiotics targets include inhibition of cell wall synthesis, cell membrane functions, protein or nucleic acid synthesis, folic acid or mycolic acid production, and other metabolic processes (Anderson et al., 2012). Bacteria has devised mechanisms of evading these bactericidal effects shrinking the pipeline of effective antibiotics (O'Connell et al., 2013, Mamun et al., 2021). Bacteria develop resistance to antibiotics by modifying the target site for antibiotics activity, modifying the pathway of the target synthesis, reducing the antibiotics concentration in the cell or

destroying the antibiotics (Levy and Marshall, 2004). There is a minimum of one mechanism of bacterial resistance to all the classes of antibiotics available (Levy and Marshall, 2004, O'Connell et al., 2013).

With the rise in multidrug-resistant (MDR) bacteria, there is an urgent need for new antibacterial agents with targets that have low possibility of developing resistance through mutation, and that can overcome latest bacterial resistance mechanisms (O'Connell et al., 2013, Jackman et al., 2016). It is desired that novel antibacterial agents inhibit bacteria via multiple mechanisms with bactericidal actions that do not involve specific biochemical pathways. In recent years, great attention has been directed to the use of antimicrobial nanoparticles (NPs) as alternative antimicrobials with novel non-specific low-mutation bacterial targets (Jackman et al., 2016, Mamun et al., 2021). Antimicrobial NPs inactivate microorganisms via non-specific pathways with multiple targets involving a combination of cell membrane lysis and ROS generation to degrade cellular compounds (Aruguete et al., 2013, Mamun et al., 2021). Thus, antimicrobial NPs have a high barrier against resistance development. Moreover, the use of nanoscale antimicrobials allows for increased bioavailability by promoting transport through the cell membrane to the target site (Gao et al., 2014, Abed et al., 2015, Mamun et al., 2021).

Silver nanoparticles (AgNPs) have gained wide use in different antimicrobial research areas because they significantly inhibit several Gram-positive and Gram-negative bacteria and have lower tendency for antibacterial resistance development (Aruguete et al., 2013, Cao et al., 2017, Abdellatif et al., 2021). Moreover, AgNPs have high affinity towards sulphur and phosphorus in biomolecules (Yin et al., 2015). Consequently, several studies have been conducted to fully understand the antibacterial mechanisms of AgNPs to

promote its antimicrobial applications (Mijnendonckx et al., 2013, Aruguete et al., 2013, Yan et al., 2018).

Recent studies have elucidated that the antibacterial action of AgNPs is mainly based on the localized release of silver ions ( $\text{Ag}^+$ ) from the surface of AgNP core. The released  $\text{Ag}^+$  enables bacterial inactivation due to interaction with enzymes and proteins, and high ROS production (Aruguete et al., 2013, Cao et al., 2017, Salomoni et al., 2017, Yan et al., 2018, Elashnikov et al., 2019). Therefore, AgNPs act as a reservoir of  $\text{Ag}^+$ , which release  $\text{Ag}^+$  ions by oxidative dissolution in aerobic or other oxidative conditions (Ho et al., 2010, Siriwardana et al., 2015). The design of novel AgNP-based materials that increase the oxidation of AgNPs to enhance the release of  $\text{Ag}^+$  ions will have a major impact on the antimicrobial features of AgNPs. Tremendous efforts have been made to further the clinical application of antimicrobial AgNPs and improve the release of  $\text{Ag}^+$  by modifying the surface coating (Kvítek et al., 2008, Neethu et al., 2020, Abdellatif et al., 2021), varying its size (Agnihotri et al., 2014, Pareek et al., 2018), infusing silver in biodegradable core (Richter et al., 2015, Cao et al., 2017) and, more recently, conjugation with photosensitizers (PS) (Xie et al., 2017, Elashnikov et al., 2019, Shabangu et al., 2020).

PS are known to generate reactive oxygen species (ROS) that inactivate bacteria by causing oxidative stresses or damage to cellular components when irradiated with visible light in an antimicrobial approach called photodynamic inactivation (PDI) (Yin et al., 2015, Hurst et al., 2019). PDI is becoming popular as an alternative antimicrobial therapy to conventional antibiotics (Elashnikov et al., 2019, Shabangu et al., 2020). PDI involves the combination of nontoxic dyes called photosensitizers (PS) with harmless visible light to produce reactive oxygen species (ROS) that can selectively eliminate microbial cells (Yin

et al., 2015, Elashnikov et al., 2019, Hurst et al., 2019). PDI is an excellent alternative to kill ARB without generating resistance because it deals with cytotoxic ROS generation. Protoporphyrin IX (PpIX), one of the most effective ROS producing PS, has been extensively used as an effective antimicrobial agent either as single molecule or attached to different materials (Vzorov et al., 2002, Almeida et al., 2011). However, it has been observed that Gram-positive bacteria are more susceptible to PDI than Gram-negative bacteria (Huang et al., 2010, Hurst et al., 2019). The complex outer membrane of Gram-negative bacteria offers a relatively impermeable barrier to PS than in Gram-positive bacteria.

Recent studies have shown that PS and AgNPs conjugates have synergistic antimicrobial effect in PDI (Xie et al., 2017, Elashnikov et al., 2019, Shabangu et al., 2020, Ghasemi et al., 2021, Malá et al., 2021). However, most of these studies did not investigate the fundamental mechanisms responsible for antibacterial synergy in PS and AgNPs conjugates. In the quest against AR using new AgNPs formulations, it is important to understand their mechanistic bactericidal effect to avoid misuse or sublethal exposure that may promote bacterial resistance development (Aruguete et al., 2013, Mijndonckx et al., 2013). This work is designed to answer the following research questions relating to the antimicrobial property of a novel surface-modified porphyrin-AgNPs complex:

1. Is there a synergistic effect in the bactericidal action of PS-NPs complex?
2. Does resistance to antibiotics mean tolerance to PDI?
3. Is porphyrin-AgNPs complex equally effective against Gram-positive and Gram-negative ARB and ARGs?

### 3.2. Hypothesis and Objectives of this Chapter

It was hypothesized that conjugating porphyrin on AgNPs will result in a synergistic antimicrobial effect and promote Ag<sup>+</sup> release via ROS from porphyrin. Also, we hypothesize that AgNPs will promote the transport of porphyrin through the membranes of Gram-negative bacteria. The following objectives were designed to answer the above questions:

- i. Evaluate of the inactivation of Gram-positive and Gram-negative ARB using porphyrin-AgNP conjugates.
- ii. Determine the bactericidal mechanism of light-activated NPs.
- iii. Assess the degradation of ARGs using porphyrin-AgNP conjugates.

### 3.3. Study Overview

This is a study targeting the mechanisms causing synergistic antimicrobial activity in porphyrin-AgNP conjugates: cysPpIX-AgNP and PEI-cysPpIX-AgNP. Herein, the inactivation of a methicillin resistant *Staphylococcus aureus* (MRSA) strain and a MDR *Escherichia coli* strain were examined as model organisms of Gram positive and Gram-negative bacteria respectively. Also, the influence of positive charge surface coating of polyethyleneimine (PEI) on antimicrobial activity of porphyrin- AgNP conjugates was examined.

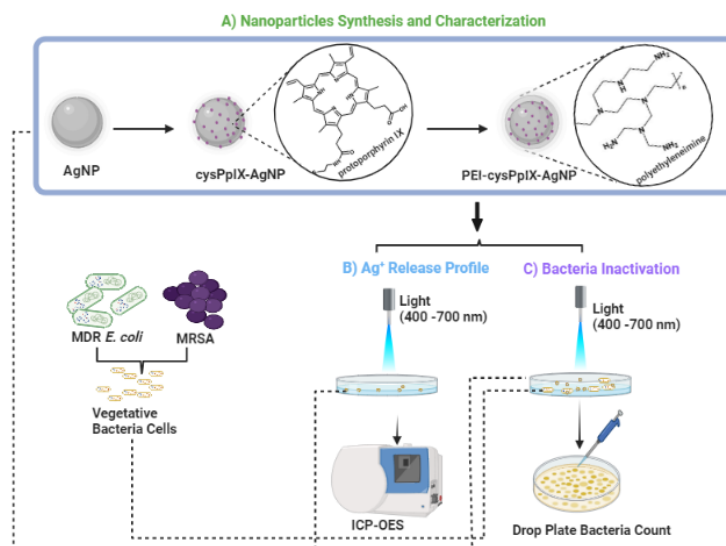


FIGURE 3. 1 Schematics of the ARB inactivation experiments using porphyrin-AgNP conjugates. **A)** Synthesis and Characterization of cysPpIX-AgNPs and PEI-cysPpIX-AgNPs. **B)** Ag<sup>+</sup> release profile obtained post light activation using ICP-OES. **C)** Antimicrobial activity of the light irradiated nanoparticles assessed by drop plate colony count method.

### 3.4. Materials and Method

#### 3.4.1. Test Organisms

Based on the World Priority List of ARB for Research and Development of new antibiotics given by WHO (2017), the test organisms chosen for this study are: extended-spectrum beta-lactams resistance *E. coli* (Critical Priority) and methicillin resistant *Staphylococcus aureus* (High Priority). It is noteworthy that half of 85-90% of all clinically reported infections from seven organisms are caused by *S. aureus* and *E. coli* (Reisner and Woods, 1999, Richards et al., 2018).

The antimicrobial activities of AgNPs, cysPpIX-AgNPs and PEI-cysPpIX-AgNPs were examined against a MRSA strain (BAA 44) purchased from ATCC and a wild-type MDR *E. coli* strain (accession number PRJNA806466). The MDR *E. coli* was isolated from Class B biosolids amended soil (Mays et al., 2021). It was confirmed to be resistant to tetracycline, gentamicin, ampicillin, sulfamethoxazole-trimethoprim and ciprofloxacin using the CLSI M100 Performance Standards (Weinstein et al., 2018). A non-resistant *E. coli* K-12 strain (Sigma-Aldrich) was used to as a control strain during the evaluation of the tolerance of MDR *E. coli* to PDI by various PS.

#### 3.4.2. MDR *E. coli* Library Preparation and Sequencing

A single bacterial colony of each strain was aseptically picked from the top of a LB agar plate using a sterile loop and inoculated into sterile LB broth media supplemented with tetracycline, ampicillin and sulfamethoxazole-trimethoprim at 50, 100 and 200  $\mu\text{g}/\text{mL}$  respectively. Bacteria cells were grown overnight (~ 18 hours) at 37 °C under continuous gentle mixing at 200 rpm. Overnight cells were harvested the following day by centrifugation at 7000 rpm for 5 min. Genomic DNA was extracted using QIAamp<sup>®</sup> DNA Mini kit (QIAGEN) following the manufacturer's protocol for bacterial extraction. The extracted DNA sample was quantified using Qubit<sup>®</sup> 3.0 fluorometer (3.0) based on the Qubit dsDNA HS Assay (Thermo Scientific<sup>™</sup>). The purity of the DNA was confirmed by measuring the concentration using a Nanodrop<sup>™</sup> UV-Vis spectrophotometer (Thermo Scientific<sup>™</sup>). The concentration and A260/A280 were 65.8 ng/ $\mu\text{L}$  and 2.02 respectively and confirmed to be of high purity for sequencing application. Sequencing was carried out on PromethION48 (Oxford Nanopore Technologies) using the SQK-LSK-109 ligation

sequencing kit. This MDR *E. coli* sample was sequenced alongside 14 other bacteria isolates for use in another study. Thus, EXP-NBD196 native barcoding was used for the pooled sequencing run to identify individual samples. The library preparation step, barcode ligation, adapter ligation and clean up, followed the Nanopore Native barcoding genomic DNA with EXP-NBD196 and SQK-LSK-109 (version NBE\_9129\_v109\_revB\_19Jan2021). For all isolates, 400 ng gDNA was used. DNA fragmentation step was not included in the protocol and Longer DNA fragments were enriched by washing pooled barcoded sample beads with long fragment buffer (LFB). The concentration of pooled DNA samples quantified after the adapter ligation and clean-up was obtained as 23.8 ng/ $\mu$ L. A volume of 12  $\mu$ L DNA library was added to a mixture of loading beads and sequencing buffer and loaded onto a new PromethION flow cell (FLO-PRO112). The flow cell used passed the flow cell check and it was primed before loading samples whilst observing standard procedure to prevent the introduction of air bubbles. In all library preparation steps, LoBind consumables (Eppendorf) were used and nuclease-free certified reagents as recommended in the protocol.

### 3.4.3. Nanoparticles Synthesis and Characterization

AgNPs, cysPpIX-AgNPs and PEI-cysPpIX-AgNPs were synthesized and characterized by Varsha Godakhindi (a PhD Student in the Department of Chemistry at the University of North Carolina Charlotte, USA). Details of the synthesis and characterization can be found in the resulting publication titled: *Enhancing the Inactivation of Antibiotic-Bacteria using Light-Activated Silver Nanoparticles: Influence of Silver Ion Release* (Article no 2 in List of Publications). Briefly, AgNPs was fabricated based on the co-

reduction method using sodium citrate and tannic acid (Bastus et al., 2014). cysPpIX-AgNPs was synthesized in two stages. First, PpIX was functionalized with cysteamine to afford a thiol derivative of PpIX called cysPpIX. Thereafter, AgNPs was functionalized with cysPpIX to form cysPpIX-AgNPs. The synthesis of PEI-cysPpIX-AgNPs was carried out by coating cysPpIX-AgNPs with PEI by electrostatic interaction (Figure 3.1).

#### 3.4.4. Bacterial Inactivation Experiment

AgNPs and cysPpIX-AgNPs stock solutions were prepared in dimethylformamide (DMF); while PEI-cysPpIX-AgNPs was prepared in nanopure water (18 M $\Omega$ .cm). A single bacterial colony of each strain was aseptically picked from the top of a LB agar plate using a sterile loop and inoculated into sterile LB broth media. Bacteria cells were grown overnight (~ 18 h) at 37 °C under continuous gentle shaking at 200 rpm. Overnight cells were harvested the following day by centrifugation at 7000 rpm for 5 min, washed twice with PBS and resuspended in 1X DPBS to achieve an absorbance of 0.5 McFarland turbidity standard (~1.5 x 10<sup>8</sup> CFU/mL). Before light irradiation, 2,970  $\mu$ L bacteria cells in 1X DPBS were incubated at room temperature (~37  $\pm$  2 °C) in the dark for 30 min with 30  $\mu$ L of each sample to achieve a working concentration of 1.5  $\mu$ g/mL for AgNPs, and 1  $\mu$ M cysPpIX-1.5  $\mu$ g/mL AgNPs for cysPpIX-AgNPs. The resulting DMF concentration in the reaction volume was  $\leq$  1%. Thereafter, cells were irradiated for 20 min without stirring in a Petri dish (60 x 15 mm) with a white light source (400–700 nm; 56 $\pm$  2 mW/cm<sup>2</sup>). The surviving cells were enumerated after 0, 4, and 24 h post irradiation in triplicate using the drop plate colony count method (Hurst et al., 2019). At specific time point, 100  $\mu$ L of the sample was withdrawn, serially diluted and 20  $\mu$ L of each dilution was spotted on LB agar.

The bacterial log inactivation was estimated using Equation 3.1. In all experimental groups, negative control and dark control samples were enumerated. A physical mixture of AgNO<sub>3</sub> and cysPpIX was used as a positive control. The concentration of AgNO<sub>3</sub> used corresponds to the amount of maximum Ag<sup>+</sup> (μg/L) released from the conjugate samples as determined from Ag<sup>+</sup> release profile (See Figure 3.7).

$$\text{Log inactivation of bacteria} = \log \frac{C_o}{C_t} \quad (3.1)$$

where  $C_o$  is the concentration (CFU/mL) of bacteria without the addition of nanoparticles and  $C_t$  is the bacterial concentration after the addition of nanoparticles and (or) light irradiation after time  $t$ .

#### 3.4.5. ARG Degradation Experiment

The MDR *E. coli* hosted a plasmid that contained *tetA* and *sulI* genes (Details in Section 2.4.2). The integrity of *tetA* and *sulI* genes in NPs treated MDR *E. coli* after 4 h and 24 h exposure was examined by qPCR and compared to untreated MDR *E. coli* (intracellular-ARG). Also, extracellular plasmids were directly exposed to AgNPs, cysPpIX-AgNPs, and PEI-cysPpIX-AgNPs for 24 h to examine the effect of ROS and Ag<sup>+</sup> on ARG degradation. AgNO<sub>3</sub> and cysPpIX were used as controls in all experimental groups.

#### 3.4.6. qPCR Quantification of ARG Degradation

The total volume of the qPCR reaction mixture was 20 μL consisting of 0.5 μL of each primer, 2 μL of DNA sample, 10 μL of SYBR green, and 7 μL of sterile nuclease-free water. The qPCR reaction cycle included one cycle at 95 °C for 2 min, 30 cycles at 95

°C for 5 s, an annealing step at T<sub>A</sub> (Table 3.1) for 1 min, and an elongation at 72 °C for 30 s, followed by a melt curve analysis from 65 °C to 95 °C. Each sample was analysed in triplicate independent experiments.

TABLE 3. 1 List of primers and qPCR amplification conditions

qPCR Amplicons	Forward primer (5' – 3')	Reverse primer (5' – 3')	T <sub>A</sub> * (°C)	Reference
<i>tetA</i> (210 bp)	GCTACATCCTGCTTGCCTTC	CATAGATCGCCGTGAAG AGG	55	(Zhang et al., 2019)
<i>sul1</i> (162 bp)	CGCACCGGAAACATCGCTG CAC	TGAAGTTCCGCCGCAAGG CTCG	55.9	(Pei et al., 2006)

\* Annealing temperature

### 3.5. Results and Discussion

#### 3.5.1. MDR *E. coli* Sequence Data Analysis, Classification and Identification

For the MDR *E. coli* (barcode 1), 378,283 total reads were analyzed and 343,575 were successfully aligned to NCBI complete genomes. Implementing a 1% abundance cutoff, the most abundant species in this mixed sample were *E. coli*, *S. aureus*, *P. fermentans*, *K. pneumoniae*, *P. aeruginosa*, and *L. granuli* with 158,479, 72,002, 22,492, 13,733, 6,043, and 3,503 reads respectively. For *E. coli*, 154,686 reads were species classified and the remaining reads were split amongst 112 child taxa/strains, with the largest amount of hits belonging to the CE10 strain. The de novo assembly of the reads generated a final genome consensus sequence. The MDR *E. coli* was identified as a K12 lineage, serotype O17:K52:H18 with a 99.98% match.

Of this *E. coli* portion of reads, 11,775 aligned to 327 unique entries in the Comprehensive Antibiotic Resistance Database (CARD) with an average accuracy of 91.4%. The highest abundance ARG entry was APH(3')-Ia; a transposon-encoded aminoglycoside phosphotransferase with 837 aligned reads. This was followed by *E. coli* rrsH gene modifications at 458 reads conferring resistance to spectinomycin in K-12 strains, and rpoB at 198 reads conferring resistance to rifampicin in O157 strains.

### 3.5.2. Bacterial Inactivation Experiment

MRSA and MDR *E. coli* are one of the most common causes of human and animal antibiotic resistant infections (Weese, 2010, Salomoni et al., 2017, Richards et al., 2018). These pathogens are considered as serious threats by the Centers for Disease Control and Prevention (CDC) and are part of the 'nine bacteria of international concern' (WHO, 2017, CDC, 2019). The antimicrobial properties of AgNP, cysPpIX-AgNP and PEI-cysPpIX-AgNP were tested against MRSA (ATCC BAA 44 strain) and a wild type MDR *E. coli*. For all cases, the concentration of AgNP in all samples was kept constant at 1.5  $\mu\text{g/mL}$  while cysPpIX concentration was 1  $\mu\text{M}$  in cysPpIX-AgNP and PEI-cysPpIX-AgNP. These concentrations were chosen based on the results from preliminary concentration optimization experiments (Figure 3.2). All NPs were individually incubated in the dark with microbes for 30 min prior to visible light irradiation for 20 min. The log bacterial inactivation of MRSA and MDR *E. coli* achieved using these NPs under dark and after light irradiation for 20 minutes are presented in Figure 3.3. The data showed that cysPpIX achieved a significantly higher inactivation of MRSA than any of the NPs. One reason for the higher inactivation of cysPpIX compared to NPs is the exposure time-dependent and

dose-dependent bactericidal action of silver-based NPs. Since intracellular  $\text{Ag}^+$  is responsible for the bactericidal action of silver-based NPs, it is required that  $\text{Ag}^+$  has sufficient time to diffuse through the cell membranes of bacteria for lethal action (De Matteis et al., 2015, Ishida, 2018). Whereas cysPpIX inactivate bacterial from ROS generated which outside the bacteria cell (Yin et al., 2015). On the other hand, no significant bacterial inactivation was recorded for MDR *E. coli*. This result suggests the tolerance of MDR *E. coli* to PDI relative to MRSA. Previous studies have shown that some Gram-negative bacteria tolerated PDI (Yin et al., 2015, Hurst et al., 2019)

To allow for adequate  $\text{Ag}^+$  contact time, samples were withdrawn post irradiation at 0h (i.e., immediately after 20 min irradiation), 4h and 24h post irradiation (for the light conditions); and at corresponding time point for the dark control. In a separate control experiment, the stability of the bacterial strains in PBS over 24 h was monitored to ensure that recorded inactivation was not due to nutrient starvation (Figure 3.4). The log bacterial inactivation achieved using these NPs under dark and light conditions are presented in Figures 3.5 and 3.6 for MRSA and MDR *E. coli* respectively. The results indicate that 1.5  $\mu\text{g}/\text{mL}$  of AgNP achieved  $< 1$ -log inactivation of MRSA both under light and dark conditions even after 24 h of exposure (Figures 3.5a and 3.5b). Similar results were obtained for cysPpIX-AgNP and PEI-cysPpIX-AgNP under dark conditions for time 0h, 4h and 24h ( $p > 0.05$ ). This low inactivation by AgNP at 1.5  $\mu\text{g}/\text{mL}$  was expected because typical minimum inhibitory concentrations (MIC) reported for AgNPs of similar sizes used in this study are about 3-10 folds higher (Martínez, 2008, Agnihotri et al., 2014, Malá et al., 2021). However, after light activation of these NPs, MRSA inactivation by cysPpIX-AgNP increased to  $\sim 1.5$ -log following immediate irradiation for 20 min (i.e., 0h) and

continuously increased to 2.3-log and 6.2-log after 4h and 24h contact time, respectively. For PEI-cysPpIX-AgNP, MRSA inactivation also increased in the order 0.2-log, 0.7-log and 3.2-log, as contact time increased in the order 0h, 4h and 24h, respectively. cysPpIX-AgNP achieved the highest inactivation of MRSA amongst the three NPs examined regardless of the contact time (Figures 3.5b).

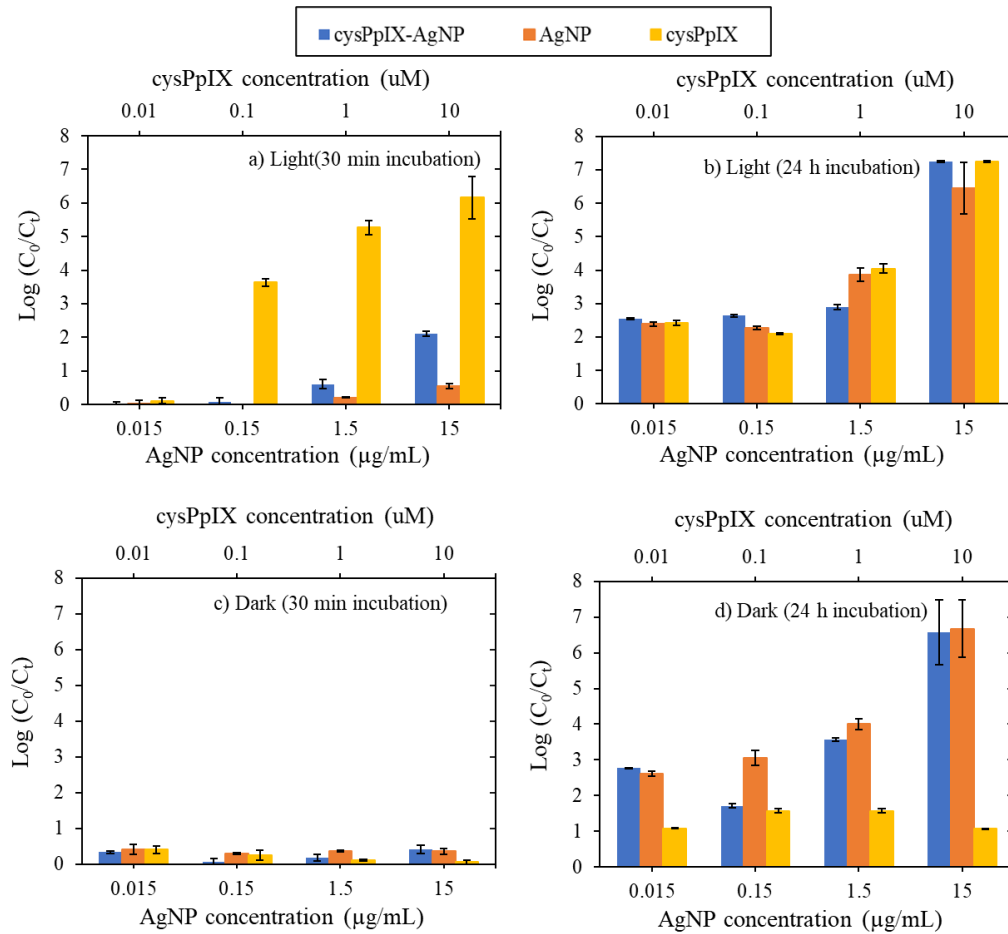


FIGURE 3. 2 Evaluating the Bacterial inactivation of MRSA after 20 minutes irradiation.

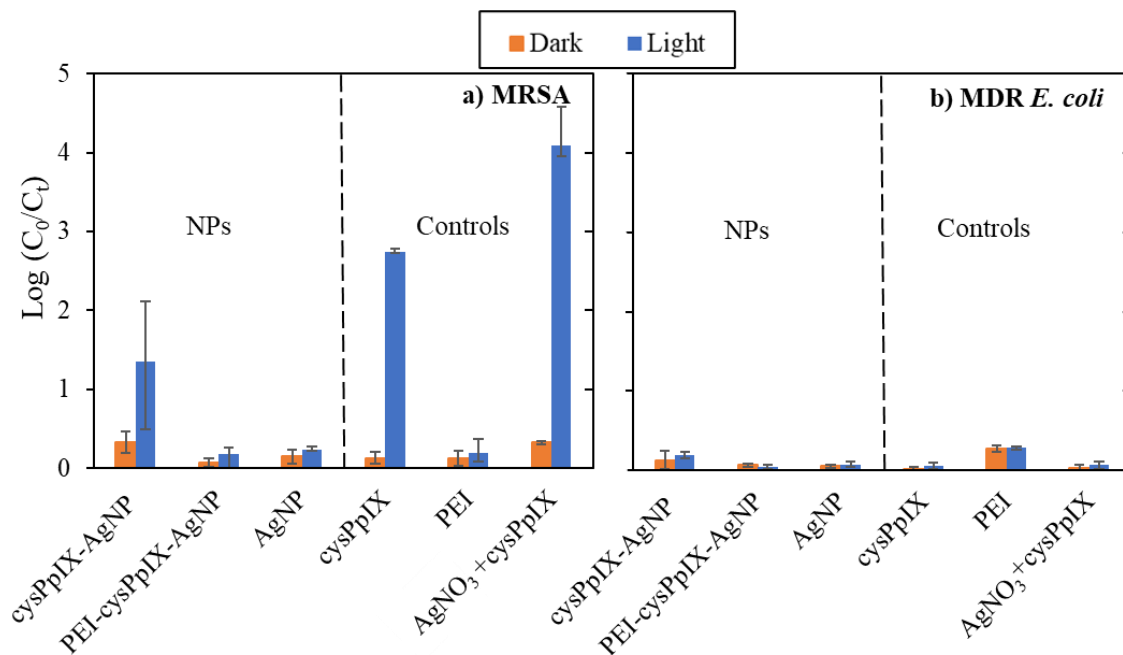


FIGURE 3. 3 Bacterial inactivation between MRSA and MDR *E. coli* after 20 minutes irradiation (30 minutes dark incubation prior to irradiation).

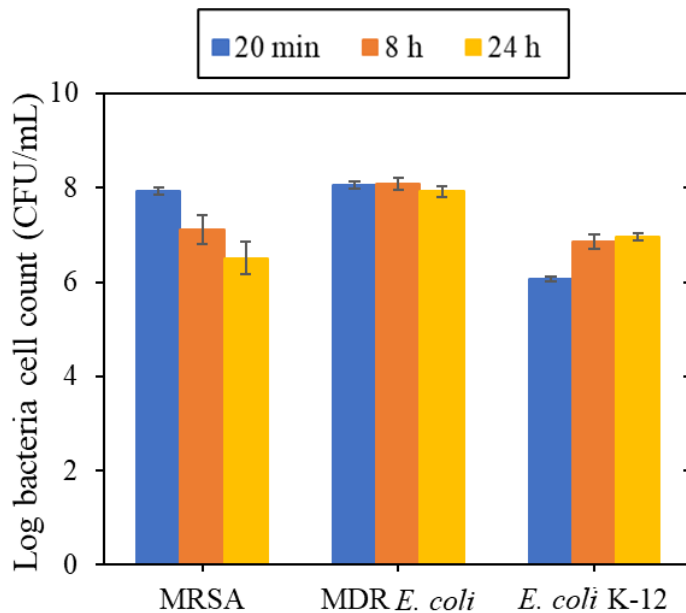


FIGURE 3. 4 Changes in the bacteria cell count in PBS with time (microbe stability test).

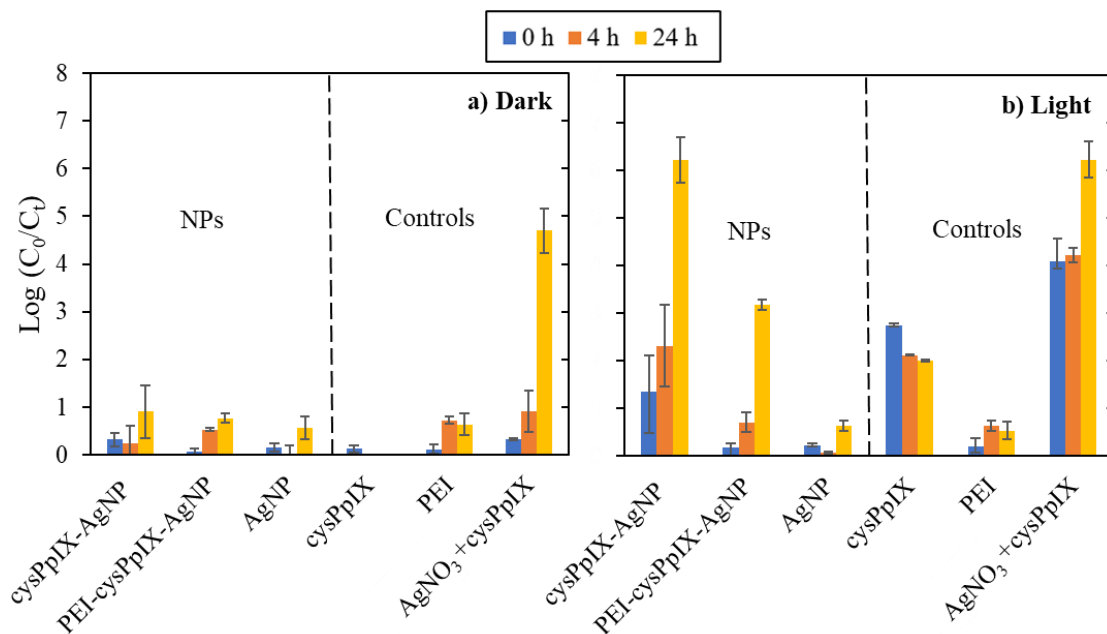


FIGURE 3. 5 Inactivation of MRSA under light activated conditions. 0 h time point indicates the achieved inactivation after light irradiation for 20 minutes. 4 h and 24 h show the bactericidal effect post-irradiation. Error bar is the standard error of mean (SEM) of three independent replicate experiments.

The inactivation of the Gram-negative MDR *E. coli* showed a similar trend as the inactivation of the Gram-positive MRSA. Under dark conditions, the log inactivation was  $<0.5$  log for all three NPs for time 0h, 4h and 24h ( $p > 0.05$ ) (Figures 3.6a). Similarly, cysPpIX-AgNP achieved the highest inactivation of  $\sim 8$ -logs after 24 hrs under light conditions (the limit of quantification since the starting bacteria concentration  $\sim 10^8$  CFU/mL) (Figures 3.6b). The increase in bacterial inactivation of MRSA and MDR *E. coli* by cysPpIX-AgNP following light irradiation is consistent with the patterns recorded in literature (Xie et al., 2017, Chen et al., 2019, Elashnikov et al., 2019, Shabangu et al., 2020, Malá et al., 2021, Ghasemi et al., 2021). Also, studies have reported complete elimination of MRSA and *E. coli* using AgNP only, however, MIC are at least  $5\mu\text{g/mL}$  depending on

the physiochemical properties of the examined AgNP (Martínez, 2008, Agnihotri et al., 2014, Pareek et al., 2018, Malá et al., 2021). Whereas, in this study, only 1.5  $\mu\text{g/mL}$  AgNP in cysPpIX-AgNP resulted in complete inactivation of MRSA and MDR *E. coli*. This again outlines the antimicrobial synergy of AgNP PS conjugates.

The incorporation of positive charges in molecules or NPs has been an important strategy to enhance the antimicrobial properties of PS (Hurst et al., 2019). The rationale is that an electrostatic interaction between the positively charged agents and the negatively charged surface of bacteria will bring them in close proximity, resulting in an improved antimicrobial effect (Yin et al., 2015, Hurst et al., 2019). In this work cysPpIX-AgNPs was functionalized with PEI following the same rationale where the positive surface charge of PEI would promote electrostatic interaction with bacteria cells, thus resulting in higher bacterial inactivation by PEI-cysPpIX-AgNP (Zhang et al., 2011, Meng et al., 2020). Nevertheless, the results showed a lower antimicrobial effect of PEI-cysPpIX-AgNP as compared with cysPpIX-AgNPs (Figure 3.5b and 3.6b). The observed pattern reveals that the addition of PEI did not enhance the antimicrobial property of cysPpIX-AgNP even though its positive surface charge should promote ROS interaction with cells due to increased electrostatic attraction (Merchat et al., 1996a, Merchat et al., 1996b). This lower antimicrobial activity of PEI-cysPpIX-AgNP compared to cysPpIX-AgNP can be explained from the lower concentration of  $\text{Ag}^+$  released by PEI-cysPpIX-AgNP (Figure 3.7). It has been reported that PEI is a chelating agent and can potentially bind  $\text{Ag}^+$ , reducing its amount in solution, and consequently its concentration in bacteria cells (Kobayashi et al., 1987, Zhou et al., 2006, Liu et al., 2018). This outcome suggests that cationic surface coatings are less likely to improve bacterial inactivation if they do not

promote  $\text{Ag}^+$  release, regardless of the electrostatic interaction promoted by opposite charge between cationic PEI-cysPpIX-AgNP and net-negative bacteria cells wall.

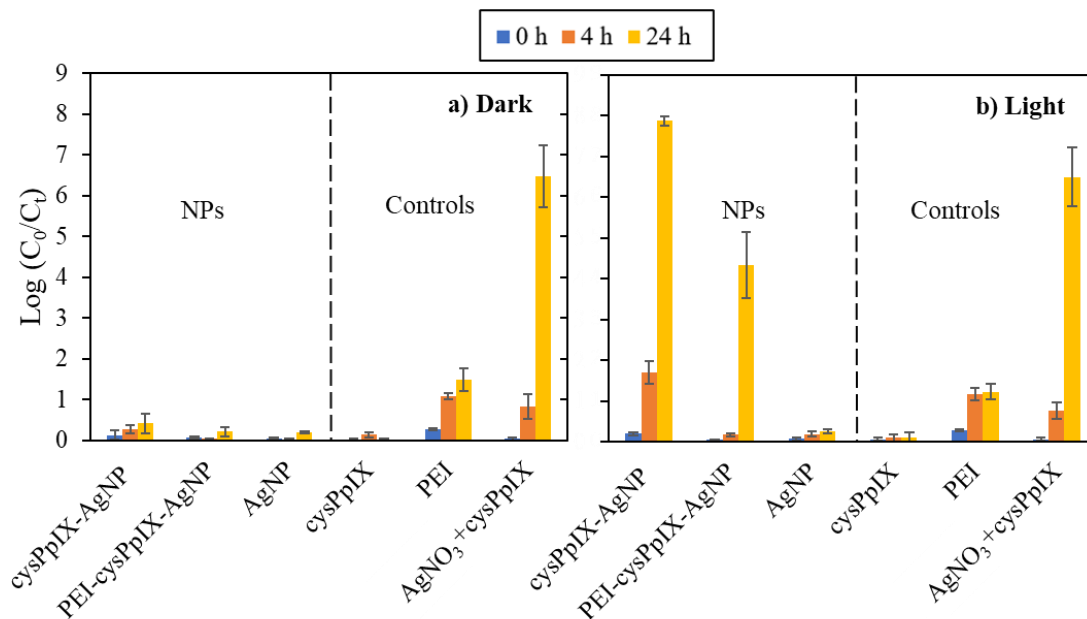


FIGURE 3. 6 Inactivation of MDR *E. coli* under light activated conditions. 0 h time point indicates the achieved inactivation after light irradiation for 20 minutes. 4 h and 24 h show the bactericidal effect post-irradiation. Error bar is the standard error of mean (SEM) of three independent replicate experiments.

Overall, the log inactivation of MRSA and MDR *E. coli* was in the order cysPpIX-AgNP > PEI-cysPpIX-AgNP > AgNP under light conditions irrespective of the contact time (Figures 3.5b and 3.6b). The order of bacterial log inactivation correlates with the trend of  $\text{Ag}^+$  release profile (cysPpIX-AgNP > PEI-cysPpIX-AgNP > AgNP) (Figure 3.7). This observation confirms the crucial role of optimized  $\text{Ag}^+$  release for enhanced AgNP-based antimicrobials, which in this platform is controlled by using light. Other reports have shown the importance of combining a PS with AgNPs to eliminate bacteria (Xie et al.,

2017, Chen et al., 2019, Elashnikov et al., 2019, Shabangu et al., 2020, Ghasemi et al., 2021, Malá et al., 2021). The broad-spectrum antimicrobial property demonstrated by cysPpIX-AgNP makes it a promising material for antimicrobial therapy.

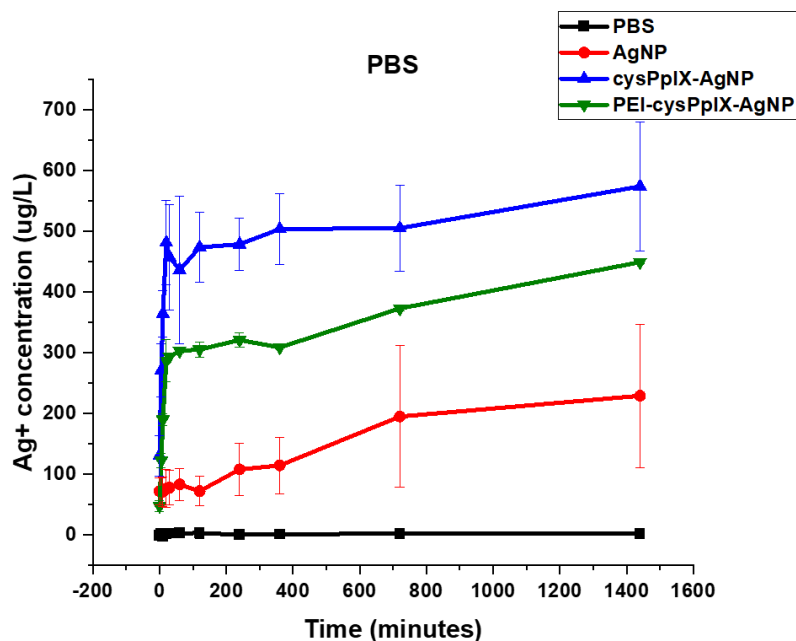


FIGURE 3. 7 Ag<sup>+</sup> release profile of AgNP, cysPpIX-AgNP and PEI-cysPpIX-AgNP under light condition. (Experiment by Varsha Godakhindi, 2022. Details in publication: *Enhancing the Inactivation of Antibiotic- Bacteria using Light-Activated Silver Nanoparticles: Influence of Silver Ion Release*. Article no 2 in List of Publications).

### 3.5.3. Roles of ROS in ARB Inactivation using Porphyrin-AgNP Conjugates

To further elucidate the role of ROS in the reported antimicrobial synergy in cysPpIX-AgNP conjugates, separate control experiments were conducted using cysPpIX alone for MRSA and *E. coli* treatment at 1 µM under the same experimental conditions as the NPs (Figures 3.5 and 3.6). The results show that cysPpIX achieved a maximum of 2.75

log inactivation of MRSA under light conditions (Figure 3.5). This suggests that ROS generated in PDI partially inactivated MRSA and therefore, contributed to the observed increase in the log inactivation of MRSA by cysPpIX-AgNP and PEI-cysPpIX-AgNP. Nevertheless, the total sum of the log inactivation by cysPpIX alone and AgNP only (i.e., 2.75-log + 0.64-log = 3.39-logs) was still much lower than the total inactivation achieved by cysPpIX-AgNP (6.2-log) after 24 h. This indicates that other factors such as increased  $\text{Ag}^+$  concentration contributed to the log inactivation (Figure 3.7). The inactivation of MRSA by PEI-cysPpIX-AgNP is comparable to the sum of the log inactivation by cysPpIX only and AgNP (3.18-logs vs 3.39-logs) after 24 h exposure ( $p > 0.05$ ). This again highlights that the positive charge of the PEI coat afforded did not improve the overall bacterial inactivation as expected.

On the other hand, MDR *E. coli* tolerated PDI using cysPpIX even up to 10  $\mu\text{M}$  concentration after light irradiation for 20 minutes (Figure 3.8). This pattern is consistent with reports in the literature (Merchat et al., 1996a, Yin et al., 2015, Hurst et al., 2019). It has been observed that Gram-negative bacteria are less susceptible to anionic PS (like porphyrins) than Gram-positive bacteria (Merchat et al., 1996a, Yin et al., 2015, Hurst et al., 2019). *E. coli* K-12, a non-resistant bacterial strain, was used as a control strain to observe whether this observation was related to the Gram stain or dependent on the *E. coli* strain. The results showed that the tolerance to PDI was strain-dependent because *E. coli* K-12 was inactivated at 1  $\mu\text{M}$  cysPpIX concentration. MDR *E. coli* is a strain isolated from an environmental sample, while *E. coli* K-12 is a laboratory strain. The physiological welfare of laboratory bacterial strains that have been cultured and sub-cultured in nutrient-rich and stress-free laboratory environments is readily affected by stressors Aldsworth

(Aldsworth et al., 1999). However, MDR *E. coli* is well adjusted to stressful environmental conditions such as heat, antibiotics, low nutrients and other oxidative stresses of the environments it was isolated (Roszak and Colwell, 1987).

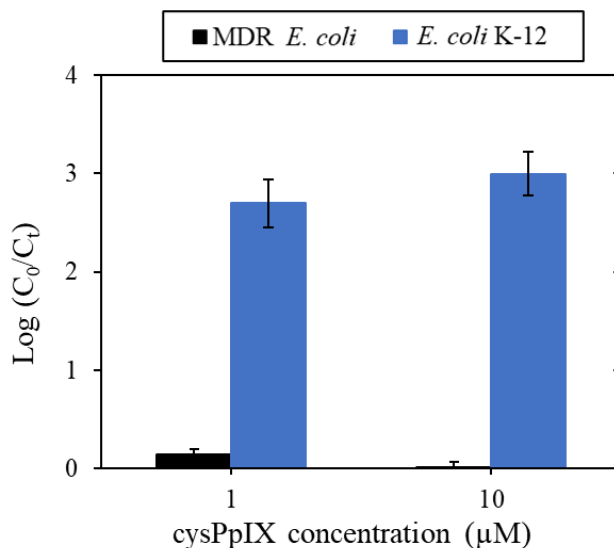


FIGURE 3. 8 Tolerance of MDR *E. coli* to PDI using cysPpIX (30 min dark incubation and 20 min irradiation time).

Upon conjugation of cysPpIX with AgNP, MDR *E. coli* was inactivated to below quantification limits (Figure 3.6b). This shows that cysPpIX-AgNP conjugates not only have synergistic antimicrobial property but enhanced application as a broad-spectrum antimicrobial agent (Gram-positive and Gram-negative). Control experiment with AgNO<sub>3</sub> having the same Ag<sup>+</sup> concentration as the maximum concentration of Ag<sup>+</sup> released by light-activated cysPpIX-AgNP (in Figure 3.7), showed that Ag<sup>+</sup> concentration was vital to the inactivation of the MDR *E. coli* (Figure 3.9). It is sufficient to say that the increased log inactivation of MDR *E. coli* by cysPpIX-AgNP and PEI-cysPpIX-AgNP was due to

increased  $\text{Ag}^+$  released from the interaction of ROS with AgNP core as confirmed by ICP-OES experiment (Figure 3.7).

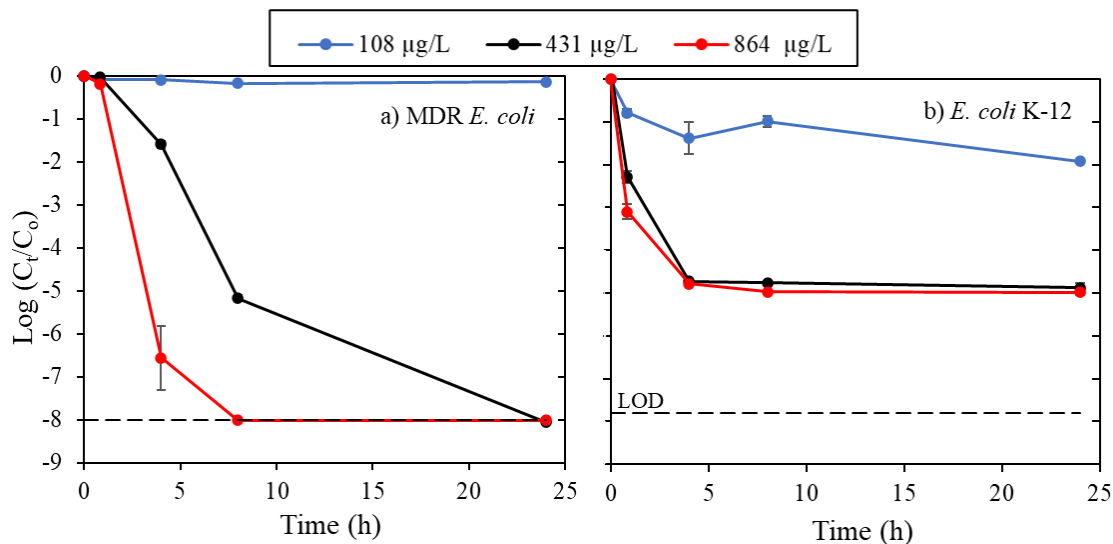


FIGURE 3. 9 Inactivation of bacteria using  $\text{AgNO}_3$ . Concentration is expressed in  $\mu\text{g/L}$   $\text{AgNO}_3$  as  $\text{Ag}^+$ .

#### 3.5.4. ARG Degradation using Porphyrin-AgNPs

The study further used qPCR analysis to investigate possible damages to *tetA* and *sull* genes encoded on the MDR *E. coli* plasmid after bacterial inactivation by AgNP, cysPpIX-AgNP and cysPpIX. The standard curves for *tetA* and *sull* amplicons are given in Figure 3.10. The degradations of *tetA* and *sull* in extracellular plasmids and intracellular plasmids were examined. Figures 3.11 and 3.12 show that the recorded cell death from AgNP, cysPpIX-AgNP and cysPpIX may not have resulted from damage to ARGs in MDR *E. coli* based on qPCR assay. Although ROS generated by PS cause DNA damage ranging from single-strand breaks to double-strand breaks (Fiel et al., 1981), cysPpIX at 1  $\mu\text{M}$  did not result in significant damage to the monitored *tetA* and *sull* amplicons relative to the

control untreated samples (Figures 3.11). This could be because qPCR measures only a small segment of the DNA and ROS oxidation damage to DNA may have occurred outside the monitored qPCR amplicon region (He et al., 2019).

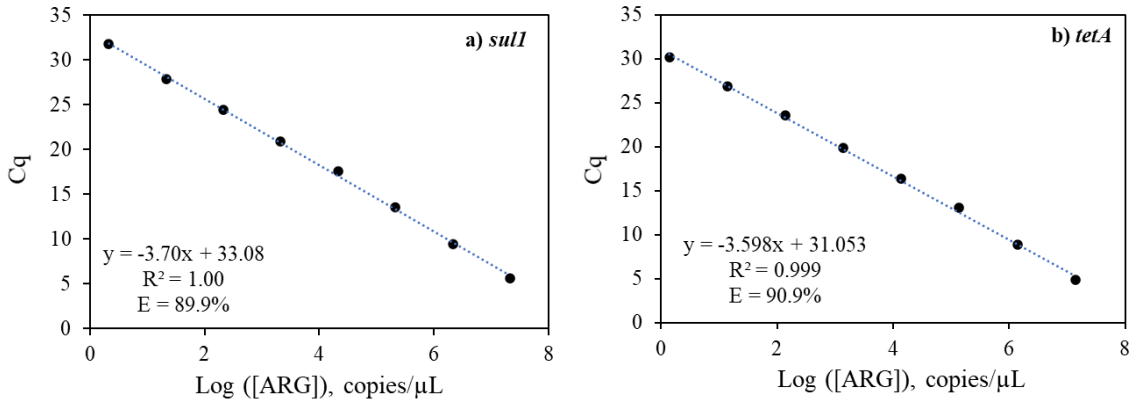


FIGURE 3. 10 Standard curves for *sull* and *tetA* ARG amplicons.

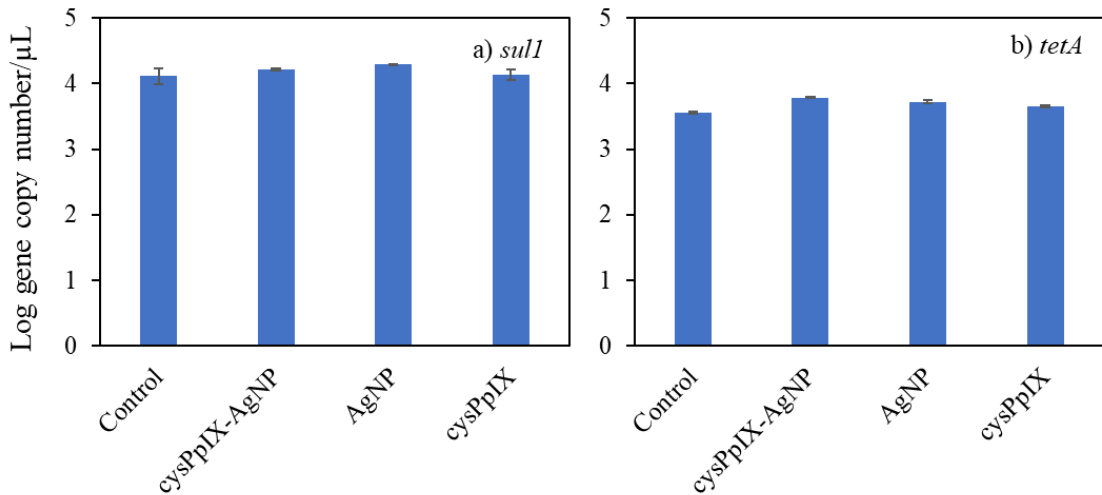


FIGURE 3. 11 Degradation of extracellular ARG encoded on MDR *E. coli* plasmid using AgNP, cysPpIX-AgNP and cysPpIX (1.5  $\mu\text{g}/\text{mL}$  AgNP and 1  $\mu\text{M}$  cysPpIX). Contact time was 24 hrs. Control refers to samples that were not treated with any of the NPs or PS.

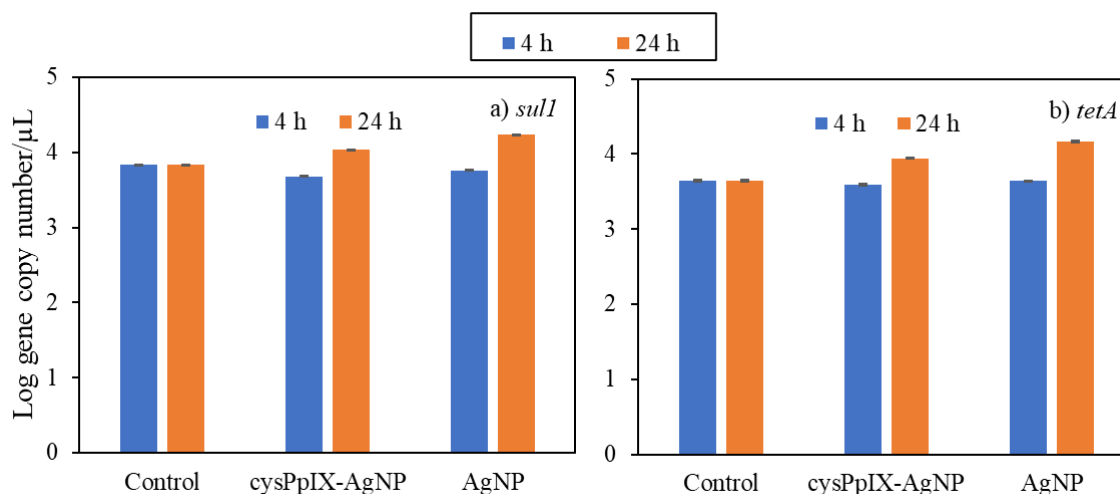


FIGURE 3.12 Degradation of intracellular ARG in MDR *E. coli* plasmid using AgNP and cysPpIX-AgNP (1.5 μg/mL AgNP and 1 μM cysPpIX). Control refers to samples that were not treated with any of the NPs or PS.

Moreover, several studies have reported DNA damage due to AgNPs and Ag<sup>+</sup> using assays based on DNA damage signaling pathways (Piao et al., 2011, AshaRani et al., 2012, Ahn et al., 2014, McShan et al., 2014, Ishida, 2018), circular dichroism spectroscopy (Rahban et al., 2010) and gel electrophoresis assay (Fiel et al., 1981, Lin et al., 2016). However, the qPCR assay used here suggests that no damage occurred to the *sull* amplicon monitored even at an extremely high concentration of 5.4 mg/L Ag<sup>+</sup> (Figure 3.13). It is noteworthy that the maximum Ag<sup>+</sup> release by cysPpIX-AgNP causing 7-log bacterial inactivation was only 0.4 mg/L. This implies that Ag<sup>+</sup> induced DNA damages were not detectable by the qPCR amplicons measured in this study. Similar results were obtained by Ahn et al. (2014) in a study that showed oxidative DNA damage based on significant increase in 8-OHdG levels in AgNO<sub>3</sub> and AgNP treated *Caenorhabditis elegans*. Whereas, no DNA damage was detectable by qPCR. This could be because Ag<sup>+</sup> induced DNA

damage are small oxidative modification of bases that are not polymerase-inhibiting DNA lesion (Meyer, 2010, Ahn et al., 2014). Thus, are hard to detect by qPCR.

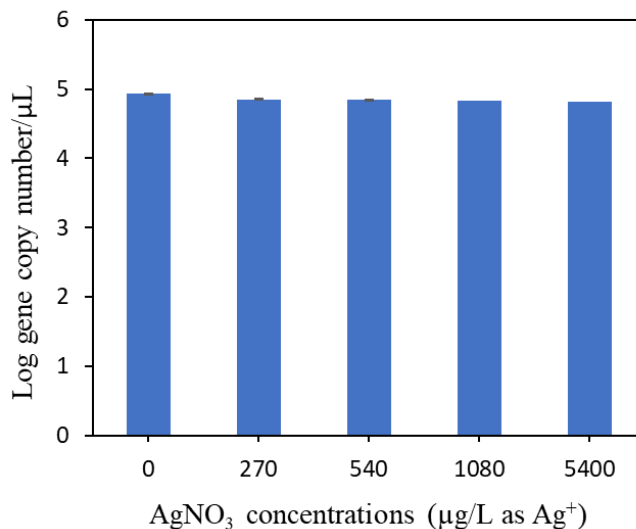


FIGURE 3. 13 Effect of Ag<sup>+</sup> on the degradation of *sull* gene in MDR *E. coli* plasmid after 24 hrs exposure.

### 3.6. Summary

The results showed that bacterial inactivation increased with an increase in Ag<sup>+</sup> release profile of porphyrin-AgNP conjugates. Porphyrin-AgNP conjugates (cysPpIX-AgNPs and PEI-cysPpIX-AgNPs) demonstrated broad-spectrum antibacterial action resulting in > 7 log inactivation of MRSA and MDR *E. coli*. Bacterial inactivation achieved by silver-based NPs was independent of the Gram-stain classification of the examined bacterial strains. The cationic surface coating of PEI in PEI-cysPpIX-AgNPs did not improve bacterial inactivation since it did not promote Ag<sup>+</sup> release in comparison with cysPpIX-AgNP. Potential damage to ARGs by Ag<sup>+</sup> was not detectable by the qPCR amplicons monitored in this study.

## CHAPTER 4. ANTIBACTERIAL AND ANTIVIRAL ACTIVITY OF MONOGLYCERIDE NANO-EMULSIONS

### 4.1. Literature Review

Broad-spectrum antibacterial agents with novel bacterial targets for which microorganisms cannot develop resistance via genetic evolution or mutation are in great demand (Jackman et al., 2016). The rise in antimicrobial resistance (AMR) has led to renewed interest in antimicrobial lipids because they are membrane-active antimicrobial agents with a low frequency of resistance development (Jackman et al., 2016, Fletcher et al., 2020). Antimicrobial lipids are composed of free fatty acids and monoglycerides. Free fatty acids are made up of saturated and unsaturated carbon chains and a carboxylic acid group (Jackman et al., 2016) (Figure 4.1). Monoglycerides are made of fatty acids and glycerol linked by an ester bond (Yoon et al., 2018a). Antimicrobial lipids are known to kill enveloped viruses, Gram-positive and Gram-negative bacteria. The antiviral and the antimicrobial activities of lipids have been studied extensively (Kabara et al., 1972, Kabara et al., 1977, Kabara, 1978, Kristmundsdóttir et al., 1999, Thormar et al., 1999, Bergsson et al., 2001, Bergsson et al., 2002, Thorgeirsdottir et al., 2003, Thormar et al., 2006, Fletcher et al., 2020). Monoglycerides have become attractive as broad-spectrum antibacterial agents (Kabara et al., 1972, Kabara et al., 1977, Jackman et al., 2016). Monoglycerides formulations have high antiviral properties relative to the free fatty acids (Thorgeirsdottir et al., 2003).

Monocaprin, the 1-monoglyceride of capric acid, has been recorded to rapidly inactivate Gram-negative and Gram-positive bacterial species (Thorgeirsdottir et al., 2003, Thormar et al., 2006). Moreover, these molecules are cheap, naturally abundant,

biocompatible and have a low frequency of bacterial resistance development (Kabara, 1978, Jackman et al., 2016, Churchward et al., 2018, Churchward et al., 2020). In addition to its potential use for the treatment of established infections, monocaprin formulations can be manufactured as a topical antimicrobial to prevent the transfer of pathogens through mucosal membranes into the body (Thorgeirsdottir et al., 2003, Thormar et al., 2013). Also, it has a structure similar to the lipids of the natural immune system in humans (Thorgeirsdottir et al., 2003, Thormar et al., 2013). However, monocaprin has a very low water solubility which is a limitation to its use in pharmaceutical formulations. Attempts to improve the solubility of monocaprin in pharmaceutical formulations involve the use of co-solvent (Thorgeirsdottir et al., 2003), surfactants (Thorgeirsdottir et al., 2003, Thormar et al., 2006) and excipient (Kristmundsdóttir et al., 1999, Thormar et al., 1999). All these methods have always included the addition of one or more inactive reagents that potentially lower the antiviral activity of monocaprin (Kristmundsdóttir et al., 1999, Thorgeirsdottir et al., 2003).

In recent years, nanotechnology has been exploited to improve the biological and chemical activities of antimicrobial agents (São Pedro et al., 2013, Fernandes et al., 2014, Yariv et al., 2015, Fernandes et al., 2016, Gupta et al., 2019, Mamun et al., 2021, Tan et al., 2021). Materials at the nanoscale display higher chemical reactivities than their bulk form due to the large surface area to volume ratio of materials in sizes between 1 to 100 nm (Xu et al., 2012, Singh et al., 2014, Yariv et al., 2015). Hence, lower MICs have been reported for antimicrobial agents at the nanoscale relative to bulk compounds (Yariv et al., 2015). Organic NPs penetrate more into cells than the bulk form. Sonochemistry, one of the earliest methods of nanomaterial fabrication, is a simple technique for generating

organic nanoparticles (Suslick and Crum, 1997, Gedanken, 2003, Gedanken, 2004, Qiao et al., 2011). The sonochemistry technique involves an acoustic cavitation process that occurs from the application of powerful ultrasound radiation (20 kHz–10 MHz) to a molecule causing chemical bonds to break (Gedanken, 2003, Qiao et al., 2011) (Figure 4.2). This technique has been used to improve the pharmacological activity of other organic compounds such as penicillin and Vitamin B<sub>12</sub> (Fernandes et al., 2014, Yariv et al., 2015, Fernandes et al., 2016). Herein, it was hypothesized that the preparation of monocaprin at the nanoscale using simple sonochemistry techniques will improve its solubility and antimicrobial property without the addition of any co-solvent or surfactant.

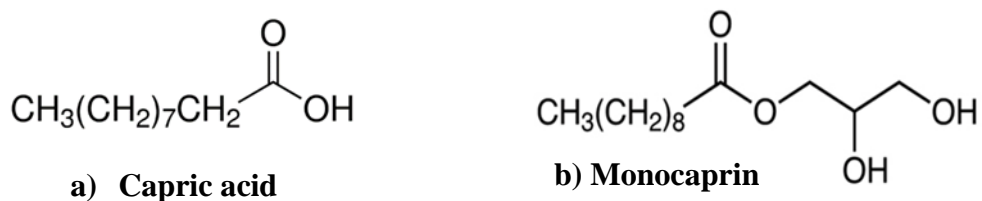


FIGURE 4. 1 Chemical structure of capric acid (Free fatty acid) and Monocaprin (Monoglyceride).

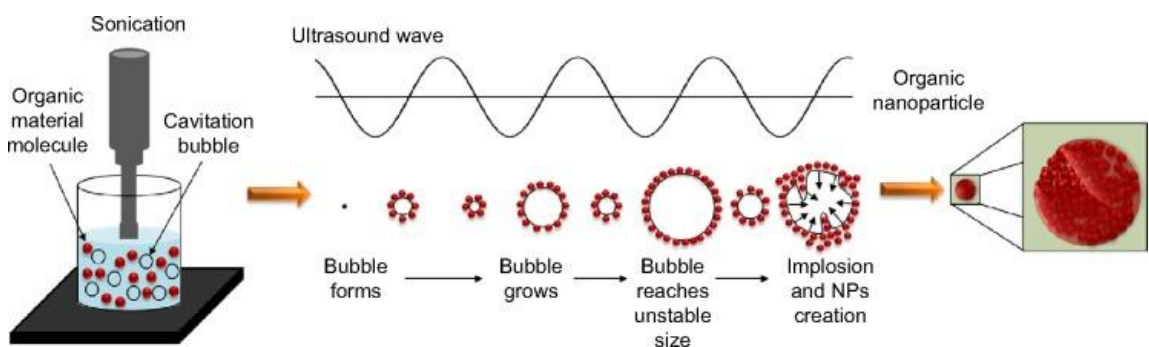


FIGURE 4. 2 The generation of organic nanoparticle due to acoustic cavitation phenomenon during sonochemistry. During sonication, bubbles are generated in the liquid and organic molecules form a shell around bubbles. Bubbles grow in volume as solvent or

solute vapour diffuses into the bubbles. A stage is reached when bubbles become unstable resulting in implosion and the collapse of molecules shell into the center of the bubble. This process creates nanoparticles (NPs) shown in the magnified form at the end of the process. Adapted from Yariv et al. (2015).

#### 4.2. Objectives of the Chapter

- i. Prepare and characterize nano-monocaprin as an antimicrobial agent.
- ii. Compare the antimicrobial activity of nano-monocaprin with the bulk-monocaprin suspension.
- iii. Examine the antimicrobial action of nano-monocaprin at various pH.
- iv. Examine the cytotoxicity of the synthesized nano-monocaprin.

#### 4.3. Study Overview

The study evaluated the use of nanoscale monocaprin as the first line of defense antimicrobials agent to prevent the entrance of intracellular pathogens such as *E. coli*, SARS-CoV-2 etc. The study compared the efficacy of nanoscale and bulk form monocaprin emulsions. Nano-monocaprin was prepared using sonochemistry technique. The antiviral activity of the two forms of nano-monocaprin: intermediate versus continuous sonication processes were examined. Enveloped bacteriophage phi6 was used as a surrogate for SARS-CoV-2 (Sands, 1977). The overall schematic of the study is shown in Figure 4.3.

#### 4.4. Materials and Method

##### 4.4.1. Biological and Chemical Reagent

Agar (VWR Life Science), tryptic soy broth (TSB) (Sigma Aldrich), ampicillin, streptomycin, monocaprin ( $\geq 98\%$  GC grade, TCI America, Inc), Dulbecco's modified Eagle's medium (DMEM) (Thermo Fisher Scientific), Roswell Park Memorial Institute (RPMI) media (Corning), Fetal Bovine Serum (FBS) (Corning), penicillin-streptomycin (pen-strep) (Corning), Glutamax (Gibco), non-essential amino acids (NEAA), 1X Dulbecco's phosphate buffer saline (DPBS) (Corning), phosphate buffered saline solution (10 mM, Sigma Aldrich), tween20 (Fisher Scientific), pH buffer 7 and 4.

##### 4.4.2. Preparation of Bulk- and Nano-monocaprin

Bulk-monocaprin was prepared in a Pyrex glass bottle by manually mixing monocaprin ( $\geq 99\%$ ) in nanopure water (18 M $\Omega$ .cm) to obtain a stock solution of 4 mM (Figure 4.3). Nano-monocaprin was prepared using a part of the bulk-monocaprin stock solution by sonochemistry technique (Yariv et al., 2015). Briefly, sonication was done intermittently (30 sec sonication, 30 sec manual mixing to a total of 7 min) and continuously for 20 min using an ultrasonic cleaner ( $47 \pm 3$  kHz,  $28 \pm 2$  °C, Branson 2210R-MTH). Nano-monocaprin at pH 4 and pH 7 were prepared in pH buffered solutions instead of nanopure water. For nano-monocaprin + tween20, tween20 was added after nano-monocaprin was prepared, just before the antiviral experiment. The absorbance spectra of bulk-monocaprin and nano-monocaprin (continuous and intermittent) were determined using a Hach DR 6000<sup>TM</sup> UV-Vis Spectrophotometer.

#### 4.4.3. Preparation of Bacteriophage Stock Suspension

phi6 (HER 102) and host bacteria *Pseudomonas syringae* (HER 1102) were purchased from Félix d'Hérelle Reference Center for Bacterial Viruses Université Laval (Québec, Canada). MS2 (ATCC 15597-B1) and host bacteria *E. coli* HS(pFamp)R (ATCC 700891) were purchased from the American Type Culture Collection (ATCC, USA). Stock suspensions of phi6 and MS2 were prepared using the top agar overlay technique (Wood et al., 2020). Bacteriophage was propagated using 100 µL of lyophilized bacteriophage stock mixed with 100 µL of overnight host bacteria in 5 mL of molten soft tryptic soy agar (TSA) (0.6% agar). The mixture was uniformly spread over hard TSA (1.5%) plates and allowed to solidify. Subsequently, agar plates were incubated for 18 h. *P. syringae* was incubated at  $24 \pm 2^\circ\text{C}$  while *E. coli* HS(pFamp)R (ATCC 700891) was cultured at  $37^\circ\text{C}$  on TSA supplemented with 15 µg/mL of ampicillin and streptomycin and 2.25 mM CaCl<sub>2</sub>. Top agar with lysed bacteria cells was aseptically harvested, 15 mL of TSB added and centrifuged at 7000 rpm for 15 min. The supernatant was removed and filtered through a sterile 0.2 µm syringe filter to remove residual bacteria. Stock bacteriophage was stored at  $4^\circ\text{C}$  for subsequent use.

#### 4.4.4. Bacteriophage Inactivation using Nano- and Bulk-monocaprin

phi6 and MS2 suspensions (phi6 and MS2) were used at a concentration of  $\sim 1 \times 10^7$  PFU/mL in TSB. The titer of the bacteriophage was determined by using the double agar overlay plaque assay. Bacteriophage inactivation experiments were carried out by mixing 500 µL of bacteriophage suspensions and 500 µL each sample (i.e., nano-monocaprin or bulk-monocaprin) under varying contact time (1 to 5 min). After

predetermined time points, 100  $\mu\text{L}$  of bacteriophage and 100  $\mu\text{L}$  of  $1.5 \times 10^8$  CFU/mL of overnight host bacteria were mixed in 5 mL of molten soft tryptic soy agar (TSA) (0.6% agar). The mixture was uniformly spread over hard TSA (1.5%) plates and allowed to solidify. Agar plates were incubated for 18 h at conditions described in Section 4.4.3. Bacteriophage were treated with pH buffer solution and(or) TSB (500  $\mu\text{L}$ ) as negative control. Bacteriophage inactivation was obtained based on Equation 4.1.

$$\text{Log inactivation of bacteriophage} = \log \frac{C_o}{C_t} \quad (4.1)$$

where  $C_o$  is the concentration (PFU/mL) of bacteriophage without the addition of nano/bulk monocaprin and  $C_t$  is the bacteriophage concentration after the addition of nano/bulk monocaprin for time  $t$ .

#### 4.4.5. *E. coli* Inactivation using Nano-monocaprin

The antibacterial action of nano-monocaprin was evaluated using a wild-type *E. coli* strain isolated from a class B biosolid amended soil (Mays et al., 2021). Briefly, 500  $\mu\text{L}$  of bacterial suspension in PBS ( $1.5 \times 10^8$  CFU/mL) and 500  $\mu\text{L}$  of two-fold serially diluted nano-monocaprin solutions (0 - 2.5 mM) were mixed for a contact time of 5 min. pH buffer solution (500  $\mu\text{L}$ ) was added instead of nano-monocaprin solution as the negative control. The reduction in bacterial cell count following the treatment was evaluated using the drop plate method. Bacteria inactivation was obtained based on Equation 4.2.

$$\text{Log inactivation of bacteria} = \log \frac{C_o}{C_t} \quad (4.2)$$

where  $C_o$  is the concentration (CFU/mL) of bacteria without the addition of nano-monocaprin and  $C_t$  is the bacteria concentration after the addition of nano-monocaprin for time  $t$ .

#### 4.4.6. Cytotoxicity of Nano-monocaprin

The CellTiter 96® AQueous One Solution Cell Proliferation Assay (MTS) was carried out to evaluate the biocompatibility of the synthesized nano-monocaprin. Human Pancreatic Duct Epithelial Cell (HPDE) and HeLa cervical cancer cell lines were used for the cell viability assay to represent the effect of nano-monocaprin on normal and cancer cell lines, respectively. HPDE was cultured in DMEM supplemented with 10% FBS, 1% penicillin/streptomycin, 1% Glutamax and 1% non-essential amino acids. HeLa cells were cultured in RPMI media supplemented with 10% FBS and 1% penicillin/streptomycin. Cells were seeded in 96 well plates (1,000 cells per well) and incubated overnight (5% CO<sub>2</sub>, 37 °C). Thereafter, cells were incubated with media containing ten-fold serially diluted nano-monocaprin (0 to 2 mM) for 24 h (5% CO<sub>2</sub>, 37 °C). Cell viability (%) was calculated using Equation 4.3.

$$\% \text{ Cell viability} = \frac{A_{\text{sample}} - A_{\text{blank}}}{A_{\text{control}} - A_{\text{blank}}} \times 100 \quad (4.3)$$

where  $A_{\text{sample}}$ ,  $A_{\text{control}}$  and  $A_{\text{blank}}$  are the absorbance values of the nano-monocaprin treated cells, untreated cells, and media respectively. IC<sub>50</sub> values were determined by nonlinear regression of normalized cell viability data using GraphPad Prism (v8.3.0 for Windows).

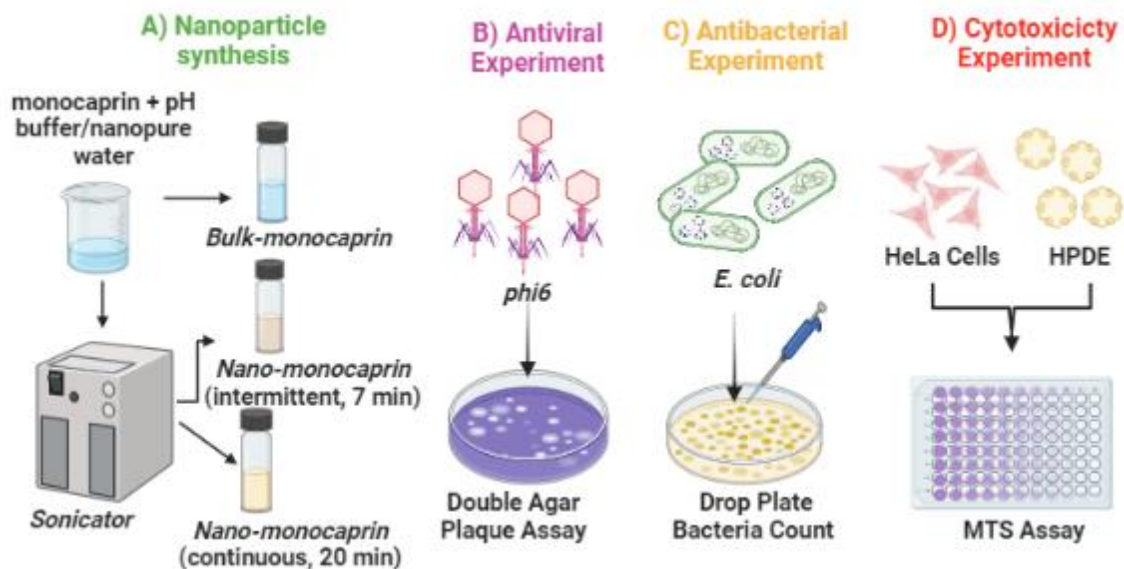


FIGURE 4. 3 Schematics of the antiviral and antibacterial assays using nano-monocaprin.

## 4.5. Results and Discussion

### 4.5.1. Characterization of Nano-monocaprin

The size of NPs generated by sonochemistry is influenced by the sonication time (Yariv et al., 2015). This study evaluated the influence of sonication time by testing two sonication patterns: intermittent sonication (every 30 sec for 7 mins) and continuous sonication for 20 minutes. The stock solution (4 mM) of the nano-monocaprin (continuous) appeared as a clear solution compared to the milky formations of the nano-monocaprin (intermittent) and bulk-monocaprin (Figure 4.4). This suggests an improved solubility by the sonication process (Figure 4.4). The absorption spectra of the nano-monocaprin and bulk-monocaprin were observed to verify that the chemical structure of monocaprin was unaltered (Figure 4.5). Figure 4.5 shows that bulk-monocaprin and nano-monocaprin had the same absorption spectra. This indicates that no structural changes occurred due to

sonication. Nano-monocaprin (20 minutes sonication time) has a lower absorption value than the bulk-monocaprin because of it is a clear solution compared to the milky solution of bulk-monocaprin (Figure 4.4)

#### 4.5.2. Antimicrobial Effect of Nano-monocaprin and Bulk-monocaprin

Figure 4.6 shows that at 2 mM (pH 7), nano-monocaprin prepared by continuous sonication (20 min) achieved 2.5 times higher phi6 inactivation than that prepared by intermittent sonication (7 min) after 1 min contact time. It has been reported that the particle size of molecules significantly decreases with sonication time in sonochemistry (Yariv et al., 2015). Thus, a longer sonication time means smaller particle size resulting in greater penetration and interaction with the lipid envelope of the virus (Thormar et al., 2013, São Pedro et al., 2013, Yariv et al., 2015). However, after 5 mins contact time, no difference was observed in the antiviral activity of the two forms of nano-monocaprin (Figure 4.6). This shows the time-dependent antiviral action of monocaprin. This time-dependent antiviral activity of antimicrobial lipids is reported in literature (Sands, 1977, Wang and Johnson, 1992, Bergsson et al., 1998). With this observation, subsequent antiviral and antimicrobial tests were carried out using the nano-monocaprin prepared by continuous sonication (called nano-monocaprin henceforth).

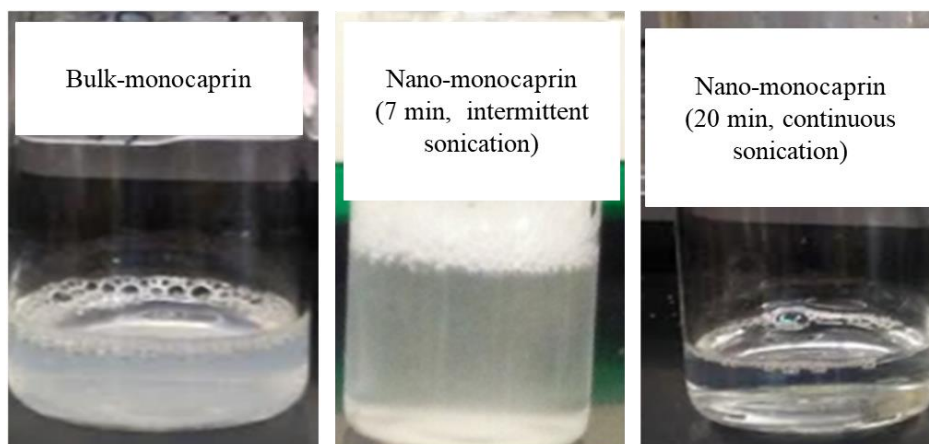


FIGURE 4. 4 Physical appearance of nano-monocaprins and bulk-monocaprin at 4 mM concentration.

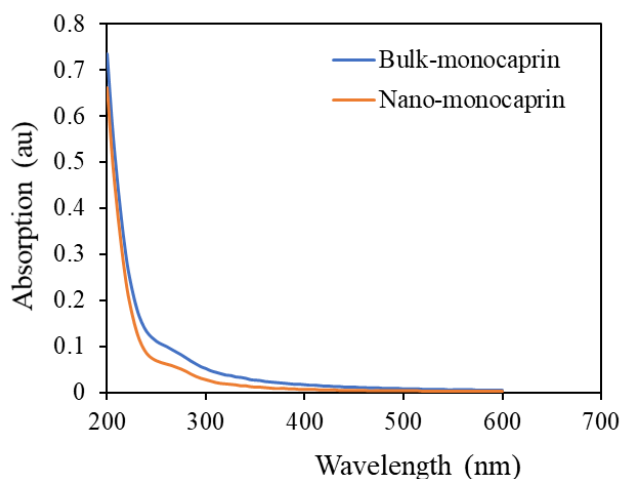


FIGURE 4. 5 Absorbance spectra of bulk-monocaprin and nano-monocaprin (20 min sonication, continuous) (4 mM, in nano-pure water).

Figure 4.7 shows that  $> 7$ -log  $\phi 6$  inactivation was achieved at 2 mM and 5 min contact time using nano-monocaprin. Whereas only  $\sim 4$  log inactivation of  $\phi 6$  was recorded for bulk-monocaprin. This result is because compounds in nanoscale have higher reactivities than in bulk form due to the high surface area to volume ratio (Fernandes et al., 2014, Singh et al., 2014). Thus, nano-monocaprin interacted better with the lipid envelope

of phi6 than bulk-monocaprin, causing faster lysis of the lipid envelope. Tween20, a surfactant commonly used to improve the solubility of monocaprin (Thormar et al., 2006), added (1.5% v/v) to nano-monocaprin (2 mM) further improved the antiviral activity of nano-monocaprin at a short contact time of 1 min (Figure 4.8).

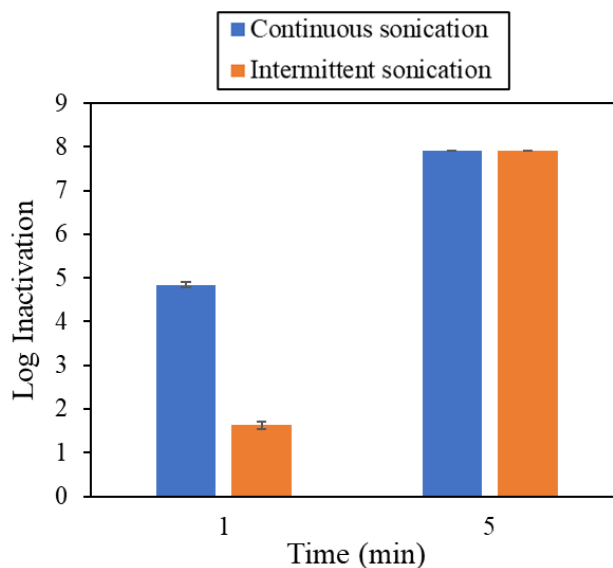


FIGURE 4. 6 Optimization of nano-monocaprin preparation method (2 mM, pH 7). Error bars are the standard deviation of triplicate plaque counts for each experiment condition.

pH is a factor that has been recorded to influence the antimicrobial activity of monocaprin (Petschow et al., 1996, Thormar et al., 2006, Thormar et al., 2013). The study compared the antiviral activity of nano-monocaprin at pH 4 and 7 with the goal of lowering the inhibitory concentration (Figure 4.9). At a high concentration of 2 mM and 5 min contact time, no difference in antiviral activity was recorded for nano-monocaprin at pH 4 and pH 7. The replication of phi6 was inhibited more using nano-monocaprin at an acidic pH 4 than pH 7 at 0.25 and 0.5 mM. High acidity weakens the outer lipid coat and allows more lipids to penetrate cellular components (Thormar et al., 2013). This implies that the

inhibitory concentration of nano-monocaprin against phi6 can be reduced using formulation at acidic. The effectiveness of nano-monocaprin at acidic pH opens the possibility for its use in many pharmaceutical formulations.

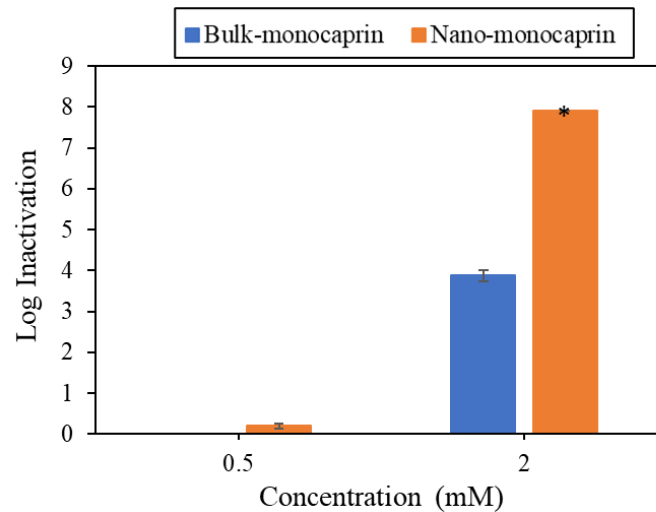


FIGURE 4. 7 Inactivation of phi6 using bulk- and nano-monocaprin solutions at pH 7 with exposure time of 5 min. (\*) indicates the limit of quantification. Error bars are the standard deviation of triplicate plaque counts for each experiment condition.

As mentioned earlier, the antiviral activity of monocaprin is based on the disintegration of the lipid envelope present in enveloped viruses (Sands, 1977, Thormar and Bergsson, 2001, Thormar et al., 2013). Hence, it is generally not applied to treating non-enveloped viruses that lack this lipid envelope. To examine whether the specific antiviral activity was unaltered due to sonication, MS2 – a non-enveloped virus was treated with nano-monocaprin. MS2 was not inactivated by both nano-monocaprin and bulk-monocaprin (Figure 4.10). This indicates that nano-monocaprin retained the specific antiviral action of monocaprin. Also, monocaprin has a high antibacterial effect against Gram-negative and Gram-positive bacteria and has been reported to be effective against

skin and food-borne pathogens (Thormar et al., 2006, Thormar and Hilmarsson, 2012, Wang and Johnson, 1992). Nano-monocaprin (pH 7) achieved  $> 7$  log inactivation of *E. coli* at a low concentration of 0.63 mM in 5 mins. This value is lower than those reported in the above literature that examined bulk-monocaprin (Figure 4.11).

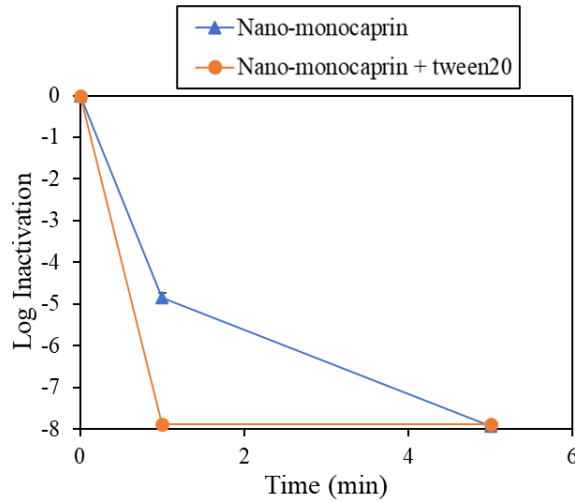


FIGURE 4. 8 Effect of surfactant tween20 on the on phi6 inactivation using nano-monocaprin (2 mM, pH 7).

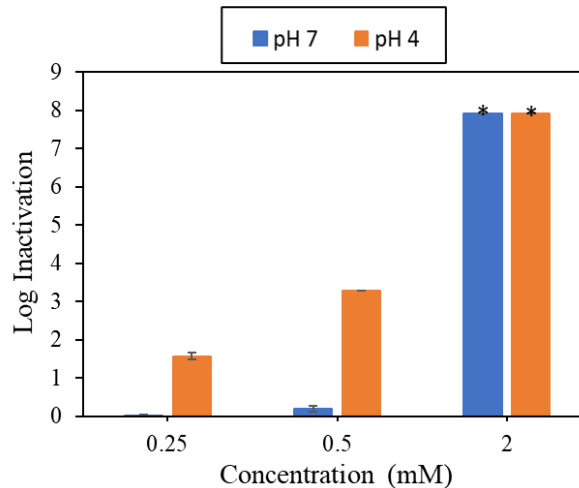


FIGURE 4. 9 Effect of nano-monocaprin solution pH on phi6 inactivation for 5 min exposure time. (\*) indicates the limit of quantification. Error bars are the standard deviation

of triplicate plaque counts for each experiment condition. Control experiment indicates that pH 4 buffer + nano pure water achieved 0.21 ( $\pm$  0.02) log inactivation of phi6.

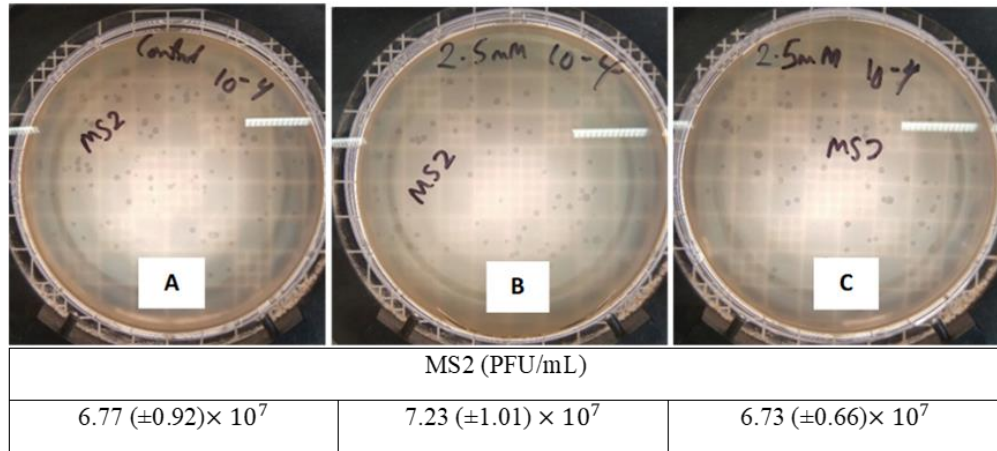


FIGURE 4. 10 Plaque assay results of the antiviral experiment of samples against MS2. A). MS2 + TSB (control); B) MS2 + 2.5 mM bulk-monocaprin; C) MS2 + 2.5 mM nano-monocaprin. Treatment conditions are 5 min contact time and pH 7. Images show comparable number of plaques at 10-4 dilution.

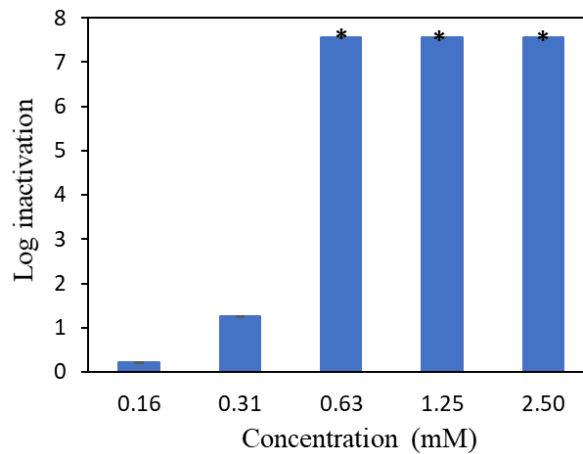


FIGURE 4. 11 Inactivation of *E. coli* using nano-monocaprin solution at pH 4 with exposure time of 5 min. No bacterial inactivation was observed when *E. coli* cells were

exposed to pH 4 buffer solution alone in a control experiment. (\*) indicates the limit of quantification.

#### 4.5.3. Cytotoxicity of nano-monocaprin

HPDE and HeLa cervical cancer cell lines were used for the cell viability assay to represent the effect of nano-monocaprin on normal and cancer cell lines, respectively. Figure 4.12 shows that nano-monocaprin was cytotoxic at the antiviral concentration of 2 mM. The  $IC_{50}$  values were obtained as 0.22 mM and 0.2 mM for HeLa and HPDE respectively. Several studies have reported cell death when emulsions of antimicrobial lipids are directly exposed to monolayers of mammalian cells using standard cell viability assays like MTS (Bergsson et al., 1998, Thormar et al., 1999, Thormar et al., 2013, Jackman et al., 2016). Nevertheless, this nano-monocaprin formulation is suggested for use against the transmission of pathogens through the skin or mucus layer into the body. We expect that they should be suited for these applications because the sensitive mucosal membranes are protected from the environment by the mucus layer. Besides, the stomach of suckling infants has a high concentration of antimicrobial lipids after feeding which does not harm the gastric mucosa (Isaacs et al., 1986, Thormar et al., 2013). This is an indication that the mucus layer protects mucosal membranes.

#### 4.6. Summary

The present study demonstrated that simple sonochemistry techniques to generate nanoparticles can improve the solubility and the antimicrobial activity of monocaprin. The particle size of nano-monocaprin generated decreased and antiviral activity increased as

sonication time increased from 7 min to 20 min. The absorbance spectra of nano-monocaprin and bulk-monocaprin showed that the sonication process did not alter the chemical structure of monocaprin. Moreover, the specific antiviral activity of monocaprin was unchanged by the sonication process since nano-monocaprin inactivated phi6 and *E. coli* having lipid envelope and cell membranes, but MS2 was not inactivated. The synthesized nano-monocaprin exhibited higher antiviral activity against phi6 than the bulk-monocaprin at pH 7. The inhibitory concentration of nano-monocaprin was lower at pH 4 compared to pH 7. Although cytotoxicity of nano-monocaprin was observed for monolayers of HeLa and HPDE cells, we present that the synthesized nano-monocaprin can be suited to prevent the transmission of pathogens such as SARS-CoV-2 through the mucosal membrane due to the protective mucus layer.

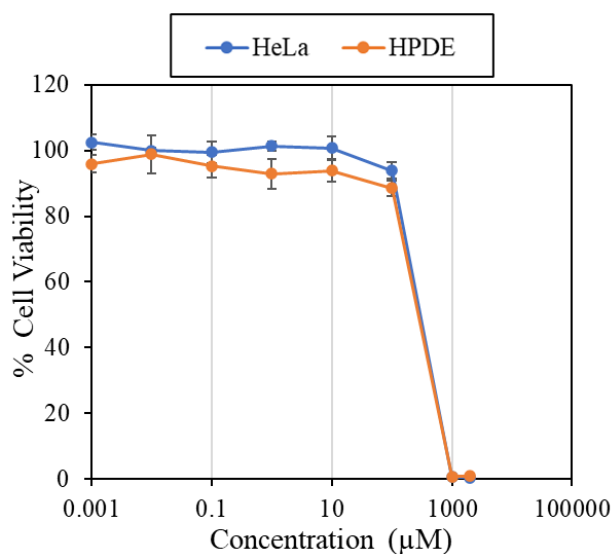


FIGURE 4. 12 Cytotoxicity of nano-monocaprin on HeLa and HPDE cells

## CHAPTER 5. CONCLUSIONS AND RECOMMENDATIONS

### 5.1. Conclusions

This study presented AOPs that utilize the strong oxidizing power of hydroxyl radical ( $HO\cdot$ ) and sulphate radical ( $SO_4^{\cdot-}$ ) as promising technologies for ARGs degradation. We also presented antimicrobial nanoparticles (NPs) that inactivate microorganisms via non-specific actions as alternatives to conventional antibiotics against pathogens of clinical concerns. Herein, we assessed the degradation of ARGs using  $HO\cdot$  and  $SO_4^{\cdot-}$  AOPs; evaluated the inactivation of clinically relevant ARB using photo-activated silver NPs; and examined the antimicrobial and antiviral activity of nano-monocaprin. The overall conclusions from the studies are:

- Results indicate that extracellular ARGs degradation kinetics of the treatments followed an order  $UV_{254}/S_2O_8^{2-} > UV_{254}/H_2O_2 > UV_{254}$  ( $k'_{UV_{254}/S_2O_8^{2-}} \sim 0.45-9.95 \times 10^{-2}$ ;  $k'_{UV_{254}/H_2O_2} \sim 0.49-7.16 \times 10^{-2}$  and  $k_{UV_{254}} \sim 0.47-5.73 \times 10^{-2} \text{ cm}^2/\text{mJ}$ ). The base pair specific kinetic constants with respect to  $HO\cdot$  and  $SO_4^{\cdot-}$  at pH 7 were between  $1.86 \times 10^9$ - $1.65 \times 10^{11} \text{ M}^{-1}\text{s}^{-1}$  and  $2.87 \times 10^9$ - $5.84 \times 10^{11} \text{ M}^{-1}\text{s}^{-1}$  respectively.
- e-ARGs degradation was at least 2-fold higher than i-ARGs degradation for all treatments.  $UV_{254}/S_2O_8^{2-}$  was most effective for ARG degradation under acidic pH (5-6) while  $UV_{254}/H_2O_2$  was most effective between pH 7 and 8.
- Higher ARG degradation rates were recorded for AT-rich *amp<sup>R</sup>* and longer qPCR amplicons. Deactivation rates by  $UV_{254}/H_2O_2$  and  $UV_{254}/S_2O_8^{2-}$  were 2.6-times higher than that of  $UV_{254}$ .

- Generally, deactivation kinetics were ~8-13 times faster than degradation kinetics observed for short *amp<sup>R</sup>* amplicon. These findings show an overestimation of the potential risks of ARG presence using short qPCR target amplicons and the impact of nucleotide composition on ARG damage.
- The synthesized PpIX-AgNPs achieved >7 log inactivation of MRSA and MDR *E. coli*. The order of bacterial log inactivation was PpIX-AgNPs > PEI-PpIX-AgNPs > AgNPs and this correlates with the trend of Ag<sup>+</sup> concentration released by the NPs (PpIX-AgNPs > PEI-PpIX-AgNPs > AgNPs).
- The synthesized nano-monocaprin exhibited higher antiviral activity against phi6 than the bulk-monocaprin at pH 7. The inhibitory concentration of nano-monocaprin was lower at pH 4 compared to pH 7.

## 5.2. Novel Contributions

- **Chapter 3:** This research provided fundamental first-order for ARG degradation during UV<sub>254</sub>, UV<sub>254</sub>/H<sub>2</sub>O<sub>2</sub> and UV<sub>254</sub>/S<sub>2</sub>O<sub>8</sub><sup>2-</sup>. Amplicon specific second-order kinetic constants with respect to HO· and SO<sub>4</sub><sup>-</sup> were determined. The study promoted an understanding of factors that influence ARGs degradation. This quantitative information is useful for deciding treatment processes, setting operating conditions in wastewater and drinking water treatments, and reactor designs for effective ARGs degradation. Moreover, the study showed that longer qPCR amplicons are better indicators of ARGs treatment efficiencies and environmental AR status.
- **Chapter 4:** The novelty of the photoactivated silver-NPs study is based on the combination of photosensitizers with nanoparticles to improve the performance of

photodynamic inactivation against clinical AR pathogens. The study confirmed a synergistic effect between PpIX and AgNPs in the inactivation of AR pathogens. The results outlined the crucial role of optimized  $\text{Ag}^+$  release for enhanced performance of AgNP-based antimicrobials.

- **Chapter 5:** This work showed, for the first time, that nano-monocaprin can be generated using a simple sonochemistry technique. We also demonstrated that the antimicrobial properties of monocaprin can be enhanced by this formulation method and be applicable for the elimination of clinically relevant pathogens.

### 5.3. Recommendations

- **Chapter 2:** He et al. (2019) and Zhang et al. (2019) recommended that qPCR amplicons for evaluating treatment performance and selecting optimum operating conditions for AR mitigation should contain nucleotide contents equivalent to a ‘critical sequence’ required for transformation. Obtaining such critical sequence would require evaluating damages to other important DNA segments such as the promoter region and origin of replication for plasmids in addition to ARG regions. Such analysis will enable the determination of the minimum length of qPCR amplicon that will accurately predict deactivation of a plasmid of given bp length. Moreover,  $\text{HO}\cdot$  and  $\text{SO}_4^{\cdot-}$  kinetic studies on the degradation qPCR amplicons of other types of ARGs should be examined to enable the development of a complex multivariable regression model that captures all the important sequence elements in a single model. Such a model will provide a more accurate prediction of ARG degradation during treatments with  $\text{HO}\cdot$  and  $\text{SO}_4^{\cdot-}$  AOPs.  $\text{HO}\cdot$  and  $\text{SO}_4^{\cdot-}$  radicals did not significantly contribute to i-ARG degradation in *E. coli*

used in this study. However, some studies have reported significant contributions of radicals to *i*-ARG degradation in some *pseudomonas. Sp* (Meng et al., 2022). Mechanistic studies as described by Meng et al. (2022) are needed to further understand the roles of EPS components in *i*-ARG degradation of various ARB species during  $UV_{254}/H_2O_2$  and  $UV_{254}/S_2O_8^{2-}$ .

- **Chapter 3:** AgNPs-PS conjugates should be examined for their antimicrobial action against other ARB that have heavy metal resistance genes (MRGs). This is to observe whether this NPs conjugate can overcome the issue of Ag resistance that has been reported in some bacteria. Also, a generation study should be carried out to determine the frequency of the development of resistance against this novel AgNPs-PS platform.
- **Chapter 4:** The stability of the nano-monocaprin under various environmental conditions such as temperature and ionic strength should be examined. This information is needed to understand how biological media/temperature affects its antimicrobial activity and optimum conditions for its use. *In vivo* assays should be carried out to examine the application of nano-monocaprin against intracellular pathogens.

## LIST OF PUBLICATIONS

1. **Sorinolu, A. J.**, Mamun, M., Vadarevu, H., Vivero-Escoto, J. L., Eric P. Vejerano and Munir, M. Antiviral Activity of Nano-monocaprin against phi6 as a Surrogate for SARS-CoV-2. (Submitted: *Research in Microbiology*)
2. **Sorinolu, A. J.**, Godakhindi, V., Siano, P., Vivero-Escoto, J. L., and Munir, M. Influence of Silver Ion Release on the Inactivation of Antibiotic Resistant Bacteria using Light-Activated Silver Nanoparticles. (Under Review: *RSC Materials Advances*)
3. **Sorinolu, A. J.**, and Munir, M. Degradation and Horizontal Gene Transfer Analysis of Plasmid-encoded Antibiotic Resistance Genes during UV<sub>254</sub>, Hydroxyl Radical and Sulphate Radical treatments. (Accepted: *Chemical Engineering Journal*)
4. Barua, V.B., Juel, M.A.I., Blackwood, A.D., Clerkin, T., Ciesielski, M., **Sorinolu, A.J.**, Holcomb, D.A., Young, I., Kimble, G., Sypolt, S., Engel, L.S., Noble, R. T. and Munir, M. 2022. Tracking the temporal variation of COVID-19 surges through wastewater-based epidemiology during the peak of the pandemic: A six-month long study in Charlotte, North Carolina. *Science of The Total Environment*, p.152503.
5. Mamun, M.M., **Sorinolu, A.J.**, Munir, M. and Vejerano, E.P., 2021. Nanoantibiotics: Functions and properties at the nanoscale to combat antibiotic resistance. *Frontiers in chemistry*, 9, p.348.
6. **Sorinolu, A.J.**, Tyagi, N., Kumar, A. and Munir, M., 2020. Antibiotic Resistance Development and Human Health Risks during Wastewater Reuse and Biosolids Application in Agriculture. *Chemosphere*, p.129032.

## REFERENCES

- ABDELLATIF, A. A., ALTURKI, H. N. & TAWFEEK, H. M. J. S. R. 2021. Different cellulosic polymers for synthesizing silver nanoparticles with antioxidant and antibacterial activities. *Scientific reports*, 11, 1-18.
- ABED, N., SAÏD-HASSANE, F., ZOUHIRI, F., MOUGIN, J., NICOLAS, V., DESMAËLE, D., GREF, R. & COUVREUR, P. 2015. An efficient system for intracellular delivery of beta-lactam antibiotics to overcome bacterial resistance. *Scientific Reports*, 5, 13500.
- AGNIHOTRI, S., MUKHERJI, S. & MUKHERJI, S. 2014. Size-controlled silver nanoparticles synthesized over the range 5–100 nm using the same protocol and their antibacterial efficacy. *RSC Advances*, 4, 3974-3983.
- AHN, J.-M., EOM, H.-J., YANG, X., MEYER, J. N. & CHOI, J. J. C. 2014. Comparative toxicity of silver nanoparticles on oxidative stress and DNA damage in the nematode, *Caenorhabditis elegans*. *Chemosphere*, 108, 343-352.
- AHN, Y., LEE, D., KWON, M., CHOI, I.-H., NAM, S.-N. & KANG, J.-W. 2017. Characteristics and fate of natural organic matter during UV oxidation processes. *Chemosphere*, 184, 960-968.
- ALDSWORTH, T., SHARMAN, R. & DODD, C. 1999. Bacterial suicide through stress. *Cellular Molecular Life Sciences*, 56, 378-383.
- ALMEIDA, A., CUNHA, A., FAUSTINO, M., TOMÉ, A. & NEVES, M. 2011. Porphyrins as antimicrobial photosensitizing agents. *J Photodynamic inactivation of microbial pathogens: medical*, 11, 83-160.
- AMARASIRI, M., SANO, D. & SUZUKI, S. 2020. Understanding human health risks caused by antibiotic resistant bacteria (ARB) and antibiotic resistance genes (ARG) in water environments: Current knowledge and questions to be answered. *Critical Reviews in Environmental Science and Technology*, 50, 2016-2059.
- ANDERSON, R., GROUNDWATER, P. W., TODD, A. & WORSLEY, A. 2012. *Antibacterial agents: chemistry, mode of action, mechanisms of resistance and clinical applications*, John Wiley & Sons.
- ANJUM, M., MIANDAD, R., WAQAS, M., GEHANY, F. & BARAKAT, M. 2019. Remediation of wastewater using various nano-materials. *Arabian Journal of Chemistry*, 12, 4897-4919.
- ARUGUETE, D. M., KIM, B., HOHELLA, M. F., JR., MA, Y., CHENG, Y., HOEGH, A., LIU, J. & PRUDEN, A. 2013. Antimicrobial nanotechnology: its potential for the effective management of microbial drug resistance and implications for research needs in microbial nanotoxicology. *Environ Sci Process Impacts*, 15, 93-102.
- ASHARANI, P., SETHU, S., LIM, H. K., BALAJI, G., VALIYAVEETIL, S. & HANDE, M. P. 2012. Differential regulation of intracellular factors mediating cell cycle, DNA repair and inflammation following exposure to silver nanoparticles in human cells. *Genome integrity*, 3, 1-14.
- BALASUBRAMANIAN, B., POGOZELSKI, W. K. & TULLIUS, T. D. 1998. DNA strand breaking by the hydroxyl radical is governed by the accessible surface areas

- of the hydrogen atoms of the DNA backbone. *Proceedings of the National Academy of Sciences*, 95, 9738-9743.
- BASTUS, N. G., MERKOCI, F., PIELLA, J. & PUNTES, V. 2014. Synthesis of Highly Monodisperse Citrate-Stabilized Silver Nanoparticles of up to 200 nm: Kinetic Control and Catalytic Properties. *Chemistry of Materials*, 26, 2836-2846.
- BEN, Y., FU, C., HU, M., LIU, L., WONG, M. H. & ZHENG, C. 2019. Human health risk assessment of antibiotic resistance associated with antibiotic residues in the environment: A review. *Environmental Research*, 169, 483-493.
- BERENDONK, T. U., MANAIA, C. M., MERLIN, C., FATTA-KASSINOS, D., CYTRYN, E., WALSH, F., BÜRGMANN, H., SØRUM, H., NORSTRÖM, M., PONS, M. N., KREUZINGER, N., HUOVINEN, P., STEFANI, S., SCHWARTZ, T., KISAND, V., BAQUERO, F. & MARTINEZ, J. L. 2015. Tackling antibiotic resistance: the environmental framework. *Nat Rev Microbiol*, 13, 310-7.
- BERGSSON, G., ARNFINNSSON, J., KARLSSON, S. M., STEINGRÍMSSON, Ó. & THORMAR, H. 1998. In vitro inactivation of *Chlamydia trachomatis* by fatty acids and monoglycerides. *Antimicrobial agents & chemotherapy*, 42, 2290-2294.
- BERGSSON, G., ARNFINNSSON, J., STEINGRÍMSSON, Ó. & THORMAR, H. 2001. Killing of Gram-positive cocci by fatty acids and monoglycerides Note. *Apmis*, 109, 670-678.
- BERGSSON, G., STEINGRÍMSSON, Ó. & THORMAR, H. 2002. Bactericidal effects of fatty acids and monoglycerides on *Helicobacter pylori*. *International journal of antimicrobial agents*, 20, 258-262.
- BOLTON, J. R. & LINDEN, K. G. 2003. Standardization of methods for fluence (UV dose) determination in bench-scale UV experiments. *Journal of environmental engineering*, 129, 209-215.
- BRIGGS, C. E. & FRATAMICO, P. M. 1999. Molecular characterization of an antibiotic resistance gene cluster of *Salmonella typhimurium* DT104. *Antimicrobial agents & chemotherapy*, 43, 846-849.
- CALERO-CÁCERES, W. & MUNIESA, M. 2016. Persistence of naturally occurring antibiotic resistance genes in the bacteria and bacteriophage fractions of wastewater. *Water Research*, 95, 11-18.
- CAO, F., JU, E., ZHANG, Y., WANG, Z., LIU, C., LI, W., HUANG, Y., DONG, K., REN, J. & QU, X. 2017. An efficient and benign antimicrobial depot based on silver-infused MoS<sub>2</sub>. *ACS nano*, 11, 4651-4659.
- CDC. 2019. *Antibiotic Resistance Threats in the United States* [Online]. Atlanta, GA: U.S. Department of Health and Human Services. Available: <https://www.cdc.gov/drugresistance/pdf/threats-report/2019-ar-threats-report-508.pdf> [Accessed 17 March, 2021].
- CHANG, P. H., JUHREND, B., OLSON, T. M., MARRS, C. F. & WIGGINTON, K. R. 2017. Degradation of Extracellular Antibiotic Resistance Genes with UV254 Treatment. *Environmental Science & Technology*, 51, 6185-6192.
- CHANG, Q., WANG, W., REGEV-YOCHAY, G., LIPSITCH, M. & HANAGE, W. P. 2015. Antibiotics in agriculture and the risk to human health: how worried should we be? *Evolutionary applications*, 8, 240-247.

- CHEN, H. & ZHANG, M. 2013. Effects of advanced treatment systems on the removal of antibiotic resistance genes in wastewater treatment plants from Hangzhou, China. *Environmental Science & Technology*, 47, 8157-8163.
- CHEN, J., YANG, L., CHEN, J., LIU, W., ZHANG, D., XU, P., DAI, T., SHANG, L., YANG, Y. & TANG, S. 2019. Composite of silver nanoparticles and photosensitizer leads to mutual enhancement of antimicrobial efficacy and promotes wound healing. *Chemical Engineering Journal*, 374, 1373-1381.
- CHOI, Y., HE, H., DODD, M. C. & LEE, Y. 2021. Degradation Kinetics of Antibiotic Resistance Gene *mecA* of Methicillin-Resistant *Staphylococcus aureus* (MRSA) during Water Disinfection with Chlorine, Ozone, and Ultraviolet Light. *Environmental Science & Technology*, 55, 2541-2552.
- CHURCHWARD, C. P., AL-KINANI, A. A., ABDELKADER, H., SWINDEN, J., SIWOKU, O., VARNAKULASINGAM, T., ALANY, R. G. & SNYDER, L. A. 2020. Monocaprin eye drop formulation to combat antibiotic resistant gonococcal blindness. *J Scientific Reports*, 10, 1-10.
- CHURCHWARD, C. P., CALDER, A. & SNYDER, L. A. 2018. Mutations in *Neisseria gonorrhoeae* grown in sub-lethal concentrations of monocaprin do not confer resistance. *PLoS One*, 13, e0195453.
- COLOMER-LLUCH, M., JOFRE, J. & MUNIESA, M. 2011. Antibiotic resistance genes in the bacteriophage DNA fraction of environmental samples. *PloS one*, 6, e17549.
- CULLY, M. 2014. Public health: the politics of antibiotics. *Nature*, 509, S16-S17.
- CUTLER, T. D. & ZIMMERMAN, J. J. 2011. Ultraviolet irradiation and the mechanisms underlying its inactivation of infectious agents. *Anim Health Res Rev*, 12, 15-23.
- CZEKALSKI, N., IMMINGER, S., SALHI, E., VELJKOVIC, M., KLEFFEL, K., DRISSNER, D., HAMMES, F., BÜRGMANN, H. & VON GUNTEN, U. 2016. Inactivation of Antibiotic Resistant Bacteria and Resistance Genes by Ozone: From Laboratory Experiments to Full-Scale Wastewater Treatment. *Environmental Science & Technology*, 50, 11862-11871.
- DE MATTEIS, V., MALVINDI, M. A., GALEONE, A., BRUNETTI, V., DE LUCA, E., KOTE, S., KSHIRSAGAR, P., SABELLA, S., BARDI, G. & POMPA, P. P. 2015. Negligible particle-specific toxicity mechanism of silver nanoparticles: the role of Ag<sup>+</sup> ion release in the cytosol. *Nanomedicine: Nanotechnology, Biology & Medicine*, 11, 731-739.
- DENG, Y. & ZHAO, R. 2015. Advanced Oxidation Processes (AOPs) in Wastewater Treatment. *Current Pollution Reports*, 1, 167-176.
- DHANASEKARAN, S., DOHERTY, T. M., KENNETH, J. & GROUP, T. T. S. 2010. Comparison of different standards for real-time PCR-based absolute quantification. *Journal of immunological methods*, 354, 34-39.
- DI MARTINO, P. 2018. Extracellular polymeric substances, a key element in understanding biofilm phenotype. *AIMS microbiology*, 4, 274.
- EGGEN, R. I., HOLLENDER, J., JOSS, A., SCHÄRER, M. & STAMM, C. 2014. Reducing the discharge of micropollutants in the aquatic environment: the benefits of upgrading wastewater treatment plants. ACS Publications.
- ELASHNIKOV, R., RADOCHA, M., PANOV, I., RIMPELOVA, S., ULBRICH, P., MICHALCOVA, A., SVORCIK, V. & LYUTAKOV, O. 2019. Porphyrin-silver

- nanoparticles hybrids: synthesis, characterization and antibacterial activity. *Materials Science Engineering: C*, 102, 192-199.
- FERNANDES, M. M., FRANCESKO, A., TORRENT-BURGUÉS, J., CARRIÓN-FITÉ, F. J., HEINZE, T. & TZANOV, T. 2014. Sonochemically processed cationic nanocapsules: efficient antimicrobials with membrane disturbing capacity. *Biomacromolecules*, 15, 1365-1374.
- FERNANDES, M. M., IVANOVA, K., FRANCESKO, A., RIVERA, D., TORRENT-BURGUÉS, J., GEDANKEN, A., MENDONZA, E. & TZANOV, T. 2016. Escherichia coli and Pseudomonas aeruginosa eradication by nano-penicillin G. *Nanomedicine: Nanotechnology, Biology, Medicine*, 12, 2061-2069.
- FERRO, G., GUARINO, F., CICALTELLI, A. & RIZZO, L. 2017.  $\beta$ -lactams resistance gene quantification in an antibiotic resistant Escherichia coli water suspension treated by advanced oxidation with UV/H<sub>2</sub>O<sub>2</sub>. *Journal of Hazardous Materials*, 323, 426-433.
- FIEL, R. J., DATTA-GUPTA, N., MARK, E. H. & HOWARD, J. C. 1981. Induction of DNA damage by porphyrin photosensitizers. *J Cancer Research*, 41, 3543-3545.
- FLEMING, A. 1945. *Sir Alexander Fleming - Nobel Lecture: penicillin*. [Online]. Nobel Media. Available: <https://www.nobelprize.org/uploads/2018/06/fleming-lecture.pdf> [Accessed 29 June, 2020].
- FLETCHER, N. F., MEREDITH, L. W., TIDSWELL, E. L., BRYDEN, S. R., GONÇALVES-CARNEIRO, D., CHAUDHRY, Y., SHANNON-LOWE, C., FOLAN, M. A., LEFTERI, D. A., PINGEN, M., BAILEY, D., MCKIMMIE, C. S. & BAIRD, A. W. 2020. A novel antiviral formulation inhibits a range of enveloped viruses. *J Gen Virol*, 101, 1090-1102.
- FUKUZUMI, S., MIYAO, H., OHKUBO, K. & SUENOBU, T. 2005. Electron-transfer oxidation properties of DNA bases and DNA oligomers. *The Journal of Physical Chemistry A*, 109, 3285-3294.
- FURUKAWA, T., JIKUMARU, A., UENO, T. & SEI, K. 2017. Inactivation effect of antibiotic-resistant gene using chlorine disinfection. *Water*, 9, 547.
- GAO, W., THAMPHIWATANA, S., ANGSANTIKUL, P., ZHANG, L. & NANOBIO TECHNOLOGY 2014. Nanoparticle approaches against bacterial infections. *Wiley interdisciplinary reviews: nanomedicine*, 6, 532-547.
- GEDANKEN, A. 2003. Sonochemistry and its application to nanochemistry. *Current science*, 1720-1722.
- GEDANKEN, A. 2004. Using sonochemistry for the fabrication of nanomaterials. *Ultrasonics sonochemistry*, 11, 47-55.
- GHASEMI, M., KHORSANDI, K., KIANMEHR, Z. J. W. J. O. M. & BIOTECHNOLOGY 2021. Photodynamic inactivation with curcumin and silver nanoparticles hinders Pseudomonas aeruginosa planktonic and biofilm formation: evaluation of glutathione peroxidase activity and ROS production. *World Journal of Microbiology & Biotechnology*, 37, 1-10.
- GÖRNER, H. J. J. O. P. & BIOLOGY, P. B. 1994. New trends in photobiology: Photochemistry of DNA and related biomolecules: Quantum yields and consequences of photoionization. *Journal of Photochemistry Photobiology B: Biology*, 26, 117-139.

- GUO, M.-T., YUAN, Q.-B. & YANG, J. 2015. Distinguishing effects of ultraviolet exposure and chlorination on the horizontal transfer of antibiotic resistance genes in municipal wastewater. *J Environmental science & technology*, 49, 5771-5778.
- GUPTA, N., RAI, D. B., JANGID, A. K. & KULHARI, H. 2019. Use of nanotechnology in antimicrobial therapy. *Methods in Microbiology*. Elsevier.
- HANAHAN, D., JESSEE, J. & BLOOM, F. R. 1991. Plasmid transformation of *Escherichia coli* and other bacteria. *Methods in enzymology*, 204, 63-113.
- HE, H., ZHOU, P., SHIMABUKU, K. K., FANG, X., LI, S., LEE, Y. & DODD, M. C. 2019. Degradation and Deactivation of Bacterial Antibiotic Resistance Genes during Exposure to Free Chlorine, Monochloramine, Chlorine Dioxide, Ozone, Ultraviolet Light, and Hydroxyl Radical. *Environmental Science & Technology*, 53, 2013-2026.
- HO, C. M., YAU, S. K. W., LOK, C. N., SO, M. H. & CHE, C. M. 2010. Oxidative dissolution of silver nanoparticles by biologically relevant oxidants: a kinetic and mechanistic study. *Chemistry—An Asian Journal*, 5, 285-293.
- HOUSE, D. A. 1962. Kinetics and Mechanism of Oxidations by Peroxydisulfate. *Chemical Reviews*, 62, 185-203.
- HU, Y., ZHANG, T., JIANG, L., YAO, S., YE, H., LIN, K. & CUI, C. 2019. Removal of sulfonamide antibiotic resistant bacterial and intracellular antibiotic resistance genes by UVC-activated peroxymonosulfate. *Chemical Engineering Journal*, 368, 888-895.
- HUANG, G., NG, T. W., AN, T., LI, G., XIA, D., YIP, H. Y., ZHAO, H. & WONG, P. K. 2017. Probing the intracellular organic matters released from the photocatalytic inactivation of bacteria using fractionation procedure and excitation-emission-matrix fluorescence. *Water research*, 110, 270-280.
- HUANG, J. J., HU, H. Y., TANG, F., LI, Y., LU, S. Q. & LU, Y. 2011. Inactivation and reactivation of antibiotic-resistant bacteria by chlorination in secondary effluents of a municipal wastewater treatment plant. *Water Res*, 45, 2775-81.
- HUANG, L., DAI, T. & HAMBLIN, M. R. 2010. Antimicrobial photodynamic inactivation and photodynamic therapy for infections. *Photodynamic Therapy*. Springer.
- HURST, A. N., SCARBROUGH, B., SALEH, R., HOVEY, J., ARI, F., GOYAL, S., CHI, R. J., TROUTMAN, J. M. & VIVERO-ESCOTO, J. L. 2019. Influence of Cationic meso-Substituted Porphyrins on the Antimicrobial Photodynamic Efficacy and Cell Membrane Interaction in *Escherichia coli*. *Int J Mol Sci*, 20.
- ISAACS, C. E., THORMAR, H. & PESSOLANO, T. 1986. Membrane-disruptive effect of human milk: inactivation of enveloped viruses. *Journal of Infectious Diseases*, 154, 966-971.
- ISHIDA, T. 2018. Availability of Ag<sup>+</sup> Ions Having Most Highly Bactericidal Activity to Suppression by Inhibitions of Viral and Cancerous Cell Growth. *Clinical Research in Immunology*, 1, 1-11.
- JACANGELO, J. G. & TRUSSELL, R. R. 2002. International report: water and wastewater disinfection - trends, issues and practices. *Water Supply*, 2, 147-157.
- JACKMAN, J. A., YOON, B. K., LI, D. & CHO, N. J. 2016. Nanotechnology Formulations for Antibacterial Free Fatty Acids and Monoglycerides. *Molecules*, 21, 305.
- JØRGENSEN, S. E. & HALLING-SØRENSEN, B. 2000. Drugs in the environment. *Chemosphere*, 40, 691-699.

- KABARA, J., VRABLE, R. & LIE KEN JIE, M. 1977. Antimicrobial lipids: natural and synthetic fatty acids and monoglycerides. *Lipids*, 12, 753-759.
- KABARA, J. J. 1978. Structure-function relationships of surfactants as antimicrobial agents. *SOC. COSMET. CHEMISTS*; 29, 733-741.
- KABARA, J. J., SWIECZKOWSKI, D. M., CONLEY, A. J., TRUANT, J. P. J. A. A. & CHEMOTHERAPY 1972. Fatty acids and derivatives as antimicrobial agents. *Antimicrobial agents & chemotherapy*, 2, 23-28.
- KEEN, P. L. & MONTFORTS, M. H. M. M. 2012. Antimicrobial Resistance in the Environment. Hoboken, New Jersey: John Wiley & Sons, Inc.
- KILIC, M. Y., ABDELRAHEEM, W. H., HE, X., KESTIOGLU, K. & DIONYSIOU, D. D. 2019. Photochemical treatment of tyrosol, a model phenolic compound present in olive mill wastewater, by hydroxyl and sulfate radical-based advanced oxidation processes (AOPs). *Journal of hazardous materials*, 367, 734-742.
- KOBAYASHI, S., HIROISHI, K., TOKUNOH, M. & SAEGUSA, T. 1987. Chelating properties of linear and branched poly (ethylenimines). *Macromolecules*, 20, 1496-1500.
- KOLTHOFF, I. M. & MILLER, I. K. 1951. The Chemistry of Persulfate. II. The Reaction of Persulfate with Mercaptans Solubilized in Solutions of Saturated Fatty Acid Soaps1. *Journal of the American Chemical Society*, 73, 5118-5122.
- KRISTMUNDSÓTTIR, T., ÁRNADÓTTIR, S. G., BERGSSON, G. & THORMAR, H. 1999. Development and evaluation of microbicidal hydrogels containing monoglyceride as the active ingredient. *Journal of pharmaceutical sciences*, 88, 1011-1015.
- KÜMMERER, K. 2009. Antibiotics in the aquatic environment—a review—part I. *Chemosphere*, 75, 417-434.
- KVÍTEK, L., PANÁČEK, A., SOUKUPOVA, J., KOLÁŘ, M., VEČEŘOVÁ, R., PRUCEK, R., HOLECOVÁ, M. & ZBOŘIL, R. 2008. Effect of surfactants and polymers on stability and antibacterial activity of silver nanoparticles (NPs). *The Journal of Physical Chemistry C*, 112, 5825-5834.
- LAMBA, M. & AHAMMAD, S. Z. 2017. Performance comparison of secondary and tertiary treatment systems for treating antibiotic resistance. *Water Res*, 127, 172-182.
- LEE, Y., GERRITY, D., LEE, M., GAMAGE, S., PISARENKO, A., TRENHOLM, R. A., CANONICA, S., SNYDER, S. A. & VON GUNTEN, U. 2016. Organic Contaminant Abatement in Reclaimed Water by UV/H<sub>2</sub>O<sub>2</sub> and a Combined Process Consisting of O<sub>3</sub>/H<sub>2</sub>O<sub>2</sub> Followed by UV/H<sub>2</sub>O<sub>2</sub>: Prediction of Abatement Efficiency, Energy Consumption, and Byproduct Formation. *Environmental Science & Technology*, 50, 3809-3819.
- LEVY, S. B. & MARSHALL, B. 2004. Antibacterial resistance worldwide: causes, challenges and responses. *Nat Med*, 10, S122-9.
- LI, W., PATTON, S., GLEASON, J. M., MEZYK, S. P., ISHIDA, K. P. & LIU, H. 2018. UV Photolysis of Chloramine and Persulfate for 1,4-Dioxane Removal in Reverse-Osmosis Permeate for Potable Water Reuse. *Environmental Science & Technology*, 52, 6417-6425.

- LIN, W., LI, S., ZHANG, S. & YU, X. 2016. Reduction in horizontal transfer of conjugative plasmid by UV irradiation and low-level chlorination. *Water Res*, 91, 331-8.
- LINDBERG, R., JARNHEIMER, P.-Å., OLSEN, B., JOHANSSON, M. & TYSKLIND, M. 2004. Determination of antibiotic substances in hospital sewage water using solid phase extraction and liquid chromatography/mass spectrometry and group analogue internal standards. *Chemosphere*, 57, 1479-1488.
- LIU, N., SIJAK, S., ZHENG, M., TANG, L., XU, G. & WU, M. 2015. Aquatic photolysis of florfenicol and thiamphenicol under direct UV irradiation, UV/H<sub>2</sub>O<sub>2</sub> and UV/Fe (II) processes. *Chemical Engineering Journal*, 260, 826-834.
- LIU, S., WANG, Z., BAN, M., SONG, P., SONG, X. & KHAN, B. 2018. Chelation-assisted in situ self-assembly route to prepare the loose PAN-based nanocomposite membrane for dye desalination. *Journal of Membrane Science*, 566, 168-180.
- LONG, G., ZHU, P., SHEN, Y. & TONG, M. 2009. Influence of extracellular polymeric substances (EPS) on deposition kinetics of bacteria. *Environmental science & technology*, 43, 2308-2314.
- MA, L., LI, B., JIANG, X. T., WANG, Y. L., XIA, Y., LI, A. D. & ZHANG, T. 2017. Catalogue of antibiotic resistance and host-tracking in drinking water deciphered by a large scale survey. *Microbiome*, 5, 154.
- MA, S., ZHAN, S., JIA, Y. & ZHOU, Q. 2015. Highly Efficient Antibacterial and Pb(II) Removal Effects of Ag-CoFe<sub>2</sub>O<sub>4</sub>-GO Nanocomposite. *ACS Applied Materials & Interfaces*, 7, 10576-10586.
- MALÁ, Z., ŽÁRSKÁ, L., BAJGAR, R., BOGDANOVÁ, K., KOLÁŘ, M., PANÁČEK, A., BINDER, S. & KOLÁŘOVÁ, H. 2021. The application of antimicrobial photodynamic inactivation on methicillin-resistant *S. aureus* and ESBL-producing *K. pneumoniae* using porphyrin photosensitizer in combination with silver nanoparticles. *Photodiagnosis & Photodynamic Therapy*, 33, 102140.
- MAMUN, M. M., SORINOLU, A. J., MUNIR, M. & VEJERANO, E. P. 2021. Nanoantibiotics: Functions and Properties at the Nanoscale to Combat Antibiotic Resistance. *Frontiers in chemistry*, 9.
- MANAIA, C. M. 2017. Assessing the Risk of Antibiotic Resistance Transmission from the Environment to Humans: Non-Direct Proportionality between Abundance and Risk. *Trends in Microbiology*, 25, 173-181.
- MARTÍNEZ, J. L. 2008. Antibiotics and antibiotic resistance genes in natural environments. *Science*, 321, 365-7.
- MATYAR, F. 2012. Antibiotic and heavy metal resistance in bacteria isolated from the Eastern Mediterranean Sea coast. *Bull Environ Contam Toxicol*, 89, 551-6.
- MAYS, C., GARZA, G. L., WAITE-CUSIC, J., RADNIECKI, T. S. & NAVAB-DANESHMAND, T. 2021. Impact of biosolids amendment and wastewater effluent irrigation on enteric antibiotic-resistant bacteria—a greenhouse study. *Water research X*, 13, 100119.
- MCSHAN, D., RAY, P. C. & YU, H. 2014. Molecular toxicity mechanism of nanosilver. *Journal of food & drug analysis*, 22, 116-127.
- MEMMING, R. 1969. Mechanism of the electrochemical reduction of persulfates and hydrogen peroxide. 116, 785.

- MENG, F., KWON, S., WANG, J. & YEO, Y. 2020. Immunoactive drug carriers in cancer therapy. *Biomaterials for Cancer Therapeutics*. Elsevier.
- MENG, X., LI, F., YI, L., DIEKETSENG, M. Y., WANG, X., ZHOU, L. & ZHENG, G. 2022. Free radicals removing extracellular polymeric substances to enhance the degradation of intracellular antibiotic resistance genes in multi-resistant *Pseudomonas Putida* by UV/H<sub>2</sub>O<sub>2</sub> and UV/peroxydisulfate disinfection processes. *Journal of Hazardous Materials*, 430, 128502.
- MERCHAT, M., BERTOLINI, G., GIACOMINI, P., VILLANEUVA, A. & JORI, G. 1996a. Meso-substituted cationic porphyrins as efficient photosensitizers of gram-positive and gram-negative bacteria. *Journal of Photochemistry & Photobiology B: Biology*, 32, 153-157.
- MERCHAT, M., SPIKES, J., BERTOLINI, G. & JORI, G. 1996b. Studies on the mechanism of bacteria photosensitization by meso-substituted cationic porphyrins. *Journal of Photochemistry & Photobiology B: Biology*, 35, 149-157.
- MEYER, J. 2010. QPCR: a tool for analysis of mitochondrial and nuclear DNA damage in ecotoxicology. *Ecotoxicology*, 19, 804-811.
- MICHAEL-KORDATOU, I., KARAOLIA, P. & FATTA-KASSINOS, D. 2018. The role of operating parameters and oxidative damage mechanisms of advanced chemical oxidation processes in the combat against antibiotic-resistant bacteria and resistance genes present in urban wastewater. *Water Research*, 129, 208-230.
- MIJNENDONCKX, K., LEYS, N., MAHILLON, J., SILVER, S. & VAN HOUDT, R. 2013. Antimicrobial silver: uses, toxicity and potential for resistance. *Biometals*, 26, 609-621.
- MONNET, D. L. & HARBARTH, S. 2020. Will coronavirus disease (COVID-19) have an impact on antimicrobial resistance? *Euro Surveill*, 25.
- MOURA, A., PEREIRA, C., HENRIQUES, I. & CORREIA, A. 2012. Novel gene cassettes and integrons in antibiotic-resistant bacteria isolated from urban wastewaters. *Res Microbiol*, 163, 92-100.
- NEETHU, S., MIDHUN, S. J., RADHAKRISHNAN, E. & JYOTHIS, M. 2020. Surface functionalization of central venous catheter with mycofabricated silver nanoparticles and its antibiofilm activity on multidrug resistant *Acinetobacter baumannii*. *Microbial pathogenesis*, 138, 103832.
- NIHEMAITI, M., YOON, Y., HE, H., DODD, M. C., CROUÉ, J.-P. & LEE, Y. 2020. Degradation and deactivation of a plasmid-encoded extracellular antibiotic resistance gene during separate and combined exposures to UV254 and radicals. *Water Research*, 182, 115921.
- O'CONNELL, K. M., HODGKINSON, J. T., SORE, H. F., WELCH, M., SALMOND, G. P. & SPRING, D. R. 2013. Combating multidrug-resistant bacteria: current strategies for the discovery of novel antibacterials. *Angewandte Chemie International Edition*, 52, 10706-10733.
- PAK, G., SALCEDO, D. E., LEE, H., OH, J., MAENG, S. K., SONG, K. G., HONG, S. W., KIM, H.-C., CHANDRAN, K., KIM, S. J. E. S. & TECHNOLOGY 2016. Comparison of antibiotic resistance removal efficiencies using ozone disinfection under different pH and suspended solids and humic substance concentrations. *J Environmental science & technology*, 50, 7590-7600.

- PAL, C., BENGTSSON-PALME, J., KRISTIANSOON, E. & LARSSON, D. J. 2015. Co-occurrence of resistance genes to antibiotics, biocides and metals reveals novel insights into their co-selection potential. *BMC genomics*, 16, 1-14.
- PAREEK, V., GUPTA, R. & PANWAR, J. 2018. Do physico-chemical properties of silver nanoparticles decide their interaction with biological media and bactericidal action? A review. *Mater Sci Eng C Mater Biol Appl*, 90, 739-749.
- PEI, R., KIM, S.-C., CARLSON, K. H. & PRUDEN, A. 2006. Effect of river landscape on the sediment concentrations of antibiotics and corresponding antibiotic resistance genes (ARG). *Water research*, 40, 2427-2435.
- PETSCHOW, B. W., BATEMA, R. P., FORD, L. L. J. A. A. & CHEMOTHERAPY 1996. Susceptibility of *Helicobacter pylori* to bactericidal properties of medium-chain monoglycerides and free fatty acids. *Antimicrobial agents & chemotherapy*, 40, 302-306.
- PHANIENDRA, A., JESTADI, D. B. & PERIYASAMY, L. 2015. Free radicals: properties, sources, targets, and their implication in various diseases. *Indian journal of clinical biochemistry*, 30, 11-26.
- PIAO, M. J., KANG, K. A., LEE, I. K., KIM, H. S., KIM, S., CHOI, J. Y., CHOI, J. & HYUN, J. W. 2011. Silver nanoparticles induce oxidative cell damage in human liver cells through inhibition of reduced glutathione and induction of mitochondria-involved apoptosis. *Toxicology letters*, 201, 92-100.
- QIAO, S. Z., LIU, J. & LU, G. Q. M. 2011. Synthetic chemistry of nanomaterials. *Modern Inorganic Synthetic Chemistry*. Elsevier.
- QIU, Z., YU, Y., CHEN, Z., JIN, M., YANG, D., ZHAO, Z., WANG, J., SHEN, Z., WANG, X., QIAN, D., HUANG, A., ZHANG, B. & LI, J. W. 2012. Nanoalumina promotes the horizontal transfer of multiresistance genes mediated by plasmids across genera. *Proc Natl Acad Sci U S A*, 109, 4944-9.
- RAHBAN, M., DIVSALAR, A., SABOURY, A. A. & GOLESTANI, A. 2010. Nanotoxicity and spectroscopy studies of silver nanoparticle: calf thymus DNA and K562 as targets. *The Journal of Physical Chemistry C*, 114, 5798-5803.
- REISNER, B. S. & WOODS, G. L. 1999. Times to detection of bacteria and yeasts in BACTEC 9240 blood culture bottles. *Journal of clinical microbiology*, 37, 2024-2026.
- RICHARDS, S.-J., ISUFI, K., WILKINS, L. E., LIPECKI, J., FULLAM, E. & GIBSON, M. I. J. B. 2018. Multivalent antimicrobial polymer nanoparticles target mycobacteria and gram-negative bacteria by distinct mechanisms. *Biomacromolecules*, 19, 256-264.
- RICHTER, A. P., BROWN, J. S., BHARTI, B., WANG, A., GANGWAL, S., HOUCK, K., HUBAL, E. A. C., PAUNOV, V. N., STOYANOV, S. D. & VELEV, O. D. 2015. An environmentally benign antimicrobial nanoparticle based on a silver-infused lignin core. *Nature nanotechnology*, 10, 817-823.
- RIZZO, L., MANAIA, C., MERLIN, C., SCHWARTZ, T., DAGOT, C., PLOY, M. C., MICHAEL, I. & FATTA-KASSINOS, D. 2013. Urban wastewater treatment plants as hotspots for antibiotic resistant bacteria and genes spread into the environment: A review. *Science of The Total Environment*, 447, 345-360.
- RODRÍGUEZ-CHUECA, J., GARCÍA-CAÑIBANO, C., LEPISTÖ, R. J., ENCINAS, Á., PELLINEN, J. & MARUGÁN, J. 2019a. Intensification of UV-C tertiary

- treatment: Disinfection and removal of micropollutants by sulfate radical based Advanced Oxidation Processes. *Journal of Hazardous Materials*, 372, 94-102.
- RODRÍGUEZ-CHUECA, J., VARELLA DELLA GIUSTINA, S., ROCHA, J., FERNANDES, T., PABLOS, C., ENCINAS, Á., BARCELÓ, D., RODRÍGUEZ-MOZAZ, S., MANAIA, C. M. & MARUGÁN, J. 2019b. Assessment of full-scale tertiary wastewater treatment by UV-C based-AOPs: Removal or persistence of antibiotics and antibiotic resistance genes? *Science of The Total Environment*, 652, 1051-1061.
- ROSZAK, D. & COLWELL, R. 1987. Survival strategies of bacteria in the natural environment. *Microbiological reviews*, 51, 365-379.
- SALOMONI, R., LÉO, P., MONTEMOR, A., RINALDI, B. & RODRIGUES, M. 2017. Antibacterial effect of silver nanoparticles in *Pseudomonas aeruginosa*. *Nanotechnology, science & applications*, 10, 115.
- SANDS, J. A. 1977. Inactivation and inhibition of replication of the enveloped bacteriophage  $\phi 6$  by fatty acids. *Antimicrobial agents and Chemotherapy*, 12, 523-528.
- SANGANYADO, E. & GWENZI, W. 2019. Antibiotic resistance in drinking water systems: Occurrence, removal, and human health risks. *Science of the Total Environment*, 669, 785-797.
- SÃO PEDRO, A., SANTO, I., SILVA, C., DETONI, C. & ALBUQUERQUE, E. 2013. *The use of nanotechnology as an approach for essential oil-based formulations with antimicrobial activity*, Formatex Research Center Publisher.
- SENGUPTA, I., BHATTACHARYA, P., TALUKDAR, M., NEOGI, S., PAL, S. K. & CHAKRABORTY, S. 2019. Bactericidal effect of graphene oxide and reduced graphene oxide: Influence of shape of bacteria. *Colloid and Interface Science Communications*, 28, 60-68.
- SHABANGU, S. M., BABU, B., SOY, R. C., OYIM, J., AMUHAYA, E. & NYOKONG, T. 2020. Susceptibility of *Staphylococcus aureus* to porphyrin-silver nanoparticle mediated photodynamic antimicrobial chemotherapy. *Journal of Luminescence*, 222, 117158.
- SHARMA, V. K., YU, X., MCDONALD, T. J., JINADATHA, C., DIONYSIOU, D. D. & FENG, M. 2019. Elimination of antibiotic resistance genes and control of horizontal transfer risk by UV-based treatment of drinking water: A mini review. *Frontiers of environmental science & engineering*, 13, 10.1007/s11783-019-1122-7.
- SHINOHARA, A. & OGAWA, T. 1995. Homologous recombination and the roles of double-strand breaks. *Trends in biochemical sciences*, 20, 387-391.
- SINGH, R., SMITHA, M. S. & SINGH, S. P. 2014. The role of nanotechnology in combating multi-drug resistant bacteria. *J Nanosci Nanotechnol*, 14, 4745-56.
- SINHA, R., HÄDER, D. & UV-INDUCED, D. 2002. damage and repair: A review. *Photochem. Photobiol. Sci*, 1, 225-236.
- SIRIWARDANA, K., SUWANDARATNE, N., PERERA, G. S., COLLIER, W. E., PEREZ, F. & ZHANG, D. 2015. Contradictory dual effects: organothiols can induce both silver nanoparticle disintegration and formation under ambient conditions. *The Journal of Physical Chemistry C*, 119, 20975-20984.

- SMITH, K. C. & WANG, T. C. V. 1989. recA-dependent DNA repair processes. *Bioessays*, 10, 12-16.
- SOLOMON, C., CASEY, P., MACKNE, C. & LAKE, A. 1998. *Ultraviolet Disinfection: Environmental Technology Initiative*. [Online]. Available: [http://www.nesc.wvu.edu/pdf/WW/publications/eti/UV\\_Dis\\_tech.pdf](http://www.nesc.wvu.edu/pdf/WW/publications/eti/UV_Dis_tech.pdf) [Accessed July 28, 2018].
- SORINOLU, A. J., TYAGI, N., KUMAR, A. & MUNIR, M. 2021. Antibiotic resistance development and human health risks during wastewater reuse and biosolids application in agriculture. *Chemosphere*, 265, 129032.
- SOMET, C., FOURREAU, E., LEGRANDOIS, P. & MARIS, P. 2012. Resistance to phenicol compounds following adaptation to quaternary ammonium compounds in *Escherichia coli*. *Veterinary Microbiology*, 158, 147-152.
- SUSLICK, K. S. & CRUM, L. A. 1997. Sonochemistry and sonoluminescence. *Encyclopedia of acoustics*, 1, 271-281.
- TAN, P., FU, H. & MA, X. 2021. Design, optimization, and nanotechnology of antimicrobial peptides: From exploration to applications. *Nano Today*, 39, 101229.
- TAYLOR, E. N., KUMMER, K. M., DURMUS, N. G., LEUBA, K., TARQUINIO, K. M. & WEBSTER, T. 2012. Superparamagnetic iron oxide nanoparticles (SPION) for the treatment of antibiotic-resistant biofilms. *Small*, 8, 3016-3027.
- TAYLOR, J., HAFNER, M., YERUSHALMI, E., SMITH, R., BELLASIO, J., VARDAVAS, R., BINKOWSKA-GIBBS, T. & RUBIN, J. 2014. Estimating the economic costs of antimicrobial resistance: Model and Results. *RAND Corporation, Cambridge, UK*.
- TCHOBANOGLIOUS, G., BURTON, F. L. & STENSEL, H. D. 1991. Wastewater Engineering. *Management*, 7, 1-4.
- TEMPLETON, M. R., ODDY, F., LEUNG, W.-K. & ROGERS, M. 2009. Chlorine and UV disinfection of ampicillin-resistant and trimethoprim-resistant *Escherichia coli*. *Canadian Journal of Civil Engineering*, 36, 889-894.
- THORGEIRSDOTTIR, T., THORMAR, H. & KRISTMUNDSDOTTIR, T. 2003. Effects of polysorbates on antiviral and antibacterial activity of monoglyceride in pharmaceutical formulations. *An International Journal of Pharmaceutical Sciences*, 58, 286-287.
- THORMAR, H. & BERGSSON, G. 2001. Antimicrobial effects of lipids. *Recent developments in antiviral research*, 157-173.
- THORMAR, H., BERGSSON, G., GUNNARSSON, E., GEORGSSON, G., WITVROUW, M., STEINGRIMSSON, O., DE CLERCQ, E. & KRISTMUNDSDÓTTIR, T. 1999. Hydrogels containing monocaprin have potent microbicidal activities against sexually transmitted viruses and bacteria in vitro. *Sexually transmitted infections*, 75, 181.
- THORMAR, H. & HILMARSSON, H. 2012. Glycerol monocaprate (monocaprin) reduces contamination by *Escherichia coli* and *Salmonella enteritidis* on hard surfaces. *Food control*, 25, 505-510.
- THORMAR, H., HILMARSSON, H. & BERGSSON, G. 2006. Stable concentrated emulsions of the 1-monoglyceride of capric acid (monocaprin) with microbicidal activities against the food-borne bacteria *Campylobacter jejuni*, *Salmonella* spp., and *Escherichia coli*. *Applied & Environmental Microbiology*, 72, 522-526.

- THORMAR, H., HILMARSSON, H. & BERGSSON, G. 2013. Antimicrobial lipids: Role in innate immunity and potential use in prevention and treatment of infections. *J Microbial pathogens & strategies for combating them: science, technology & education*, 3, 1474-88.
- TIWARI, D. K., BEHARI, J. & SEN, P. 2008. Application of nanoparticles in waste water treatment. *World Appl Sci J*.
- TONG, M., LONG, G., JIANG, X. & KIM, H. N. 2010. Contribution of extracellular polymeric substances on representative gram negative and gram positive bacterial deposition in porous media. *Environmental Science & Technology*, 44, 2393-2399.
- TRAN, N. H., CHEN, H., REINHARD, M., MAO, F. & GIN, K. Y.-H. 2016. Occurrence and removal of multiple classes of antibiotics and antimicrobial agents in biological wastewater treatment processes. *Water Research*, 104, 461-472.
- US EPA. 1999. *Wastewater technology fact sheet chlorine disinfection* [Online]. Washington, D.C: Office of Water Available: <https://nepis.epa.gov/Exe/ZyPDF.cgi/200044E0.PDF?Dockey=200044E0.PDF> [Accessed 23 March, 2021].
- VIKESLAND, P. J., PRUDEN, A., ALVAREZ, P. J., AGA, D., BÜRGMANN, H., LI, X.-D., MANAIA, C. M., NAMBI, I., WIGGINTON, K. & ZHANG, T. 2017. Toward a comprehensive strategy to mitigate dissemination of environmental sources of antibiotic resistance. ACS Publications.
- VON SONNTAG, C. 2006. *Free-radical-induced DNA damage and its repair*, Springer.
- VZOROV, A. N., DIXON, D. W., TROMMEL, J. S., MARZILLI, L. G. & COMPANS, R. W. 2002. Inactivation of human immunodeficiency virus type 1 by porphyrins. *Antimicrobial agents & chemotherapy*, 46, 3917-3925.
- WALSH, C. 2000. Molecular mechanisms that confer antibacterial drug resistance. *Nature*, 406, 775-781.
- WALSH, C. & WRIGHT, G. 2005. Introduction: antibiotic resistance. . *Chem Rev*, 105, 391394.
- WANG, L.-L. & JOHNSON, E. A. 1992. Inhibition of *Listeria monocytogenes* by fatty acids and monoglycerides. *Applied & environmental microbiology*, 58, 624-629.
- WEESE, J. S. 2010. Methicillin-resistant *Staphylococcus aureus* in animals. *ILAR journal*, 51, 233-244.
- WEINSTEIN, M. P., LIMBAGO, B., PATEL, J., MATHERS, A., CAMPEAU, S., MAZZULLI, T., ELIOPOULOS, G., PATEL, R., GALAS, M. & RICHTER, S. 2018. M100 performance standards for antimicrobial susceptibility testing. Wayne, PA: Clinical & Laboratory Standards Institute.
- WHO. 2014. *Antimicrobial resistance global report on surveillance*. [Online]. Available: [https://apps.who.int/iris/bitstream/handle/10665/112642/9789241564748\\_eng.pdf;sequence=1](https://apps.who.int/iris/bitstream/handle/10665/112642/9789241564748_eng.pdf;sequence=1) [Accessed 17 March, 2021].
- WHO. 2017. *World Priority List of Antibiotic-Resistant Bacteria to Guide Research, Discovery, and Development of New Antibiotics*. [Online]. Available: [http://www.who.int/medicines/publications/WHO-PPL-Short\\_Summary\\_25Feb-ET\\_NM\\_WHO.pdf](http://www.who.int/medicines/publications/WHO-PPL-Short_Summary_25Feb-ET_NM_WHO.pdf) [Accessed April 3, 2018].
- WOOD, J. P., RICHTER, W., SUNDERMAN, M., CALFEE, M. W., SERRE, S. & MICKELSEN, L. 2020. Evaluating the Environmental Persistence and Inactivation

- of MS2 Bacteriophage and the Presumed Ebola Virus Surrogate Phi6 Using Low Concentration Hydrogen Peroxide Vapor. *Environ Sci Technol*, 54, 3581-3590.
- XI, C., ZHANG, Y., MARRS, C. F., YE, W., SIMON, C., FOXMAN, B. & NRIAGU, J. 2009. Prevalence of Antibiotic Resistance in Drinking Water Treatment and Distribution Systems. *Applied & environmental microbiology*, 75, 5714-5718.
- XIAO, R., BAI, L., LIU, K., SHI, Y., MINAKATA, D., HUANG, C.-H., SPINNEY, R., SETH, R., DIONYSIOU, D. D. & WEI, Z. 2020. Elucidating sulfate radical-mediated disinfection profiles and mechanisms of Escherichia coli and Enterococcus faecalis in municipal wastewater. *Water research*, 173, 115552.
- XIE, X., MAO, C., LIU, X., ZHANG, Y., CUI, Z., YANG, X., YEUNG, K. W., PAN, H., CHU, P. K. & WU, S. 2017. Synergistic bacteria killing through photodynamic and physical actions of graphene oxide/Ag/collagen coating. *ACS applied materials & interfaces*, 9, 26417-26428.
- XU, P., ZENG, G. M., HUANG, D. L., FENG, C. L., HU, S., ZHAO, M. H., LAI, C., WEI, Z., HUANG, C., XIE, G. X. & LIU, Z. F. 2012. Use of iron oxide nanomaterials in wastewater treatment: A review. *Science of The Total Environment*, 424, 1-10.
- YAN, X., HE, B., LIU, L., QU, G., SHI, J., HU, L. & JIANG, G. 2018. Antibacterial mechanism of silver nanoparticles in Pseudomonas aeruginosa: proteomics approach. *Metallomics*, 10, 557-564.
- YAO, S., HU, Y., YE, J., XIE, J., ZHAO, X., LIU, L., LYU, S., LIN, K. & CUI, C. 2022. Disinfection and mechanism of super-resistant Acinetobacter sp. and the plasmid-encoded antibiotic resistance gene bla<sub>NDM-1</sub> by UV/peroxymonosulfate. *Chemical Engineering Journal*, 433, 133565.
- YARIV, I., LIPOVSKY, A., GEDANKEN, A., LUBART, R. & FIXLER, D. 2015. Enhanced pharmacological activity of vitamin b12 and penicillin as nanoparticles. *International journal of nanomedicine*, 10, 3593.
- YIN, R., AGRAWAL, T., KHAN, U., GUPTA, G. K., RAI, V., HUANG, Y.-Y. & HAMBLIN, M. R. 2015. Antimicrobial photodynamic inactivation in nanomedicine: small light strides against bad bugs. *Nanomedicine*, 10, 2379-2404.
- YOON, B. K., JACKMAN, J. A., VALLE-GONZÁLEZ, E. R. & CHO, N.-J. 2018a. Antibacterial free fatty acids and monoglycerides: biological activities, experimental testing, and therapeutic applications. *International journal of molecular sciences*, 19, 1114.
- YOON, Y., CHUNG, H. J., WEN DI, D. Y., DODD, M. C., HUR, H.-G. & LEE, Y. 2017. Inactivation efficiency of plasmid-encoded antibiotic resistance genes during water treatment with chlorine, UV, and UV/H<sub>2</sub>O<sub>2</sub>. *Water Research*, 123, 783-793.
- YOON, Y., DODD, M. C. & LEE, Y. 2018b. Elimination of transforming activity and gene degradation during UV and UV/H<sub>2</sub>O<sub>2</sub> treatment of plasmid-encoded antibiotic resistance genes. *Environmental Science: Water Research & Technology*, 4, 1239-1251.
- YOON, Y., HE, H., DODD, M. C. & LEE, Y. 2021. Degradation and deactivation of plasmid-encoded antibiotic resistance genes during exposure to ozone and chlorine. *Water Research*, 202, 117408.
- YU, W., ZHAN, S., SHEN, Z. & ZHOU, Q. 2018. A newly synthesized Au/GO-Co<sub>3</sub>O<sub>4</sub> composite effectively inhibits the replication of tetracycline resistance gene in water. *Chemical Engineering Journal*, 345, 462-470.

- YU, W., ZHAN, S., SHEN, Z., ZHOU, Q. & YANG, D. 2017. Efficient removal mechanism for antibiotic resistance genes from aquatic environments by graphene oxide nanosheet. *Chemical Engineering Journal*, 313, 836-846.
- YUAN, Q.-B., GUO, M.-T. & YANG, J. 2015. Fate of antibiotic resistant bacteria and genes during wastewater chlorination: implication for antibiotic resistance control. *PloS one*, 10, e0119403.
- ZHANG, B.-T., ZHANG, Y., TENG, Y. & FAN, M. 2015a. Sulfate Radical and Its Application in Decontamination Technologies. *Critical Reviews in Environmental Science and Technology*, 45, 1756-1800.
- ZHANG, M., CHEN, S., YU, X., VIKESLAND, P. & PRUDEN, A. 2019. Degradation of extracellular genomic, plasmid DNA and specific antibiotic resistance genes by chlorination. *Frontiers of Environmental Science & Engineering*, 13, 1-12.
- ZHANG, T. & LI, B. 2011. Occurrence, Transformation, and Fate of Antibiotics in Municipal Wastewater Treatment Plants. *Critical Reviews in Environmental Science and Technology*, 41, 951-998.
- ZHANG, X.-Z., ZENG, X., SUN, Y.-X. & ZHUO, R.-X. 2011. Bioactive materials in gene therapy. *Bioactive Materials in Medicine*, 179-219.
- ZHANG, X., SERVOS, M. R. & LIU, J. 2012. Surface Science of DNA Adsorption onto Citrate-Capped Gold Nanoparticles. *Langmuir*, 28, 3896-3902.
- ZHANG, Y., GU, A. Z., HE, M., LI, D. & CHEN, J. 2017. Subinhibitory concentrations of disinfectants promote the horizontal transfer of multidrug resistance genes within and across genera. *Environmental Science & Technology*, 51, 570-580.
- ZHANG, Y., ZHANG, J., XIAO, Y., CHANG, V. W. & LIM, T.-T. 2016. Kinetic and mechanistic investigation of azathioprine degradation in water by UV, UV/H<sub>2</sub>O<sub>2</sub> and UV/persulfate. *Chemical Engineering Journal*, 302, 526-534.
- ZHANG, Y., ZHUANG, Y., GENG, J., REN, H., ZHANG, Y., DING, L. & XU, K. 2015b. Inactivation of antibiotic resistance genes in municipal wastewater effluent by chlorination and sequential UV/chlorination disinfection. *Sci Total Environ*, 512-513, 125-132.
- ZHOU, C.-S., WU, J.-W., DONG, L.-L., LIU, B.-F., XING, D.-F., YANG, S.-S., WU, X.-K., WANG, Q., FAN, J.-N. & FENG, L.-P. 2020. Removal of antibiotic resistant bacteria and antibiotic resistance genes in wastewater effluent by UV-activated persulfate. *Journal of hazardous materials*, 388, 122070.
- ZHOU, Y., MA, R., EBINA, Y., TAKADA, K. & SASAKI, T. 2006. Multilayer hybrid films of titania semiconductor nanosheet and silver metal fabricated via layer-by-layer self-assembly and subsequent UV irradiation. *Chemistry of materials*, 18, 1235-1239.
- ZHUANG, Y., REN, H., GENG, J., ZHANG, Y., ZHANG, Y., DING, L. & XU, K. 2015. Inactivation of antibiotic resistance genes in municipal wastewater by chlorination, ultraviolet, and ozonation disinfection. *Environ Sci Pollut Res Int*, 22, 7037-44.

## APPENDIX A: qPCR AMPLICON SEQUENCE

### a. *tetA* (210 bp) and *tetA* (1054 bp) sequence

**GTAATTCTGAGCACTGTCGC**GCTCGACGCTGTCCGGCATCGGCCTGATTATGCCGGTGCTGCCGGGCCTCCT  
GCGCGATCTGGTTCACTCGAACGACGTCACCGCCCCTATGGCATTCTGCTGGCGCTGTATGCGTTGATGC  
AATTTGCCTGCGCACCTGTGCTGGGCGCGCTGTCCGGATCGTTTCGGGCGGCGGCCGGTCTTGCTCGTCTCG  
CTGGCCGGCGCTGCTGTGACTACGCCATCATGGCGACGGCGCCTTTCCTTTGGGTTCTCTATATCGGGCG  
GATCGTGGCCGGCATCACCAGGGGCGACTGGGGCGGTAGCCGGCGCTTATATTGCCGATATCACTGATGGCG  
ATGAGCGCGCGCGGCACCTTCGGCTTCATGAGCGCCTGTTTCGGGTTCCGGGATGGTCGCGGGACCTGTGCTC  
GGTGGGCTGATGGGCGGTTTCTCCCCCACGCTCCGTTCTTCGCCGCGGCAGCCTTGAACGGCCTCAATTT  
CCTGACGGGCTGTTTCTTTTCCGGAGTCGCACAAAGGCGAACGCCGGCCGTTACGCCGGGAGGCTCTCA  
ACCCGCTCGCTTCGTTCCGGTGGGCCCCGGGGCATGACCGTCGTCGCCGCCCTGATGGCGGTCTTCTTCATC  
ATGCAACTTGTCCGACAGGTGCCGGCCGCGCTTTGGGTCAATTTTCGGCGAGGATCGCTTTCCTGGGACGC  
GACCACGATCGGCATTTTCGCTTGCCGCATTTGGCATTCTGCATTCACTCGCCAGGCAATGATCACCAGGCC  
CTGTAGCCGCCCGGCTCGGGCGAAAGGCGGGCACTCATGCTCGGAATGATTGCCGACGGCACAG**GCTACATC**  
**CTGCTTGCCTTC**GCGACACGGGGATGGATGGCGTTCCCGATCATGGTCCTGCTTGCCTTCGGGTGGCATCGG  
AATGCCGGCGCTGCAAGCAATGTTGTCCAGGCAGGTGGATGAGGAACGTCAGGGGCAGCTGCAAGGCTCAC  
TGGCGGCGCTCACCAGCCTGACCTCGATCGTCGGACCCCT**CCTCTTCACGGCGATCTATG**

Primer set for *tetA* (210 bp):

Forward 5'-**GCTACATCCTGCTTGCCTTC**-3'

Reverse 5'-CATAGATCGCCGTGAAGAGG-3' => **CCTCTTCACGGCGATCTATG**

Primer set for *tetA* (1054 bp):

Forward 5'-**GTAATTCTGAGCACTGTCGC**-3'

Reverse 5'-CATAGATCGCCGTGAAGAGG-3' => **CCTCTTCACGGCGATCTATG**

### b. *amp<sup>R</sup>* (192 bp) and *amp<sup>R</sup>* (851 bp) sequence

**GTATTCAACATTTCCGTGTCGC**CCTTATTCCCTTTTTTGGCGCATTTTGCCTTCCCTGTTTTTGTCCACCCA  
GAAACGCTGGTGAAAGTAAAAGATGCTGAAGATCAGTTGGGTGCACGAGTGGGTTACATCGAACTGGATCT  
CAACAGCGGTAAGATCCTTGAGAGTTTTTCG**CCCCGAAGAACGTTTTCCAA**TGATGAGCACTTTTAAAGTTC  
TGCTATGTGGCGCGGTATTATCCCCTATTGACGCCGGGCAAGAGCAACTCGGTGCGCCGATACACTATTCT  
CAGAATGACTTGGTTGAGTACTCACCAGTCACAGAAAAGCATCTTACGGATGGCATGACAGTAAGAGAATT  
ATGCAGTGCTGCCATAACCATGAGTGATAACACTGCGGCCAACTTACTTCTGACAACGATCGGAGGACCGA  
AGGAGCTAACCGCTTTTTTGCACAACATGGGGGATCATGTAACCTCGCCTTGATCGTTGGGAACCGGAGCTG  
AATGAAGCCATACCAAACGACGAGCGTGACACCACGATGCCTGTAGCAATGGCAACAACGTTGCGCAAACCT  
ATTAACCTGGCGAACTACTTACTCTAGCTTCCCAGCAACAATTAATAGACTGGATGGAGGCGGATAAAGTTG  
CAGGACCACTTCTGCGCTCGGCCCTTCCGGCTGGCTGGTTTTATTGCTGATAAATCTGGAGCCGGTGAGCGT

GGGTCTCGCGGTATCATTGCAGCACTGGGGCCAGATGGTAAGCCCTCCCGTATCGTAGTTATCTACACGAC  
GGGGAGTCAGGCAACTATGGATGAACGAAATAGACAGATCGCTGAGATAGGGTGCCTCACTGATTAAGCAT

Primer set for *amp<sup>R</sup>* (192 bp):

Forward 5'-GTATTCAACATTTCCGTGTCGC-3'

Reverse 5'- TTGGAAAACGTTCTTCGGGG -3' => CCCCGAAGAACGTTTCCAA

Primer set for *amp<sup>R</sup>* (851 bp):

Forward 5'-GTATTCAACATTTCCGTGTCGC-3'

Reverse 5'- ATGCTTAATCAGTGAGGCACC -3' =>

GGTGCCTCACTGATTAAGCAT

c. *sulI* (162 bp) and *sulI* (841 bp) sequence

ATGGTGACGGTGTTCGGCATTCTGAATCTCACCGAGGACTCCTTCTCGATGAGAGCCGGCGGCTAGACCC  
CTCCGGCGCTGTACC GCGGCGATCGAAATGCTGCGAGTCGGATCAGACGTCGTGGATGTCGGACCGGCCG  
CCAGCCATCCGGACGCGAGGCCTGTATCGCCGGCCGATGAGATCAGACGTATTGCGCCGCTCTTAGACGCC  
CTGTCCGATCAGATGCACCGTGTTC AATCGACAGCTTCCAACCGGAAACCCAGCGCTATGCGCTCAAGCG  
CGGCGTGGGCTACCTGAACGATATCCAAGGATTTCTGACCCTGCGCTCTATCCCGATATTGCTGAGGCGG  
ACTGCAGGCTGGTGGTTATGCACTCAGCGCAGCGGGATGGCATCGCCACCCGCACCGGTCACCTTCGACCC  
GAAGACGCGCTCGACGAGATTGTGCGGTTCTTCGAGGCGCGGGTTTTCCGCCTTGCACGGAGCGGGGTCGC  
TGCCGACCGGCTCATCCTCGATCCGGGGATGGGATTTTTCTTGAGCCC CGCACCGGAAACATCGCTGCACG  
TGCTGTGCAACCTTCAAAGCTGAAGTCGGCGTTGGGGCTTCCGCTATTGGTCTCGGTGTCGCGGAAATCC  
TTCTTGGGCGCCACCGTTGGCCTTCTGTAAAGGATCTGGGTCCAG CGAGCCTTGCGGCGGAACTTCA CGC  
GATCGGCAATGGCGCTGACTACGTCCGCACCCACGCTCTGGAGATCTGCGAAGCGCAATCACCTTCTCGG  
AAACCCTCGCGAAATTTTCGAGTCGCGACGCCAGAGA CCGAGGGTTAGATCATGCCTAGC

Primer set for *sulI* (162 bp):

Forward 5'-CGCACCGGAAACATCGCTGCAC-3'

Reverse 5'- TGAAGTTCGCCGCAAGGCTCG -3' =>

CGAGCCTTGCGGCGGAACTTCA

Primer set for *sulI* (841 bp):

Forward 5'-ATGGTGACGGTGTTCGGCATTCTG-3'

Reverse 5'- GCTAGGCATGATCTAACCCTCGG -3' =>

CCGAGGGTTAGATCATGCCTAGC

## APPENDIX B: REACTION EQUATIONS IN UV<sub>254</sub>, UV<sub>254</sub>/H<sub>2</sub>O<sub>2</sub> AND UV<sub>254</sub>/S<sub>2</sub>O<sub>8</sub><sup>2-</sup> SYSTEMS

### B1: ARG Degradation Kinetics by UV<sub>254</sub>

The degradation rate of ARG,  $\frac{d[ARG]}{dt}$ , by UV<sub>254</sub> follows a first-order reaction kinetics defined in Equation B1.

$$-\frac{d[ARG]}{dt} = k_{ARG|UV}[ARG] \quad (B1)$$

Where ARG represents *tetA*, *amp<sup>R</sup>* or *sulI* PCR amplicons. [ARG] is the concentration of PCR amplicons in copies/μL and  $k_{ARG|UV}$  is the first-order rate constant for ARG degradation in s<sup>-1</sup>.

### B2: Determination of Second-order Kinetics Rate Constants for ARG Degradation in UV<sub>254</sub>/H<sub>2</sub>O<sub>2</sub> and UV<sub>254</sub>/S<sub>2</sub>O<sub>8</sub><sup>2-</sup> Systems

Parachlorobenzoic acid (*pCBA*) was used as a probe compound to estimate the steady-state concentrations of hydroxyl radical (*HO*·) and persulphate radical (*SO*<sub>4</sub>·<sup>-</sup>) during ARGs degradation. The degradation of *pCBA* by *HO*· and *SO*<sub>4</sub>·<sup>-</sup> is defined by a second-order reaction kinetics and the steady-state radical concentrations were calculated based on Equation B2.

$$-\frac{d[C]}{dt} = \sum k_{Radical,pCBA} [C][Radical]_{ss} \quad (B2)$$

Where  $d[C]/dt$  is the rate of degradation of *pCBA*,  $k_{Radical,pCBA}$  is the second-order rate constant for the reaction between *pCBA* and the radicals (*HO*· and/or *SO*<sub>4</sub>·<sup>-</sup>) in M<sup>-1</sup>s<sup>-1</sup>, [C] is the molar concentration of *pCBA*, and [Radical]<sub>ss</sub> is the steady-state molar

concentration of the radical species in M. The values of  $k_{Radical,pCBA}$  were found in literature.

$$k_{HO\cdot,pCBA} = 5.0 \times 10^9 M^{-1}s^{-1} \quad (\text{Ahn et al., 2017})$$

$$k_{SO_4^{\cdot-},pCBA} = 3.6 \times 10^8 M^{-1}s^{-1} \quad (\text{Ahn et al., 2017})$$

Equation B2 is rewritten as a first-order kinetics equation as in Equation B3.

$$-\frac{d[C]}{dt} = k'[C] \quad (\text{B3})$$

Where  $k' = k_{Radical,pCBA}[Radical]_{ss}$  is the pseudo first-order rate constant in  $s^{-1}$  for the degradation of *pCBA* by  $HO\cdot$  and  $SO_4^{\cdot-}$ , denoted as  $k'_{pCBA|HO\cdot}$  and  $k'_{pCBA|SO_4^{\cdot-}}$ , respectively.

Likewise, the degradation of ARG,  $\frac{d[ARG]}{dt}$ , by  $HO\cdot$  or  $SO_4^{\cdot-}$  is defined in the same format as Equation B2.

$$-\frac{d[ARG]}{dt} = \sum k_{Radical,ARG} [ARG][Radical]_{ss} \quad (\text{B4})$$

Where ARG represents *tetA*, *amp<sup>R</sup>* or *sulI* PCR amplicons.  $[ARG]$  is the concentration of ARG PCR amplicons in copies/ $\mu$ L and  $k_{Radical,ARG}$  is the second-order rate constant for the reaction between a given PCR amplicon and the radicals ( $HO\cdot$  or  $SO_4^{\cdot-}$ ). Equation B4 is rewritten as a first order kinetics equation as in Equation B5.

$$-\frac{d[ARG]}{dt} = k'[ARG] \quad (\text{B5})$$

Where  $k' = k_{Radical,ARG}[Radical]_{ss}$  is the pseudo first-order rate constant in  $s^{-1}$  for ARG degradation denoted as  $k'_{ARG|HO\cdot}$  and  $k'_{ARG|SO_4^{\cdot-}}$  for  $HO\cdot$  and  $SO_4^{\cdot-}$ , respectively.

Note: All  $k'$  were determined from linear regressions of experimental measurements.

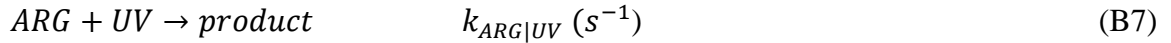
## UV<sub>254</sub>/H<sub>2</sub>O<sub>2</sub> system

### A. Relevant reactions and degradation of ARGs and probe pCBA

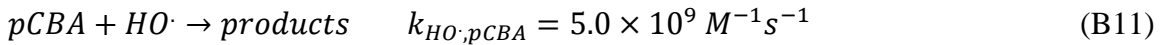
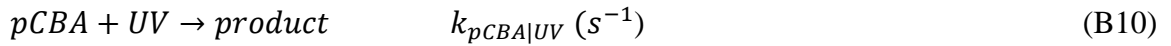
#### i. Radical generated



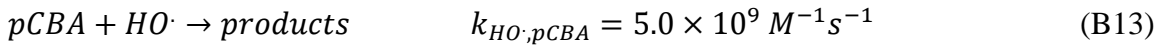
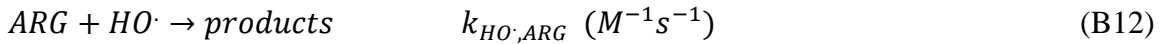
#### ii. ARG degradation (qPCR measurements)



#### iii. pCBA degradation (HPLC measurements)



#### iv. Fate of HO $\cdot$ in UV<sub>254</sub>/H<sub>2</sub>O<sub>2</sub> system



### B. The second order rate constant of ARG degradation with respect to (WRT) HO $\cdot$ i.e.

$k_{HO\cdot,ARG}$ , was calculated as follows:

#### i. Estimated pseudo-first order rate constant of pCBA probe degradation due to radicals only

$$k'_{pCBA|HO\cdot} = k'_{pCBA|UV/H_2O_2} - k_{pCBA|UV} - k'_{pCBA|H_2O_2} \quad (B14)$$

ii. *Estimated pseudo-first order constant of ARG degradation due to radicals only*

$$k'_{ARG|HO\cdot} = k'_{ARG|UV/H_2O_2} - k_{ARG|UV} - k'_{ARG|H_2O_2} \quad (B15)$$

iii. *Determined  $k'_{HO\cdot,ARG}$*

$$k'_{ARG|HO\cdot} = k_{HO\cdot,ARG}[HO\cdot]_{ss} \quad (B16)$$

$$k'_{pCBA|HO\cdot} = k_{HO\cdot,pCBA}[HO\cdot]_{ss} \quad (B17)$$

$$\frac{k'_{ARG|HO\cdot}}{k'_{pCBA|HO\cdot}} = \frac{k_{HO\cdot,ARG}}{k_{HO\cdot,pCBA}} \quad (B18)$$

$$k_{HO\cdot,ARG} = \frac{k'_{ARG|HO\cdot}}{k'_{pCBA|HO\cdot}} \times k_{HO\cdot,pCBA} \quad (B19)$$

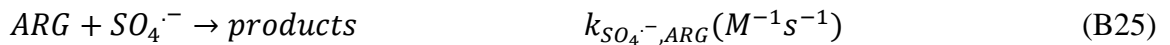
### UV<sub>254</sub>/S<sub>2</sub>O<sub>8</sub><sup>2-</sup> system

A. Relevant reactions and degradation of ARG and probe *pCBA*

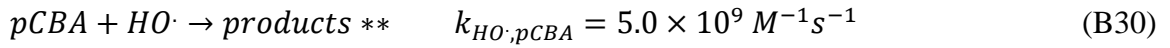
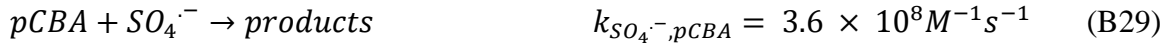
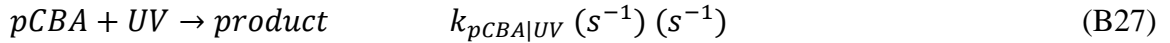
i. *Radicals expected*



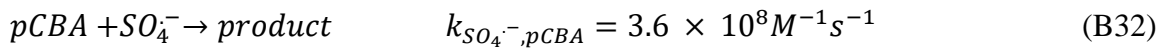
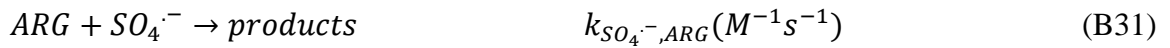
ii. *ARG degradation (qPCR measurements)*



iii. *pCBA degradation (HPLC measurements)*



iv. *Fate of  $SO_4^{\cdot-}$  in sulphate system*



\*\*Preliminary experiment indicated that the contribution of  $HO\cdot$  to ARG degradation in  $UV_{254}/S_2O_8^{2-}$  system at pH of 7 is negligible (Figure 2.7). Therefore, this equation was ignored in the kinetics analyses of  $UV_{254}/S_2O_8^{2-}$  system.

B. The second order rate constant of ARG degradation WRT  $SO_4^{\cdot-}$  i.e.  $k_{SO_4^{\cdot-},ARG}$ , was calculated as follows:

i. *Estimated pseudo-first order constant of pCBA probe degradation due to radicals only*

$$k'_{pCBA|SO_4^{\cdot-}} = k'_{pCBA|UV/S_2O_8^{2-}} - k_{pCBA|UV} - k'_{pCBA|S_2O_8^{2-}} \quad (B34)$$

ii. *Estimate pseudo-first order constant of ARG degradation due to radicals only*

$$k'_{ARG|SO_4^{\cdot-}} = k'_{ARG|S_2O_8^{2-}/UV} - k_{ARG|UV} - k'_{ARG|S_2O_8^{2-}} \quad (B35)$$

$k'_{pCBA|UV/S_2O_8^{2-}}$  was obtained without the initial log reduction from  $S_2O_8^{2-}$  (Figure 2.6).

Thus, Equation B35, was re-written as Equation B36. This was used to calculate the second order degradation rate constant of qPCR amplicons.

$$k'_{ARG|SO_4^-} = k'_{ARG|S_2O_8^{2-}/UV} - k_{ARG|UV} \quad (B36)$$

iii. *Determined  $k_{SO_4^-,ARG}$*

$$k'_{ARG|SO_4^-} = k_{SO_4^-,ARG}[SO_4^-]_{SS} \quad (B37)$$

$$k'_{pCBA|SO_4^-} = k_{SO_4^-,pCBA}[SO_4^-]_{SS} \quad (B38)$$

$$\frac{k'_{ARG|SO_4^-}}{k'_{pCBA|SO_4^-}} = \frac{k_{SO_4^-,ARG}}{k_{SO_4^-,pCBA}} \quad (B39)$$

$$k_{SO_4^-,ARG} = \frac{k'_{ARG|SO_4^-}}{k'_{pCBA|SO_4^-}} \times k_{SO_4^-,pCBA} \quad (B40)$$

**Note:** Rate constant ( $k$ ) expressed as  $cm^2/mJ$  is converted to  $k$  in  $s^{-1}$  using Equation B41.

$$k (s^{-1}) \cong k (cm^2/mJ) \times irradiance_{at\ centre\ of\ the\ dish} (mW/cm^2) \quad (B41)$$

APPENDIX C: LINEAR REGRESSION OF FIRST ORDER DEGRADATION RATE  
CONSTANT,  $K$  (CM<sup>2</sup>/MJ) VERSUS SPECIFIC NUCLEOTIDE CONTENTS OF QPCR  
AMPLICON

Name: Appendix C\_Kinetics\_Versus\_Amplicon\_Content\_Adeola\_J\_Sorinolu\_2022

File type: Microsoft Excel Worksheet (.xlsx)

Size: 26 KB

Required application software: Microsoft Excel

## APPENDIX D: UV FLUENCE CALCULATION EQUATIONS

$$UV\ fluence_{at\ dish\ centre} = irradiance_{at\ centre\ of\ the\ dish} \times exposure\ time \quad (D1)$$

Since UV fluence varies across the exposed sample surface, the average UV fluences were calculated according to the standard method described by Bolton and Linden (2003).

$$Average\ UV\ fluence = UV\ fluence_{at\ dish\ centre} \times Petri\ Factor \times \\ Reflection\ Factor \times Water\ Factor \times Divergence\ Factor \quad (D2)$$

$$Water\ factor = \frac{1-10^{-al}}{al \ln 10} \quad (Bolton\ and\ Linden,\ 2003) \quad (D3)$$

Where  $a$  is the UV absorbance of sample at 254 nm,  $l$  is the vertical path length (cm) of sample in the Petri dish (equal to the sample depth).

$$Divergence\ factor = \frac{L}{L+l} \quad (Bolton\ and\ Linden,\ 2003) \quad (D4)$$

Where  $L$  is the distance of the Petri dish from the UV lamp (cm) and  $l$  is the vertical path length (cm) of sample in the Petri dish (i.e., the sample depth).

$$Petri\ Dish\ Factor = \frac{\text{average of the incident irradiance over the area of the Petri dish}}{\text{irradiance at the center of the dish}} \quad (D5)$$

The average of the incident irradiance over the Petri dish surface was obtained as the average of at least 30 irradiance measurements at about 1cm apart across the sample surface.

The reflection factor - “the fraction of the incident beam that entered the water” was taken as 0.975 (Bolton and Linden, 2003). The water factor for the samples was taken as 1 because the UV absorbance of PBS is 0.